INVESTIGATION OF THE EFFECTS OF SILVER/ZINC OXIDE NANOCOMPOSITE DISPERSED MODIFIED ELASTIN-COLLAGEN MATRIX ON THE MECHANICAL ,THERMAL AND ANTIMICROBIAL PROPERTIES OF POLY (LACTIC ACID)

YEZIHALEM ZENA AMEHA

A Thesis Submitted to

The Department of Chemical Engineering

School of Mechanical, Chemical, and Material Engineering

Presented in Partial Fulfillment of the Requirement for the Degree of Master of science in Chemical Engineering (Specialization in Process Engineering)

Office of Graduate Studies

Adama Science and Technology University

August, 2022

Adama, Ethiopia

INVESTIGATION OF THE EFFECTS OF SILVER/ZINC OXIDE NANOCOMPOSITE DISPERSED MODIFIED ELASTIN-COLLAGEN MATRIX ON THE MECHANICAL,THERMAL AND ANTIMICROBIAL PROPERTIES OF POLY (LACTIC ACID)

YEZIHALEM ZENA AMEHA

Major Advisor

Dr. P.Selvakumar

Co-Advisors:

Dr. Zelalem Tumsa

Dr.Melakuu Tesfaye

A Thesis Submitted to

The Department of Chemical Engineering School of Mechanical, Chemical and Materials Engineering

Presented in Partial Fulfillment of the Requirement for the Degree of Master of science in Chemical Engineering (Specialization in Process Engineering)

Office of Graduate Studies

Adama Science and Technology University

August, 2022

Adama, Ethiopia

DECLARATION

I hereby declare that this Master Thesis entitled “Investigation of the effects of silver/zinc oxide nanocomposite dispersed modified elastin-collagen matrix on the mechanical thermal and antimicrobial properties of poly (lactic acid)” is my original work. That is, it has not beensubmitted for the award of any academic degree, diploma, or certificate in any other university. All sources of materials that are used for this thesis have been duly acknowledged through citation.

Yezihalem Zena Ameha	_____	_____
Name of the student	Signature	Date

RECOMMENDATION

We, the advisors of this thesis, hereby certify that we have read the revised version of the thesis entitled “Investigation of the effects of silver/zinc oxide nanocomposite dispersed modified elastin-collagen matrix on the mechanical thermal and antimicrobial properties of poly (lactic acid)” prepared under our guidance by Yezihalem Zena submitted in partial fulfillment of the requirements for the degree of Masters of Science in Chemical Engineering. Therefore, we recommend the submission of the revised version of the thesis to the department following the applicable procedures.

Dr. P.Selvakumar	_____	_____
Major advisor	Signature	Date
Dr. Zelalem Tumsa	_____	_____
Co-advisor	Signature	Date
Dr. Melakuu Tesfaye	_____	_____
Co-advisor	Signature	Date

APPROVAL PAGE

We, the advisors of the thesis entitled "Investigation of the effects of silver/zinc oxide nanocomposite dispersed modified elastin-collagen matrix on the mechanical thermal and antimicrobial properties of poly (lactic acid)" and developed by Yezihalem Zena, hereby certify that the recommendation and suggestions made by the board of examiners are appropriately incorporated into the final version of the thesis.

Dr. P.Selvakumar	_____	_____
Major advisor	Signature	Date
Dr. Zelalem Tumsa	_____	_____
Co-advisor	Signature	Date
Dr. Melakuu Tesfaye	_____	_____
Co-advisor	Signature	Date

We, the undersigned, members of the Board of Examiners of the thesis by Yezihalem Zena have read and evaluated the thesis entitled Development of Ag/ZnO Nano composite dispersed protein matrix (broiler skin) for property enhancement of poly (lactic acid) and examined the candidate during the open defense. This is, therefore, to certify that the thesis is accepted for partial fulfillment of the requirement of the degree of Master of Science in Chemical Engineering

_____	_____	_____
Chairperson	Signature	Date
_____	_____	_____
Internal Examiner	Signature	Date
_____	_____	_____
External Examiner	Signature	Date

Finally, approval and acceptance of the thesis is contingent upon submission of its final Copy to the Office of Postgraduate Studies (OPGS) through the Department Graduate Council (DGC) and School Graduate Committee (SGC).

_____	_____	_____
Department Head	Signature	Date
_____	_____	_____
School Dean	Signature	Date
_____	_____	_____
Office of Postgraduate Studies, Dean	Signature	Date

ACKNOWLEDGEMENT

I would like to acknowledge, give my warmest gratitiude and praise for the almighty GOD who was there for me through all these years and for my respected advisors P.selvakumar (PhD), Zelalem Tumsa (PhD) and Melakuu Tesfaye (PhD), words cannot express my gratitude, with out your invaluable advice and support this research would not reach this stage.

I am also greatful for my colleagues classmates for their help in editing, late night responses and moral support. All in all anybody who put a dot on this research, I would love to thank you from the bottom of my heart.

Table of Contents

LIST OF TABLES

LIST OF FIGURES

LIST OF ABBREVIATIONS AND ACRONYM

Ag NPs	Silver nanoparticles
Ag/ZnO NCs	Silver/zinc oxide Nano-composite
CNC	Cellulose Nano-composite
Cu NPs	Copper Nanoparticles
DSC	Differential scanning calorimeter
DTG	Derivative thermo gravimetric
XRD	X-ray Diffraction
EB	Elongation at break
ELL-COLL	*Elastin-collagen matrix*
m-ELL-COLL	Modified *Elastin-collagen matrix*
FTIR	Fourier-transform infrared spectroscopy
Go NPs	Grapheme-oxide Nanoparticle
GRAS	Generally recognized as safe
Hf	Heat of fusion
LA	Lactic acid
NCs	Nano-composites
NiO NPs	Nickel-oxide Nanoparticle
NPs	Nano particles
PBAT	Poly(butylene adipate-co-terephthalate)
PLA/m-ELL-COLL	Modified Elastin-collagen dispersed Poly(lactic acid) film
PLA/m-ELL-COLL/Ag/ZnO	Silver/Zinc oxide- modified Elastin-collagen dispersed Poly(lactic acid) film
PLA-Pr	Peristen poly(lactic acid)
SPR	Surface Plasmon resonance
T_{90}	Temperatures at 90% mass loss
T_{10}	Temperatures at 10% mass loss
T_{50}	temperatures at 50% mass loss
Tcc	Cold crystallization temperature
Tendset	End-set degradation temperature

Tg	Glass transition temperature
Tm	Melting temperature
Tmax	Maximum degradation temperature
Tonset	Onset degradation temperature
TS	Tensile strength
UTM	Universal testing machine
Xc	Degree of crystallinity
ZnO NPs	Zinc oxide nanoparticles

ABSTRACT

Poly(lactic acid) (PLA) has distinctive characteristics, including biodegradability, biocompatibility, thermal processability, high transparency and good film forming ability. However PLA has some poor properties that have prevented its wide applicability and these properties are low crystallization rate, poor thermal stability, and high brittleness. The main objective of this research was to investigate the effect of the modified Elastin-collagen (m-ELL-COLL) matrix and Silver/Zinc oxide dispersed modified Elastin-collagen (Ag/ZnO/m-ELL-COLL) on PLA's properties.The ELL-COLL matrix was extracted from broiler skin waste and modified by grafting using lactic acid monomer to facilitate compatibility issues with PLA. The extracted and modified ELL-COLL matrix were investigated using FTIR, and both the pre- and post-modification persistence of the α-helix and β-sheet structures were confirmed. Chemical methods were used to synthesize silver(Ag), zinc oxide (ZnO) nanoparticles (NPs), and silver-zinc oxide nanocomposite(Ag/ZnO NCs) and the synthesized nanomaterials were characterized using XRD, FTIR, UV-VIS, and PSDA. All the characterized nanomaterials showed the characterstics peaks in UV-VIS and FTIR analysis. The XRD analysis reveled that there was no additional peaks excepet for characterstics peaks of Ag, ZnO NPs and Ag/ZnO NCs which confirmed the formation of pure nanomaterials.Modified elastin-collagen dispersed Poly(lactic acid) (PLA/m-ELL-COLL) composite films were prepared using solution casting method and characterized using DSC and UTM. The effect of m-ELL-COLL as nucleating agent resulted in degree of crystallinity of 58.8% with 10wt% m-ELL/COLL loading, and the elongation at break was improved by 143.1 % for PLA/m-ELL-COLL-40% with tensile strength of 33.75 MPa compared to neat PLA. Following the same method Ag/ZnO dispersed m-ELL-COLL/PLA ternary composite films were prepared and characterized using DSC, TGA and disc diffusion method for antimicrobial activity. The results revealed that, all ternary composite films had lower thermal stability than neat PLA whereas PLA-ELL/COLL-Ag/ZnO-10% showed 43.3% degree of crystalinity. For the antibacterial properties of the ternary composite film PLA-m-ELL/COLL-Ag/ZnO-10% had the largest inhibition zone, which was approximately 12.5 mm for Staphylococcus aureus (gram-ve) and 13 mm for Streptococcus pyogenes (gram+ve) bacteria compared to control (ampicillin). As a result, the eco-friendly composite films could be widely used in different area of applications specially for active packaging purposes.

***KEY WORDS**: Composite films, Degree of crystallinity, Elongation at break, Modified elastin collgen matrix, Poly(Lactic acid), Ag/ZnONCs*

CHAPTER ONE

1. INTRODUCTION

1.1. Background of the study

For many years, petroleum-based polymers have been used for various applications including packaging and a variety of other chemical products (Luchese et al., 2015; Groh et al., 2019). Most of those polymers that derived from petrochemical sources are not biodegradable, cannot be recycled after being utlized and have drawbacks when used for packaging purpose (Puscaselu et al., 2019; Rihayat et al., 2020; Hasan et al., 2021).

To solve these aformentioned limitation of petro-based polymers, bio-based polymers have been extensively explored as a feasible option for establishing a sustainable green environment by substituting conventional polymers while retaining the important properties required for end-use applications. Biofilms that are derived from biopolymers can be categorized into two; bioplastics derived from biomass such as cellulose, starch, protein, chitosan, etc… through chemical modification, and biofilms fabricated from the synthesis of biobased monomers termed synthetic biopolymers such as poly(lactic acid), and polybutylene adipate terephthalate (PBAT) (Wang et al., 2018; Thakur et al., 2019; Chen et al., 2019; Haghighi et al., 2020; Jian et al., 2020; Sharma et al., 2021). The important aspects of the aforesaid biopolymers necessary for them to be viewed as prospective substitutes for conventional polymers are their abundance, biodegradability, biocompatibility, and some unique properties possessed by the polymers (Elolimy et al., 2018; Domene-López et al., 2019; Olayi et al., 2021; Gutiérrez et al.,2021).

Among all the synthetic biopolymers, poly (lactic acid) (PLA) is bio-based, bio-degradable, and bio-compatible linear aliphatic thermoplastic biopolymer that can be produced by the most well-known production method which is ring-opening polymerization which results in the production of optical isomers of poly(lactic acid) (Nofar et al., 2019, Asadi et al., 2020, Wang et al., 2020, Yang et al., 2020). The source of this polymer is usually lactic acid which is found in nature, particularly in sugar cane, corn starch, and other bio-mass products (Dogan et a., 2017; Bindhu et al., 2018). In addition to its natural-based source, poly (lactic acid) has appealing physicochemical properties to be used as a biofilm-making biopolymer, including a

high elastic modulus and high transparency (Mallegni, et al., 2018), non-toxic and bio-compatible for foods (Bindhu et al., 2018), has good thermal processibility (Kale et al., 2018).

The sources and properties of poly (lactic acid) inspires many researchers and scholars to functionalize it in the scientific and manufacturing world however, it has been difficult to bring this compatible, non-toxic, and biodegradable material into industrial, packaging, medical, and other application areas due to its limitation such as low crystallization rate, low thermal stability (Mallegni et al.., 2018), hydrophobicity and high brittleness (Mao et al., 2019). The process of enhancing the limitations and adding values such antimicrobial, antifungal activities would be the best possible ways in the proceesing activity of PLA.

Thus in addressing those limitations different bio-polymer as nucleating agents were incorporated with PLA matrix to form and enhance the properties of the composite film. Sun et al. 2022, reported that the addition of ammonium salt-modified cellulose nanocrystals played a significant role in improving the mechanical properties of PLA/PBAT composite films, similar to how PLA's miscibility was improved when used coffee grounds were added (Suaduang et al. 2019). Tanase et al., 2014, reported that the inclusion of keratin in the PLA chitosan system reduced Tg to 58.9 °C while crystallinity increased to 19.17 %. Nilsuwan et al.,2020, reported that bilayer films of fish gelatin (FG) and poly(lactic acid) (PLA) with varied FG/PLA layer thickness ratios (9:1, 8:2, 7:3, 6:4, and 5:5) were prepared using casting. Bilayer films were found to have lower tensile strength (TS) but greater elongation at break (EAB) than PLA films.

Beside the afformentioned approach incorporating metal and metal oxide nanoparticles in single and composite forms as fillers to enhance the PLA's property have been the go-to scientific and the most recent method to form composite biofilms. Bautista-Del et al., 2020, reported that blending of PLA with copper nanoparticles increased the degree of crystallinity from 76.9% to 79.8% with 0.043 wt% of Cu and to 84.4% with 0.074 wt% of Cu. As nanofillers, graphene oxide (GO) and multiwalled carbon nanotubes containing silver particles in various concentrations were employed to construct nanoparticle dispersed poly (lactic acid) films. The inclusion of nanoparticles boosted the crystallization rate substantially, whereas the glass transition and melting temperatures of the PLA-based films remained almost constant (Li et al., 2022). The addition of TiO_2 to PLA provides no change in the $T_{onset,}$ but alters the T_{max},

while the Ag-NPs dispersion also decreases the thermal resistance of the film (de Azevedo Gonçalves Mota et al., 2021).

Elastin-collagen (ELL-COLL) matrix was selected as composite film formig polymer due to its compatibility with that of bio-based polymer which is known to be poly (lactic acid). By understanding the lack of research works on proteins as composite film forming agents this research intended to bring the ELL-COLL matrix as as composite film forming agents to enhance important features of poly (lactic acid). Also due to their high antimicrobial activity (Lizundia et al., 2018), good crystalline property (Rashidi et al., 2019) and good thermal stability of silver (Ag) and zinc oxide (ZnO) NPs and also studying their synergetic effect on the properties of PLA was the uniqiness of this study. In the process of incorporating these nanomaterials into different polymers, many researchers blended the nanomaterial with different organic materials like cellulose (Bardotet al., 2020), starch (Davoodi et al.,2016), PBAT (Girdthep et al,.2022), and so on.

In order to exploit the matrix and the NCs as a tool for improving PLA's properties, the main objective of this research was to investigate the effect of the modified Elastin-collagen (m-ELL-COLL) matrix and Silver/Zinc oxide dispersed modified Elastin-collagen (Ag/ZnO/m-ELL-COLL) on PLA's properties. Before adding the ELL-COLL matrix to the PLA, the ELL-COLL matrix was modified using a lactic acid (LA). Next, solution casting was utilized to develop the m-ELL-COLL matrix dispersed PLA binary films, and were subsequently characterized by DSC and UTM. In addition, Ag/ZnO-m-ELL-COLL/PLA ternary films were developed and were evaluated for their antibacterial activity, crystallization, and thermal characteristics by using an m-ELL-COLL matrix to promote the compatibility, stable dispersion, and confined impact of Ag/ZnO NCs.

1.2. Satement of the problem

Developing bio-based materials with a potential to substitute these conventional polymers is a better and more promising way of solving the world's crucial problems. Among these bio-based polymers Poly (lactic acid) has shown a great potential to give an additional value in finding ways to make the bio-polymers being utilized daily. Although PLA has unique properties it exhibits some poor properties such as poor crystallinity, poor thermal resistance (stability), poor flexibility, and other poor physical and chemical properties that cause the limitation in processing and make it applicable.

When looking at potential polymers for food packaging, the main quality that must be present in order to use any material as an active packaging is its antibacterial activity, which prolongs the shelf life of the food and prevents spoilage. Even though PLA is a bio-based, environmentally friendly polymer with strong mechanical and thermal characteristics, its use as an active packaging material is constrained by its lack of antibacterial activity.

In this study, m-ELL-COLL matrix and Ag/ZnO nanocomposite was extracted, synthesized, characterized and applied to enhance the properties of PLA-based films. The impact of the m-ELL-COLL matrix as a carrier, as well as the composite film forming agent and Ag/ZnO nanocomposite on the enhancement of PLA polymer properties has been examined. Thus, the current study provides a complete analysis of integrating all of the above-mentioned materials and their influence on improving the crystallization, thermal stability, mechanical and antibacterial properties of PLA.

1.3. Research question and choice of a system

Research question: This thesis was designed to answer the following question as much as possible.

- Can the Synthesized and modified Elastin-collagen matrix serve as a nucleating agent and carrier for the Nano-composite?
- How do the dispersed Ag/ZnO Nano-composite and the Elastin-collagen matrix affect the properties of poly (lactic acid)?
- Can it be possible to explain the role of Ag/ZnO Nano-composite and the modified Elastin-collagen matrix in the poly (lactic acid) property enhancement?

Choice of a System: Based on the above research questions the choice of the system, methodology and characterization procedures are framed as follows.

- Elastin-collagen matrix is selected as nucleating agent due to its compatibility with that of bio-based polymer which is known to be poly (lactic acid) (PLA).
- Due to its high anti-microbial activity, low toxicity to human cells, and intensive ultraviolet absorption Ag/ZnO composite Nano particle is selected.
- OH group of poly (lactic acid) can have a possibility to bind with an amide group of ELN/COL to form macromolecular interaction so that kit can help to regulate the properties of PLA.

1.4. Objectives

1.4.1. General Objective

The general objective of this work was to study the effect of m-ELL-COLL matrix, Ag/ZnO Nano-composite dispersed m-ELL-COLL matrix on the crystalization, mechanical, thermal and antimicrobial properties of PLA.

1.4.2. Specific Objective

The specific objectives of this study were to:

- Extract, modify and characterize the Elastin-collagen matrix.
- Synthesize and characterize Ag NPs, ZnO NPs, and Ag/ZnO NCs.
- Study the effect of m-ELL-COLL matrix on the crystallization and mechanical properties of PLA
- Study the effect of Ag/ZnO nanoparticle dispersed m-ELL-COLL matrix on the thermal, Antimicrobial, and crystalization properties of PLA.

1.5. Significance of the study

Developing a bio-degradable, bio-compatible, and multifunctional polymer in a greener way of synthesizing bio-materials plays a great role in providing a better solution to resolve the crucial impacts of conventional polymers on the nature and its habitat. Among these bio-degradable, bio-compatible, and multifunctional polymers, the poly (lactic acid) is the most promising biopolymer in addressing the problems associated with conventional polymers. The drawbacks associated with this bio-polymer halt it from being utilized abundantly, so this research is significant in resolving the poor properties associated with PLA using different matrixes which potentially may have significant and positive impacts in enhancing the specific properties.

Aspiring ways of using different matrixes to enhance the properties of PLA play a role not only in enhancing the properties but keeping the bio-related properties of the PLA which makes it a more preferable way of conducting the research. Enhancing the properties of PLA and keeping its bio-related properties using bio-based fillers and Nanoparticles have been

chosen and were implemented in the research. Generally, the significance of the research is in filling the gap of other bio-based fillers fail to achieve, and using different matrixes will show the way in enhancing the properties without compromising their bio-related properties.

1.6. Scope of the study

The scope of the thesis work within the given time and resources includes

♣ Extracting, modifying and characterizing ELN/COL.

♣ Synthesizing and characterizing Ag, ZnO, and Ag/ZnO nanoparticles.

♣ Developing and characterizing PLA-Elastin/Collagen and PLA-Ag/ZnO- Elastin/Collagen matrix biofilm.

1.7.Organization of the Thesis

The thesis was organized as follows:

Chapter 1: Introduces the background, statement of the problem, objectives, significance of and scope of the study.

Chapter 2: Discuss the relevant literature and related works regarding the structure, synthesis, and application of ELL-COLL, Nanocomposite, polylactic acid, and property enhancement of PLA using metal Nanocomposites and particles.

Chapter 3: Features the materials and methodology for the research, including extraction and characterization of ELL-COLL, Ag, ZnO, and Ag/ZnO particles and PLA/Ag-ZnO/ELL-COLL composite films.

Chapter 4: Explains the result obtained from the desired proposed work and discusses the characterization results followed by postulating the impact of Nanocomposite dispersion into the polymer matrix.

Chapter 5: Concludes on every proposed specific objective and recommend different possible direction for further studies.

CHAPTER TWO

2. LITERATURE REVIEW

Chapter Overview

This chapter aims to present the investigation of others sholars on the property enhancement of poly(lactic acid) using different bio-materials and nano-materials and also how they have presented their research results and obtained an insight of this investigation trend. In dealing with others investigation we have gained a research gap which had given us a way to develop a novel system.

2.1. Bio-polymers

Biopolymers are naturally occurring polymers that are useful in film preparation techniques fo r avariety of applications. Six fundamental and well-known biopolymers with good film-forming capabilities are cellulose, starch, protein, chitosan, poly (lactic acid), and polybutylen e adipate terephthalate. These biopolymers can be classified as synthetic and bio based biopolymers.Thefollowing section describes the scientific definition, natural sources, unique a nd basic features, and recovery techniques of those biopolymers.

2.1.1. Natural biopolymers and their modification for biofilm preparation

Based upon their source these biopolymers are generally known as natural biopolymers. These biopolymers can be considered multifunctional materials due to their source, unique features, and recovery methods. Among these cellulose is one of the most abundant hydrophobic biopolymers that is constructed from hundreds of repeating D-glucose units connected by a special connection known as -1,4 glycosidic linkages (Zhang et al.,2018; He et al., 2021). Plants (Zhao et al., 2018), mammals (Wu et al., 2022), bacteria (Khan et al., 2020), and algae are the primary natural sources of this biopolymer (Zarei et al., 2018). It can also be recovered from different sources via the subcritical water pretreatment method (Thi et al., 2017), and fermentation (Fadakar et al., 2021). Bio-degradability and biocompatibility (Gong et al., 2017), high viscosity (Nuruddin et al., 2021), nano-fibrillar three-dimensional network structure (Atta et al., 2021), optical transparency (Reimer et al., 2021), and adjustable porous structure are among its distinctive physicochemical qualities (Shi et al., 2021). Another natural

and multifunctional biopolymer which have been utlized in different application areas is starch which consists of two main polysaccharides, amylose and amylopectin (Cui et al., 2021) and the major source of this particular biopolymer is plants' photosynthesis (Bangar et al., 2021, Oyeyinka et al., 2021). Recovering starch has been possible through ultrasound-assisted extraction (Ochoa et al., 2021), pressurized liquid extraction and supercritical technology (Santana et al., 2017), wet-milling. Natural biopolymers can't be directly functionalized they all need some chemical or physical modification and these techniques are graft modification (grafting from and to) (Garcia-Valdez et.al 2018; Qiao et al., 2018 Kedzior et al., 2019; Nallasamy et al., 2020), cross-linking (Chen et al., 2019; Jeon et al., 2019; Guo et al., 2021).

2.1.2. Synthetic Biopolymers

Synthetic biopolymers are polymers that have been modified from natural polymers or chemically produced from synthetic monomers such that they can degrade naturally without leaving residues that are hazardous to living things and the environment (Mazumder et al., 2019). Also, they have become attractive alternatives to biosynthetic biopolymers due to their unique features (Kubicek et al., 2016). Among these unique biopolymers poly(lactic acid) and Polybutylene adipate terephthalate (PBAT) have been investigated widely and proved their applicability in different areas. In the following section, detailed scientific explanations of poly(lactic acid) are discussed.

2.2. Over view of Poly (lactic acid)

As numerous sectors seek to reduce their reliance on petroleum-based fuels and goods for economic and environmental sustainability, biopolymers as alternatives to synthetic and non-degradable materials have become a key emphasis. Plastic polymers derived mostly from fossil fuels now make up roughly half of all packaging products (Umer et al., 2017).

In finding ways to tackle these crucial problems looking for the very best alternative is the way out and considering their substituting capacity; synthetic biopolymers are the best option. Among them, Poly (lactic acid) is a bio-based, biodegradable, and biocompatible linear aliphatic thermoplastic biopolymer that may be manufactured by the most well-known process, ring-opening polymerization, which produces optical isomers of poly(lactic acid) (Nofar et al., 2019, Asadi et al., 2020, Wang et al., 2020, Yang et al., 2020).

The carbon in PLA originates from atmospheric carbon dioxide, which is immobilized in glucose by photosynthesis; therefore, the carbon dioxide formed by its disposal, incineration, or biodegradation does not increase the total amount of atmospheric carbon dioxide and also poly (lactic acid) and its copolymers have attracted significant attention in environmental, biomedical, and pharmaceutical applications and as alternatives to petro-based polymers (Tsuji et al., 2013).

Poly (lactic acid) (PLA), is classified as GRAS polymer based on its different characteristics like non-toxicity, and compatibility, and since it is derived from a nature-based monomer (Nilsuwan et al., 2020). PLA production involves the condensation polymerization followed by ring-opening polymerization of lactic acid (Koh et al., 2018). Lactic acid is a naturally occurring polymer that can be found in sugar cane, maize starch, and other bio-mass products (Dogan et a., 2017; Bindhu et al., 2018). The following figure explains the life cycle of poly (lactic acid) i.e it passes through the different stages of processes like pre-polymerization, oligomerization, and degradation (Guzman et al.,2011).

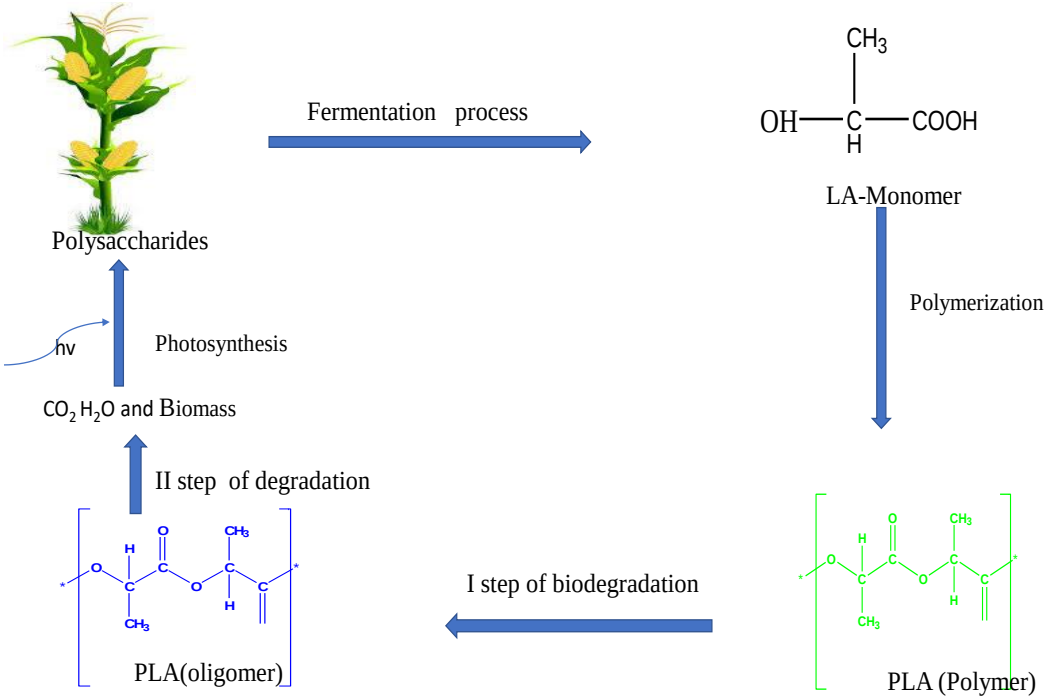

Figure 2.1: Life cycle of Poly (lactic acid)

2.2.1. Rheological, mechanical and barrier Properties

Rheological measurements are one way to look into the thermal stability of polymers and blends. Rheological qualities are important tools for evaluating thermoplastics for their preparing tasks, therefore understanding PLA's softened rheology is crucial for working with forceful handling. PLA behaved Newtonian at low shear rates and non-Newtonian (shear thinning) at high shear rates, similar to all thermoplastic polymers. (Hamad et al., 2015). The improvement of the rheological and viscoelastic properties of PLA is of great importance as it enhances the melt strength (Nofar et al.,2019).

The rheology of PLA can be concluded in the following three rheological properties and are the solution, melt, extensional rheology, and melt Strength (Di Lorenzo et al.,2018). Poly (lactic acid) exhibits poor mechanical properties like high brittleness and mow toughness which these properties are difficult in applying to this particular polymer as a multifunctional polymer (A.K. Abay et al., 2016). Barrier properties of poly (lactic acid) include permeability of gases, optical barrier properties, and water vapor permeability, i.e., related to the film materials' qualities, such as the component chemicals' hydrophilicity or hydrophobicity (Jamróz et al., 2019; Salama et al., 2020; Tarique et al., 2021). This property is directly related to packaging, a barrier property is considered enhanced when it is lower than the neat films.

2.2.2. Thermal Properties

In addition to mechanical, rheological, optical, and electrical properties, thermal properties and thermodynamics are among the most essential physicochemical features of poly(lactic acid) (PLA). PLA absorbs or releases heat during heating or cooling, just like other polymers, as seen by a change in heat capacity.

The glass transition, enthalpy relaxation, crystallization, crystal rearrangement, melting, and decomposition are all transitions that can be observed. The set of numbers and characteristics that characterize PLA's thermal properties and thermodynamics (Di Lorenzo et al.,2018). PLA is a semi-crystalline or amorphous polymer with a glass transition temperature (Tg) and melting temperature (Tm) of approximately 55°C and 180°C, respectively. The thermal properties of PLA could be affected by different structural parameters, such as molecular weights and composition (stereoisomer content) (Hamad et al., 2015).

2.2.3. Unique properties (features) of poly (lactic acid)

Poly (lactic acid) has appealing physicochemical features to be a multifunctional biopolymer, these features include high elastic modulus and transparency (Mallegni et al., 2018), as well as good mechanical qualities (tensile strength) (Liu et al., 2021). It is food-safe and biocompatible (Bindhu et al., 2018), and it has good thermal processability (Kale et al., 2018). Low thermal stability (Ciarfaglia et al., 2021), low crystallinity (Andrzejewski et al., 2021), and high brittleness (Omar et al., 2021) and biocompatibility (Bednarek et al., 2021) are some of the unique features of poly (lactic acid).

2.2.4. Limitations of poly (lactic acid)

Even though, it possesses different attractive Physical and chemical properties it has different property limitations which halt the polymer from being utilized in research, medical, manufacturing, and different area of applications. The property limitations of this particular polymer are low thermal stability, low crystallization properties, less antimicrobial and barrier properties, and also different drawbacks are related to this polymer (Huang et al 2015; Baek et al., 2018; Pena-Juarez et al., 2021; Montes-Zavala et al., 2022).

2.2.5. The Need to Improve Properties of PLA

As explained earlier PLA possesses different attractive properties such as good mechanical properties, degradability, and compatibility. But also it has some limitations to process. To bring up PLA into manufacturing and medical applications area these limitations should be tackled via different techniques. Plasticizers, polymer mixing, coupling agents, co-polymerization, and nanotechnology have all been used to overcome PLA's difficulties (Chan et al.,2017; Fan et al., 2018).

2.3. Methods to improve properties PLA

2.3.1. Nucleating agents (fillers)

The **Nucleating agents** can be classified into two main broad classes based on their source and these are bio-based and synthetic nucleating agents. These additives function by presenting a heterogeneous surface to the polymer melt, making the properties of PLA more enhanced (favorable). As a result of this effect, the temperature at which the polymer begins to

decompose is increased, as is the rate of nucleation and overall thermal stability. Nucleating agents also promote the formation of smaller and more numerous spherules, often giving enhanced properties such as flexural modulus and heat deflection temperature (HDT). Nucleating agents are most widely used in homo and random co-polymers, where they provide three main benefits: property enhancement, improved molding productivity, and increased transparency. Some special nucleating agents produce spherules so small that they do not scatter visible light, providing transparent polypropylene. Products that provide this effect are referred to as clarifiers (Kovalcik et al., 2017).

2.3.2. Synthetic nucleating agents

As the name indicates, synthetic fillers are fillers that can be synthesized in different experimental methods which can serve as property enhancement for the property of poly (lactic acid). In this thesis, we will focus on metallic nanoparticles and nanocomposites which play a vital role in enhancing the difficulties of the specific polymer. The enhancement role of these metal and metal oxide nanoparticles on crystallization, mechanical, thermal stability, and antimicrobial activity are reviewed in the following pattern.

2.3.2.1. Crystallization/nucleation property

The type of filler, as well as its size and shape, influence the crystallization enhancement of any polymer. Improving a polymer's crystallization broadens its application area and processibility (under temperature and stress conditions), as well as increasing the polymer's usage rate. Pure PLA was blended with copper nanoparticles. The crystallization enhancement was significant (from 76.9% to 79.8% with 0.043 wt% of Cu and 84.4% with 0.074 wt% of Cu) (Bautista-Del et al., 2020).

As Nanofillers, graphene oxide (GO) and multiwalled carbon nanotubes containing silver particles in various concentrations were employed to construct nanoparticle dispersed poly (lactic acid) films. The inclusion of nanoparticles boosted the crystallization rate substantially, whereas the glass transition and melting temperatures of the PLA-based films remained almost constant (Li et al., 2022). A poly (lactic acid) film distributed with silver phosphate, zinc oxide and Nano-hybrids was created. The degree of crystallization rose dramatically from 2.8

percent for the clean PLA film to 23.5, 23.2, and 25.4 percent for Ag (2 wt.%), Ag-Zn (2 wt.%), and Ag-Zn (4 wt.%), respectively (Rashidi et al., 2019).

The crystallinity of PLA increased by 95.6%, 107.1 %, 118.6 %t, 105.3 %, and 110.6 %, with the dispersion percentage of nano-Ag filler ranging from 0 to 15 wt %, respectively, and the crystallization temperature decreased by 2.7 °C in PLA nanocomposites with 15wt %t nano-Ag filler, but there was no significant difference in Tg with increasing nano-Ag content (Fan et al., 2019). For a different dispersion rate of silver nanoparticles in PLA, a thermal analysis was performed with a heating rate of 0.1 °C/min. The result showed that the glass transition (Tg) for the pure PLA occurred at around 60 °C and for the samples loaded with Ag nanoparticles, the glass transition (Tg) temperature proceeds at a higher temperature (Sirotkin et al., 2020).

2.3.2.2. Mechanical property

Improving the mechanical characteristics of any biopolymer is critical to producing eco-friendly materials that can withstand any type of force application. Many researchers have used metal nanoparticles to improve the characteristics of biopolymers. The influence of metal oxide nanoparticles on the mechanical properties of biopolymers is explored in the next section. Pure PLA film has a tensile strength of 4.2 MPa. Tensile strength increased to 7.12 MPa after 0.25 wt percent NiO was added to PLA, and the highest value of tensile strength was attained at 1 wt percent NiO. (Ramji et al., 2020). Polyethylene was used to distribute zinc oxide nanoparticles (lactic acid). Its influence on mechanical properties was studied, and the tensile strength decreased as the ZnO loading rate rose. PLA with 1% ZnO has the greatest PLA elongation at break and Young's modulus (Shafiee et al., 2018).

When compared to PLA-Pr, copper nanoparticle dispersed PLA films had a higher Cu content (0.082 wt percent), reducing the EB value by 14.9 %. Young's modulus has no statistically significant differences. Copper nanoparticles caused much more strain at break. (Bautista-Del-Ángel et al., 2020). PLA/PBAT composite film with TS of 14.5 ± 3.9 MPa was analyzed and the TS of PLA/PBAT films rose to 23.4 ± 3.9 and 26.9 ± 2.8 MPa when $ZnONP^{ZA}$ and $ZnONP^{ZC}$ were added respectively but increased to 16.8 ± 3.7 MPa when $ZnONP^{ZN}$ was added. The modulus of elasticity, on the other hand, (EM) (stiffness) increased considerably,

but elongation at break (EB) was significantly decreased in which the EB (flexibility) of PLA/PBAT film was 199.9 ± 32.2%. But when $ZnONP^{ZA}$, $ZnONP^{ZC}$, and $ZnONP^{ZN}$ were incorporated into PLA/PBAT film, it decreased to 118.1 ± 23.9, 121.8 ± 14.1, and 142.3 ± 26.8%, respectively (Shankar et al., 2019).

2.3.2.3.Thermal stability

Recently, using NPS to enhance the thermal resistance of polymers is becoming preferable due to the significant impact of the metal and metal oxide NPs. The following research reports address how the NPS incorporate with the polymers and how they affect the thermal stability of the polymers.

In the temperature range of 300 to 382 °C, neat PLA film lost 96% of its weight, corresponding to removing the ester group. When ZnO-NPs dispersed, the T_{onset}, T_{50}, and T_{endset} values of PLA films showed a decrement pattern (Kim et al., 2019; Bajwa et al., 2021). However, TiO_2 NPs dispersed film showed a higher decomposition temperature when compared to pristine PLA film. Still, there was no significant change with adding more concentrations of TiO_2-NPs (Li et al., 2020). Yu et al. (2021) reported that neat PLA's T_{max} was 379.01 ^{o}C but slightly increased when it was incorporated with acetylated cellulose nanocrystals. However, ternary composite film T_{max} values decreased and shifted further with a high concentration of ZnO NPs. The addition of TiO_2 to PLA provides no change in the $T_{onset,}$ but alters the T_{max}, while the Ag-NPs dispersion also decreases the thermal resistance of the film (de Azevedo Gonçalves Mota et al., 2021).

2.3.2.4. Antimicrobial Activity

Incorporating organic or inorganic active components into biopolymers is critical for improving the application of antibacterial biofilms. As reported by Swaroop et al., 2018, according to the FACS data, the addition of PEG killed around 22% of the bacterial cultures. Furthermore, following 24 hours of treatment, the addition of MgO NPs into PLA films killed around 47 % of the bacteria. The composite films' antimicrobial activity was evaluated against food-borne pathogenic bacteria, E. coli, and L. monocytogenes.

The neat PLA sheet had no antibacterial effect against either bacterium, as predicted. However, depending on the kind of bacterium and the quantity of ZnO NPs, PLA/ZnO NPs

composite films showed differential antibacterial efficacy against both E. coli and L. monocytogenes (Shankar et al., 2018). In the case of PLA-Ag, PLA-ZnO, and PLA-TiO_2 composite films. the antibacterial activity of metal nanoparticles decreased as the loading of the NPs increased yet the highest antimicrobial activity was reported for the case of PLA-Ag (Pušnik Črešnar et al.,2021).

2.3.3. Different bio-based nucleating agents and their efficiency

One of the valuable ways for improving PLA's characteristics without sacrificing its biodegradability is to blend it with other biopolymers or **bio-based nucleating agents** (Zhu et al., 2019; Getme et al., 2020).

2.3.3.1.Cellulose

Most PLA features, including mechanical and thermal properties, crystallization, barrier performance, degradability, and antibacterial capabilities, may be altered by incorporating different cellulose components, such as cellulose fibers, micro fibrillated cellulose, and nano-cellulose (Khosravi et al., 2020). Cellulose-incorporated composite films of PLA have been manufactured and the nucleating efficiency of this particular bio-based filler has been studied some of the property enhancements are reviewed as follows (Jin et al.,2020; Zhou et al.,2021).

The thermal stability of cellulosic filaments and PLA composites were researched utilizing thermogravimetry investigation (TGA) under a nitrogen environment at a stream pace of 60 mL/min at a heating rate of 10 ^{O}C/min and the examining range was from 30 ^{O}C to 400^{O}C. Because of the great substance of extractives and hemicellulose, MDF degrades significantly sooner than NBSK. Thusly, the maximum degradation temperature for the composites can be represented as PLA/PEG > PLA/NBSK/PEG > PLA/MDF/PEG. All in all the nucleating impact of both NBSK and MDF strands was not significant (Ding et al., 2016).

The residual mass of ABR, WABR, algal cellulose, and CNCs obtained after completion of the TGA cycle, was found to be 54 %, 60 %, 75 %, and 3 %, respectively. Faster degradation was observed in PLA/CNC bio-Nano composites (SI) (Mondal et al.,2021). The thermal stability of solution cast film samples of PLA with 1, 2, and 5 wt% CNC contents was studied. The specimens were heated from 30ºC to 600ºC at a heating rate of 10ºC/min under a nitrogen atmosphere. The TGA results of PLA and PLA/CNC Nano composites summarized as, T_{max},

T10, and *Td* of PLA were increased from 338 to 358.9, 324 to 332, *353 to 376* respectively as the loading of CNC increased (Khoo et L.,2016).

The crystallinity impact of modified cellulose fillers was studied using a differential scanning calorimeter (DSC) at different heating rates and the results are reviewed as follows. Rahman et al., 2014, reported that with 6% and 15% loading of cellulose composite (fibers) into PLA the Tg, Tc, and Tm of composite films were lower than neat PLA films which resulted in higher *Xc* compared to the presitn PLA film. The addition of cellulose reduces the crystallization peak on the chilling curves, and as a result, no matching melting peak on the heating curves has been discovered. Pure PLA has just around 2% crystallinity, and the addition of cellulose renders composites completely amorphous. This means that the inclusion of cellulose reduces the total crystallinity of composites (Šumigin et al.,2012). Similarly, Kamthai et al., 2015, reported that changes in T_g, T_{cc}, T_m, and T_c were used to investigate the influence of plasticizer concentration on the thermal characteristics of PLA/CMCB composite. The addition of 1 % (wt) CMCB in PLA composites resulted in greater T_g (55.8 oC) and lower T_m (148.1 oC) with cold crystallization at 120.9 oC. It suggests that CMCB functions as both a reinforcing filler that increases the stiffness of PLA composites and a nucleating agent. But as the concentration of the filler increased, all parameters started to decline.

Enhancing the mechanical property of PLA with different cellulose-based fillers has been under research for a long time. The process of enhancing the mechanical property of this particular polymer makes it more applicable, especially in packaging. When the mass fraction of microcrystalline cellulose was 2% or 5%, the tensile strength of the composite film was 21.86% and 50.98% higher than pure PLA film, and the elongation at break improved by 8.33% and 16.25% (Li et al., 2011).

Tensile strength falls with increasing micro fibrillated cellulose (MFC) levels in MFC-reinforced PLA, reducing by 25% at 30% MFC content (45 MPa) compared to plain PLA (60 MPa). When compared to plain PLA, Young's modulus of MFC-reinforced PLA increases by around 12%. When compared to clean PLA, the elongation at the break was similarly reduced (Li et al., 2021). The ultimate tensile strength, UTS (MPa), Young's modulus, E (MPa), and percentage elongation at break (percent E) for PLA films were determined to be 16.6 +1.1 MPa, 3.3 +0.6 MPa, and 81.5 +5.0%, respectively, for PLA films and tensile strength of bio-

nano composite films was shown to decrease as the filler (bacterial cellulose) loading increased. The insertion of 30 wt %t filler resulted in a 42 % drop in UTS (Patwa et al.,2019).

2.3.3.2. Starch

Unique features of starch play a great role in selecting this particular polymer as a filler for the PLA matrix (Nazrin et al., 2020; Yu et al., 2020). Many researchers engaged in bringing PLA polymer into the manufacturing sector by solving the drawbacks of PLA using starch and selected scientific findings are reviewed as follows. TGA investigated the effect of biodegradation on the thermal stability of PLA and starch/PLA composites. When the T_{onset}t (5 % weight loss) and T_{max} (temperature with maximum degradation rate) of nondegraded PLA and starch/PLA composite degradation curves were compared, the Tonset (5 % weight loss) and T_{max} (temperature with maximum degradation rate) of the starch/PLA composite were lower, indicating that the thermal stability was reduced with the addition of starch (Lv et al., 2018). The weight loss for samples P8C (A), P6C2S (B), P4C4S (C), P2C6S (D), and P8S(E) began at 254 °C, 253 °C, 278 °C, 249 °C, and 247 °C, with maximal weight loss at 345 °C, 385 °C, 379 °C, 379 °C, and 385 °C.

The onset temperature reduces as starch content increases (Surya et al., 2020). Without perfect miscibility of components, the S-PLA blends at both ratios, with and without compatibilizers, exhibit three degradation stages of varying intensities. The first phase, between 125 and 205 °C, corresponds to the degradation of low molecular weight components, such as plasticizers (glycerol); the main second phase, between 225 and 325 °C, is attributable to the overlapped degradation of starch and PLA because both polymers have similar degradation temperatures; and the third phase, above 330 °C (in samples with compatibilizers), would primarily correspond to the degradation of the grafted PCL with higher degradation (Collazo-Bigliardi et al., 2019).

The crystallinity impact of modified starch fillers was studied using a differential scanning calorimeter (DSC) at different heating rates and the results are reviewed as follows; composite film of PLA/TPS was prepared by melt blending and crystallinity study were performed which resulted in Tg, Tcc, Tm and Xc of PLA/TPS 59.7 °C, 110.0 °C, 148.6 °C and 28.3% before

soil burial and 55.6 °C, 106.8 °C, 141.7 °C, and 46.5% were recorded after soil burial for Tg, Tcc, T_m and Xc of PLA/TPS respectively (Palai et al., 2021).

Yu et al., 2020, reported that the thermal behavior of PLA/thermoplastic acetylated starch (TPAS) composite film was studied and resulted in a glass transition temperature of roughly pure PLA was about 60 °C. The glass transition of PLA lowers as the TPAS level increases. When the TPAS concentration exceeds 70% by weight, the glassy condition almost completely vanishes. This demonstrates that TPAS and PLA are incompatible. The composites containing TPAS exhibited considerable cold crystallization near 103 °C, but pure PLA did not exhibit cold crystallization at this temperature. This demonstrates that adding TPAS lowers the cold crystallization temperature of PLA.

For a long time, scholars have been studying how to improve the mechanical properties of PLA by using various starch-based fillers. The process of improving this polymer's mechanical properties makes it more useful, particularly in packaging. Rogovina t al., 2018, presented that the addition of starch to PLA led to a rise in elastic modulus *E*, a decrease in ultimate tensile strength σ_b, and elongation at break ϵ_b. Further increase in the starch content did not almost affect the mechanical characteristics. Because of low interfacial adhesion, mixing starch grains with PLA significantly reduces mechanical characteristics (Wu et al.,2015). Tensile and flexural strengths of the starch/PLA composite reduced substantially from 48.9 MPa to 2.4 MPa and 70.2 MPa–5.3 MPa, respectively which explains the fact that the samples can degrade faster with the presence of starch (Lv et al., 2018).

2.3.3.3. Protein

Utilizing protein as filler in enhancing the physicochemical property of poly (lactic acid) is not researched as it was supposed to be researched yet some scholars have been engaged in this pattern of work. These scientific findings are discussed as follows. Thermal properties of keratin/chitosan/PLA composite films were investigated and resulted in a neat PLA with glass transition, cold crystallization, melting temperature, and enthalpy of fusion at 59.4 °C,127.8 °C,152.97 °C, and 13.62 J/mol respectively.

The presence of keratin in the PLA chitosan system decreased Tg to 58.9 °C, while crystallinity increased to 19.17% (Tanase et al., 2014). Nilsuwan et al.,2020, reported that

bilayer films of fish gelatin (FG) and poly(lactic acid) (PLA) with varied FG/PLA layer thickness ratios (9:1, 8:2, 7:3, 6:4, and 5:5) were prepared using casting. Bilayer films were found to have lower tensile strength (TS) but greater elongation at break (EAB) than PLA films.

By understanding the lack of research works on protein fillers this research is aimed to bring the elastin/collagen matrix as a filler (nucleating agent) to enhance important features of poly (lactic acid). General explanation and application of elastin/collagen matrix are discussed.

2.4. Elastin-Collagen matrix

The extracellular matrix of many tissues, such as the urine bladder, heart valves, blood vessels, skin, neurons, skeletal muscle, ligaments, tendons, and so on, is generally harvested to acquire materials made of both proteins, collagen, and elastin. These materials may include, in addition to collagen and elastin, another ECM component, such as glycosaminoglycan, organized in a three-dimensional structure.

2.4.1. Application of Elastin- Collagen matrix

A few scaffolds obtained in such a way are commercially available, however, we have to remember that these animal-derived materials may be the cause of undesirable host responses (Schenke-Layland et al., 2003). Some research groups work also on collagen/elastin mixtures. The scaffolds are created by blending both protein solutions' inappropriate weight ratios and then lyophilized or proceed by electro spinning method (Heydarkhan-Hagvall et al.,2008).

2.5. Silver-Zinc Oxide Nano composites

Silver-zinc oxide Nano composites can be found in the form of doping, electrostatic interaction, grain size interaction so many different forms of interactions. They possess synergetic characteristics of silver and zinc oxide nanoparticles for this reason these Nano composites are more essential and applicable than single nanoparticles. In the following section, the methods of synthesis and applications of these Nano composites are discussed.

2.5.1. Synthesis of Ag-ZnO Nano composite

The size, shape, and characteristics of Ag-ZnO Nano composite are governed by the processes during the synthesis process. Many researchers have been engaged to synthesize Ag-ZnO

Nano composites using different synthesis methods. Among these synthesis techniques, some of them have been reviewed in the following section. The biological (green method) from different plant extracts like *Verbascum speciosum* (Mousavi-Kouhi et al.,2021), *Bidens Pilosa* (Kyomuhimbo et al.,2019), instrumental assisted synthesis like pulse mode ultra sonication assisted (Siva Vijayakumar et al.,2013), microwave-assisted (Phuruangrat et al.,2019), chemical methods like Sol-gel method (Rajendran et al., 2020; Rao et al.,2021), co-precipitation methods (Subhan et al., 2014; Ahmed et al.,2020; Stanley et al.,2021) and hydrothermal (Chai et al., 2014; Albadarin et al.,2021; Farbod et al.,2021).

2.5.2. Applications of Ag-ZnO nanocomposites

Due to the synergetic characteristics of Ag and ZnO nanoparticles possessed by these Nanocomposites, they have been utilized in so many application areas and some of the applications have been reviewed as follows.

Table 2.1: Applications of Ag/ZnO NCs

Name of the product	Applications	References
Screen-printed electrodes modified with multiwalled-carbon-nanotubes functionalized with silver-doped zinc oxide	Electrochemical biosensor for bisphenol	(Kunene et al., 2020)
Ag/ZnO/rGO nanocomposites	Antimicrobial activity	(Hsueh et al.,2019)
Silver-zinc oxide polyamide thin film composite membrane	Antifouling and Rejection	(Kotlhao et al.,2019)
Silver-nanoparticle (AgNPs)-decorated on polyaniline (Pani)-wrapped zinc oxide membrane	Phenol removal and hydrogen production from water	(Jilani et al., 2022)
Silver doped Zinc oxide nanowires	photocatalytic degradation for energy and environmental application	(Nagasundari et al., 2021)

2.6.Biofilms preparation methods

The commonly available biopolymers, such as starch, cellulose, proteins poly-lactic acid, and polybutylene adipate-co-terephthalate, have widely been focused on preparing biofilms typically utilized in food packaging, tissue engineering, and medical applications (Moura et al., 2015; Zhang et al., 2020). Bio-based film preparation techniques and methods are unique and different based upon the type of polymers, application areas and properties of the polymers, and the filler (Sharif et al., 2019).

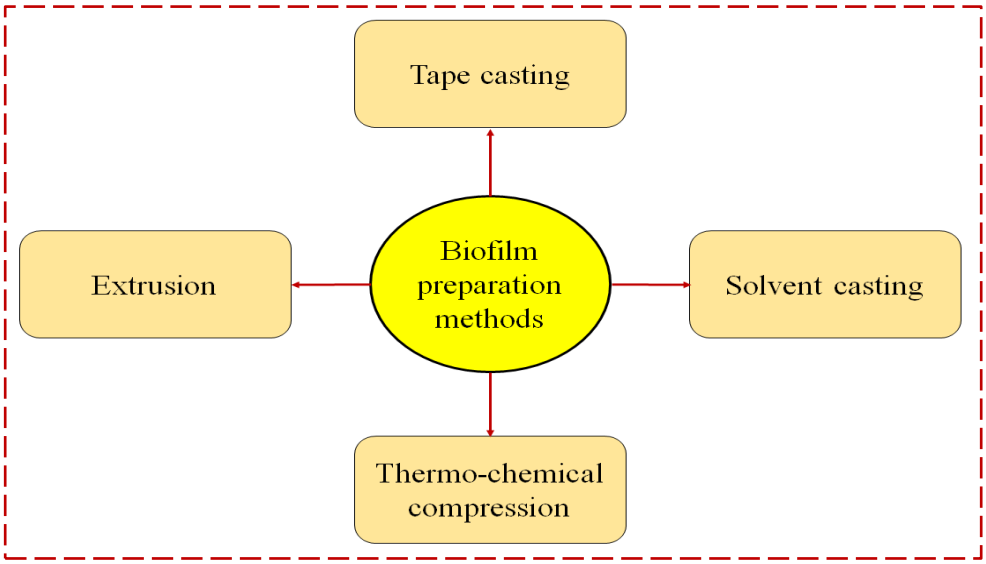

Figure 2.2: Common and basic film preparation methods

Tape-casting involves spreading the suspension using a doctor blade and shear force, whereas extrusion results in pellets, and thin films that have controlled thickness in addition to that. In point of the solvent casting method, it enables the production of films with a minimum cost yet uncontrolled film thickness. On the other hand, the synergetic effect of thermal and mechanical forces is involved in preparing films using the thermo-mechanical compression method. Solvent-supported film preparation was used to develop nano-magnesium oxide reinforced poly (lactic acid) films with the greatest improvement in tensile strength and oxygen barrier characteristics. A bird-type manual film applicator was employed for chloroform evaporation to generate consistent thickness films. (Swaroop et al., 2018). PLA films were formed using different biopolymers and plasticizer via extrusion at 11 different temperature zones which then pelletized at150 ^{o}C, 50 rpm and 150 bar (Mallegni et al., 2018).

Table 2.2: Advantage and Disavantage of film preparation methods

Film Preparation method	Advantages	Disadvantages	Reference
Tape casting	✓ Possibility of preparation of films with large dimensions ✓ Short drying time ✓ Film thickness controlling ability	✓ Energy-intensive ✓ High operating cost	✓ (Augusto et al., 2015 Laurindo et al., 2015 Ferrández-Montero et al., 2019)
Solvent/Solution Casting	✓ It can be easily performed ✓ Protects denaturation	✓ Long drying time ✓ Lack of film thickness control	✓ (Al-Ajlouni et al., 2021, Yu et al., 2019; Atta et al., 2021)
Extrusion	✓ Production of films with large film thickness ✓ films with flexibility, high tensile strength	✓ Energy-intensive ✓ Films with low water permeabilty	✓ (C. Zhang et al., 2022; wang et al., 2018; Mallegni et al., 2018)
Compression	✓ Less-time-consuming ✓ Its simplicity	✓ protein denaturation occurs	✓ (Rouf et al., 2018; C. Li et al., 2021)

Generally, this literature review can be summerised as different methods, investigations and materials were conducted and applied in order to bring a change in poly(lactic acid) properties.The changes might be positive or negative but still not many scholars have tried the effects of modified elastin-collagen matrix and also the synergetic effect of modified elastin-collagen matrix and Ag/ZnO nancomposite on the poly (lactic acid) properties therefore, a novel methodology have been conducted throught the reseach work time. In the next chapters the novel methodologies, extraceted materials and their effects was illustrated briefly.

CHAPTER THREE

3. MATERIALS AND METHODS

3.1. Chapter Overview

This chapter aims to present the materials used, sample preparation methods, and proper characterization techniques followed for various experiments that were performed in this research work. For simplicity, the utilized materials, experimental protocols, and characterization techniques were categorized into three sections. The first section describes the extraction and modification of elastin/collagen matrix from broiler skin; The second section describes the synthesis protocol techniques for Ag, ZnO and Ag/ZnO Nanocomposite; The third section describes the development of PLA/Ag-ZnO/m-ELN-COLL composite films. The fouth section describes characterization techniques for the extracted and modified elastin-collagen matrix, synthesized nanomaterials and as prepared binary and terinary composite films.

Materials and Reagents

The materials and reagents which were utilized in the research are listed as follows:

Table 3.1:The equipment, materials, and chemicals used for the thesis

Procedures	Chemicals	Equipment/Materials
Extraction of ELN/COL matrix	NaCl, Acetone, NaOH, and Distilled water.	Broiler Skin, Beaker, Cutter, Measuring cylinder, Water bath, balance, Separatory funnel, and Glove.
Synthesis of Ag, ZnO, and Ag/ZnO Nano Composite	zinc nitrate, silver nitrate, sodium borohydride, Oxalic Acid, and Distilled water	Beaker, Balance, Heating mantle with a magnetic stirrer, Thermometer, Oven, Centrifuge, and Furnace
Development of PLA/Ag-ZnO/ ELL-COLL composite films	Poly (lactic acid), Chloroform, ELL-COLL matrix, Lactic acid	Beaker, Balance, Magnetic stirrer, Sonicator, Petri dish, Spatula

3.2. Methods

3.2.1. Extraction of ELL-COLL matrix

Broiler's skin was cut into small pieces and homogenized in a 10 %vol of 1 M NaCl. After 24 h the treated broiler skin was washed with distilled water (DW) and defatted using 30 %vol acetone for 1 h. The dry skin was suspended in 30 %vol of 0.1 N NaOH and heated for 15 min in a boiling water bath with constant shaking. After cooling for 24 h, the residue was extracted again for 45min in 0.1 N NaOH at 100 °C. NaOH soluble and insoluble material was washed several times using DW from the separatory funnel and dried in an oven at 80 °C (Nadalian et al.,2013).

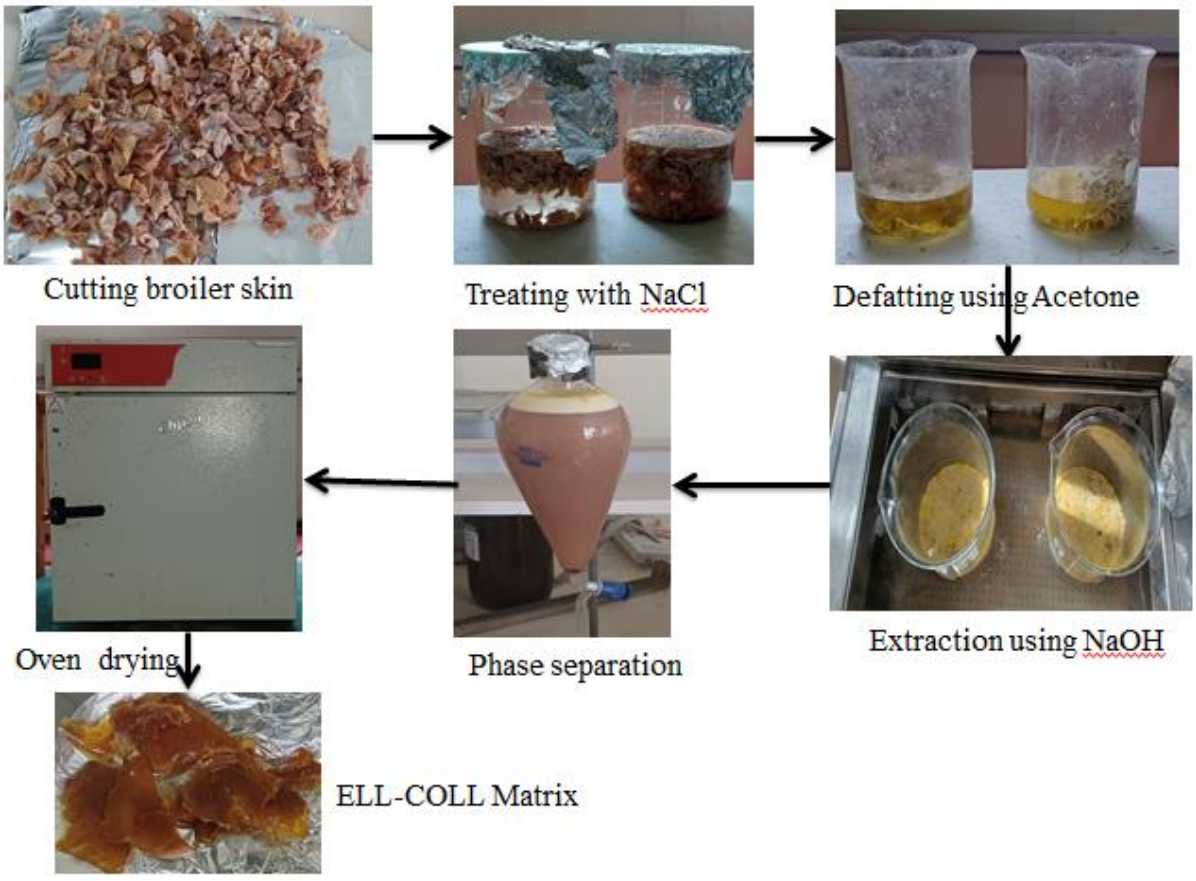

Figure 3.1: Extraction of ELL-COLL matrix

3.2.2. Modification of ELL-COLL matrix by Grafting

To form the composite films with PLA and due to the incompatibility between ELL-COLL matrix and PLA polymer the ELL-COLL matrix needed to be modified using lactic acid. This modification was done through a modification technique so called grafting and also one parameter at a time method was conducted to investigate the parametres effect on the grafting effciency. For that purpose, 10, 20, and 30 g. of ELL-COLL matrix was dissolved in 100 ml of lactic acid with an ultra sonication-assisted process. After sonication, the dissolved protein matrix was grafted at 120, 150, 180 ^{0}C for 1, 3, 5 and 7 h. The grafting efficiency (GE%) was calculated according to the following equation. In order to calculate the grafting effecincy filteration using filter paper was done to separate the grafted ELL-COLL from the ungrafted one.

$$\boldsymbol{Grafting\ efficinecy\ (GE\%) = \frac{W1}{W2} * 100}\text{.....equation 3.1}$$

where W_1 is the weight of grafted matrix (i.e., the weight of the product after extraction) and W_2 is the weight of the ungrafted matrix.

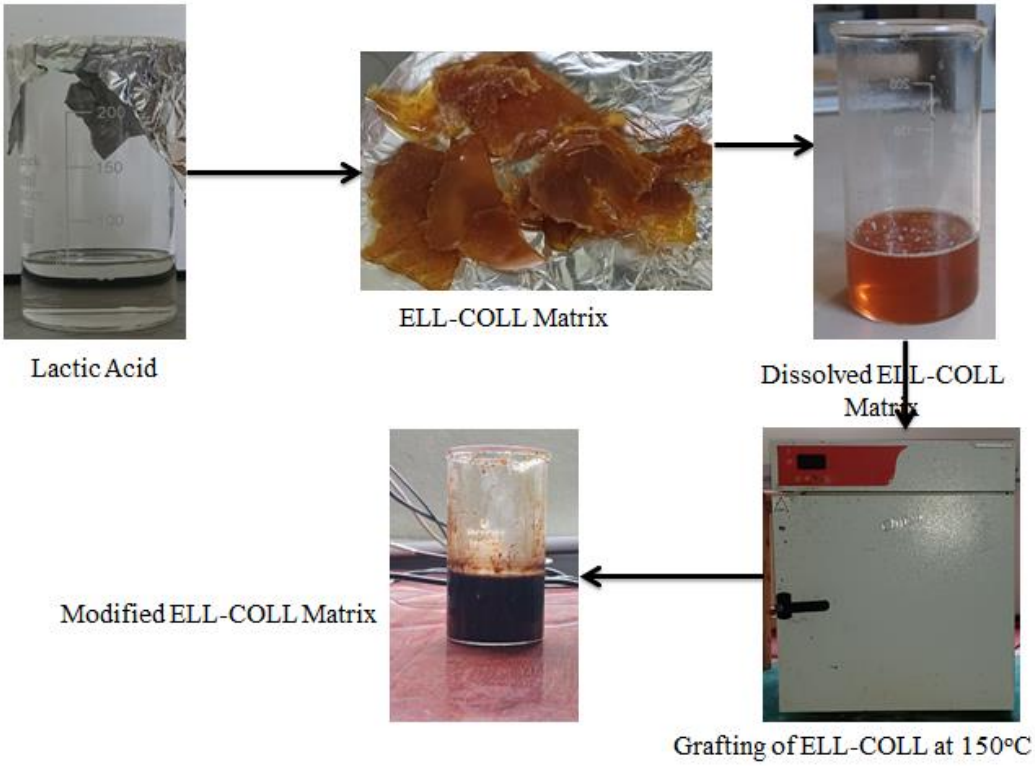

Figure 3.2: Modification of ELLA-COLL by lactic acid

3.2.3. Synthesis of Ag nanoparticles

Synthesis of Ag NPs was succesfuly performed as follows: by using silver nitrate salt and sodium borohydride as reducing agent. 5 mM of silver nitrate solution was prepared in 200 ml of DW and 0.5 M of sodium borohydride solution was prepared in 20 ml of Dw . Next to that both solutions was sonicated to facilitate dissolution. After this, the sonicated $NaBH_4$ was added drop-wise into 5 mM of silver nitrate solution at a constant stirring and addition of $NaBH_4$ was continued until no reduction reaction can be detected i.e, there were no color changes, here the addition of $NaBH_4$ was stopped and the mixture was left to be stirred for additional 30 min and additional 30 min for settling . Finally, the sample was centrifuged and dried in the oven at 100 ^{o}C for 3 h (Nguyen et al., 2019).

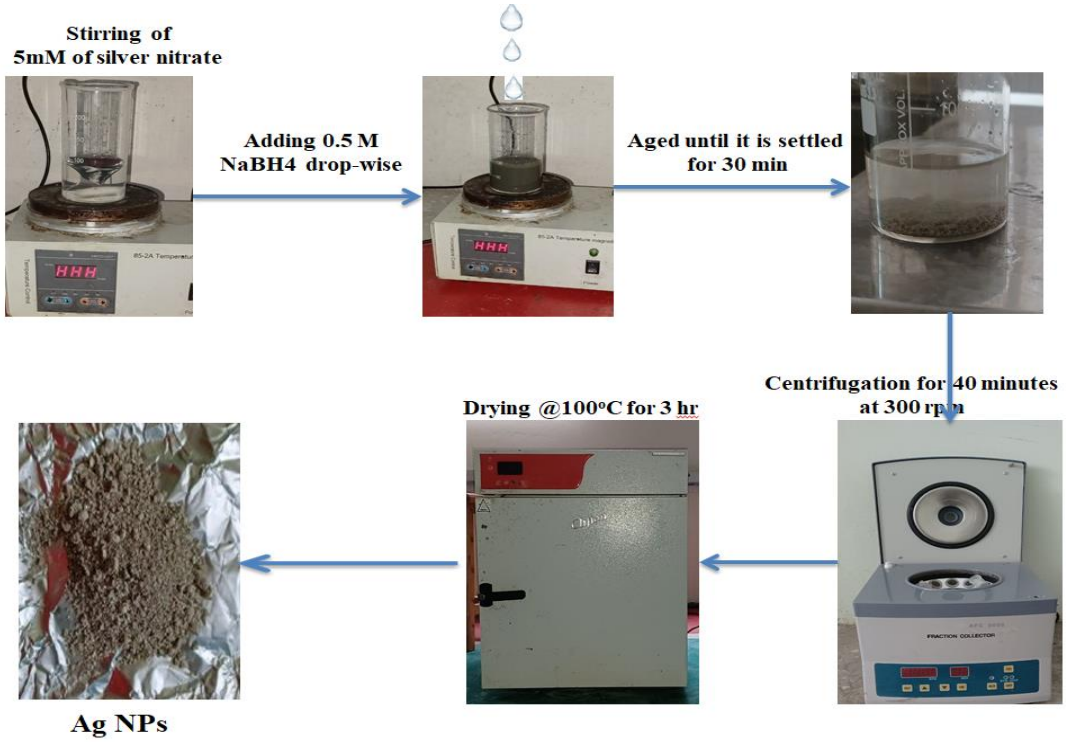

Figure 3.3: Synthesis of Ag Nanoparticles

3.2.4. Synthesis of ZnO Nanoparticle

Synthesis of ZnO NPs was succesfuly performed by following the method explained below, here zinc nitrate salt and oxalic acid as reducing agent was utilized. 0.4 M of zinc nitrate solution was prepared in 100 ml of DW and 0.6 M of oxalic acid solution was prepared in 100

ml of DW and then both solutions were heated separately until boiling point. Once the boiling point reached 0.4 M of zinc nitrate was added to 0.6 M of oxalic acid and the mixture was stirred at 300 rpm until the temperature reaches room temperature, then the mixture was left to be precipitated in open-air for 24 h. Decanting the precipitate was followed by drying the precipitated component at 100 °C for 3hrs, then the dried component was calcinated at 600 °C for 12 h. (Lucilha et al.,2016).

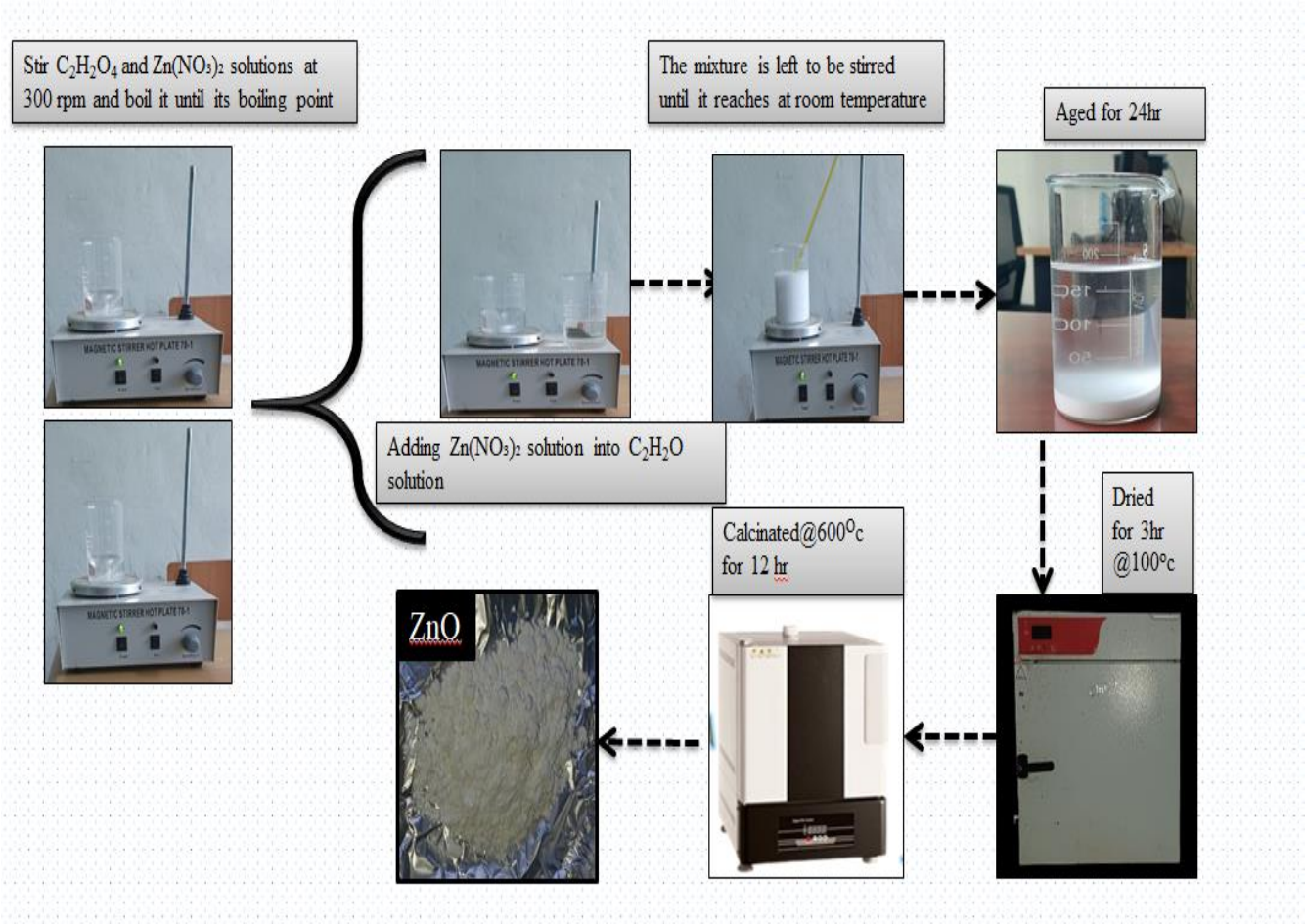

Figure 3.4. Synthesis of ZnO Nanoparticles

3.2.5. Synthesis of Ag/ZnO Nano-composite

In order to synthesise the silver-zinc oxide nanocomoposite silver nitrate and zinc nitrate salts were used, during the reaction oxalic acid served as reducing agent for both solutions. Solution of zinc nitrate and silver nitrate with 0.4 M were prepared in 50 ml of DW and solution of oxalic acid with 0.6 M was prepared in 100 ml of DW. Both 0.4 M of zinc nitrate and 0.4 M

of silver nitrate were mixed and heated until the boiling point, then the same manner was followed for oxalic acid and a mixture of 0.4 M of zinc nitrate and 0.4 M of silver nitrate solution was added to 0.6 M of oxalic acid and the mixture was stirred at 300 rpm until the room temperature reached, then it was left to be precipitated in an open-air for 24 h. Decanting the precipitate was followed by drying the precipitated component at 100 °C for 3h, then the dried component was calcinated at 400 °C for 12 h (Lucilha et al.,2016).

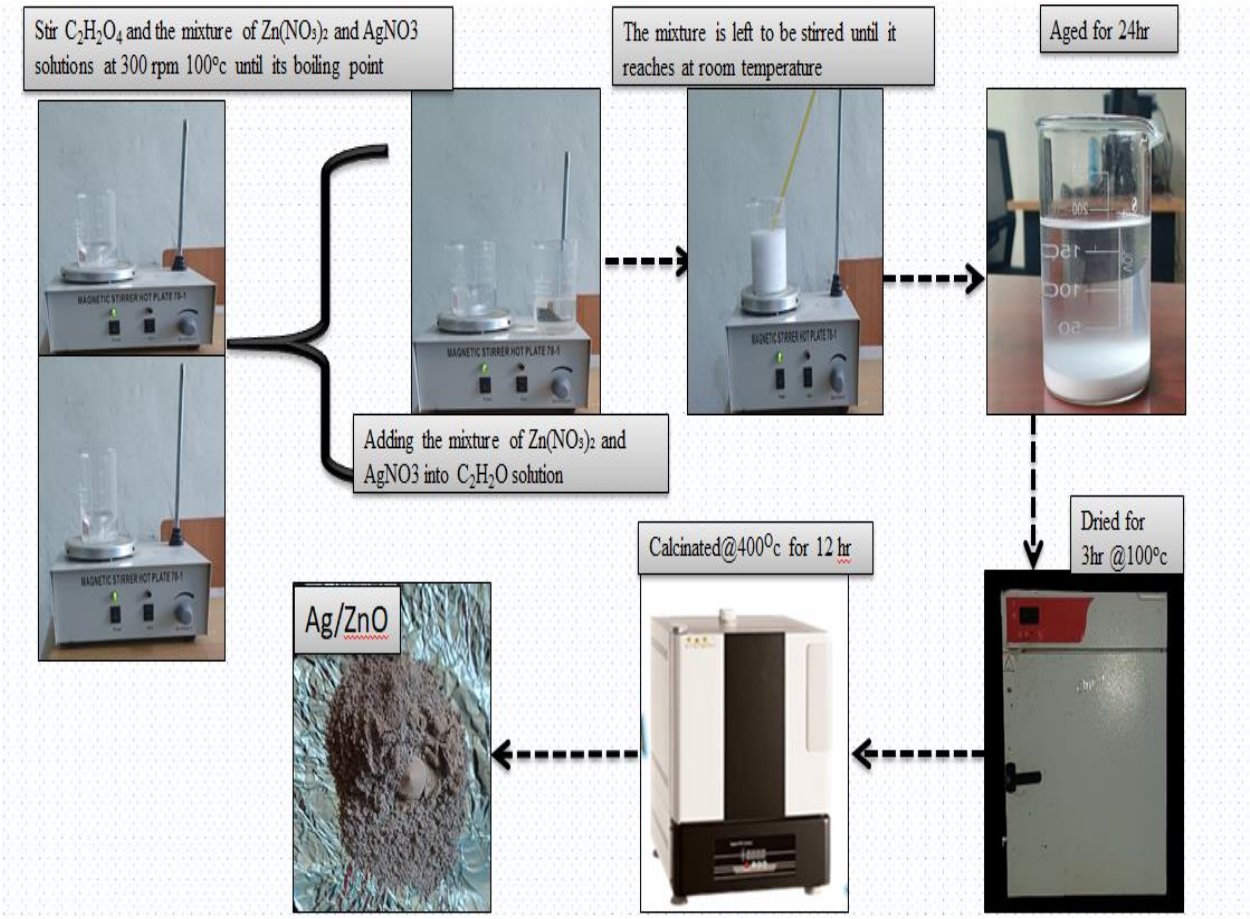

Figure 3.5: Synthesis of Ag/ZnO Nanocomposite

3.2.6. Development of poly (lactic acid)/ m-ELL-COLL matrix film and poly (lactic acid)/ Ag/ZnO dispersed m-ELL-COLL matrix composite film

A. PLA/m-ELL-COLL matrix composite film was prepared using solution casting method with different loading of m-ELL-COLL matrix (1, 3, 5, 10, 20 wt.%.), the weight percentages of m-ELL-COLL matrix was based up on the mass of PLA grains. Before

the addition of m-ELL-COLL matrix, 3 gm of PLA grain was dissolved in 70 ml and stirred for 1 h. While the PLA grains being dissolved, different weight percentage of m-ELL-COLL matrix was dissolved in 20 ml of chloroform. Since m-ELL-COLL was not fully dissolved in the chloroform filtration of ungrafted ELL-COLL matrix was performed. This mixture (PLA/ m-ELLA-COLL matrix) was stirred for additional 2 h at room temperature and then was casted on a Petri dish to obtain pre-films. After being casted the solution was left to be slowly dryed for 48 h, then prepared films were stored in a desiccator.

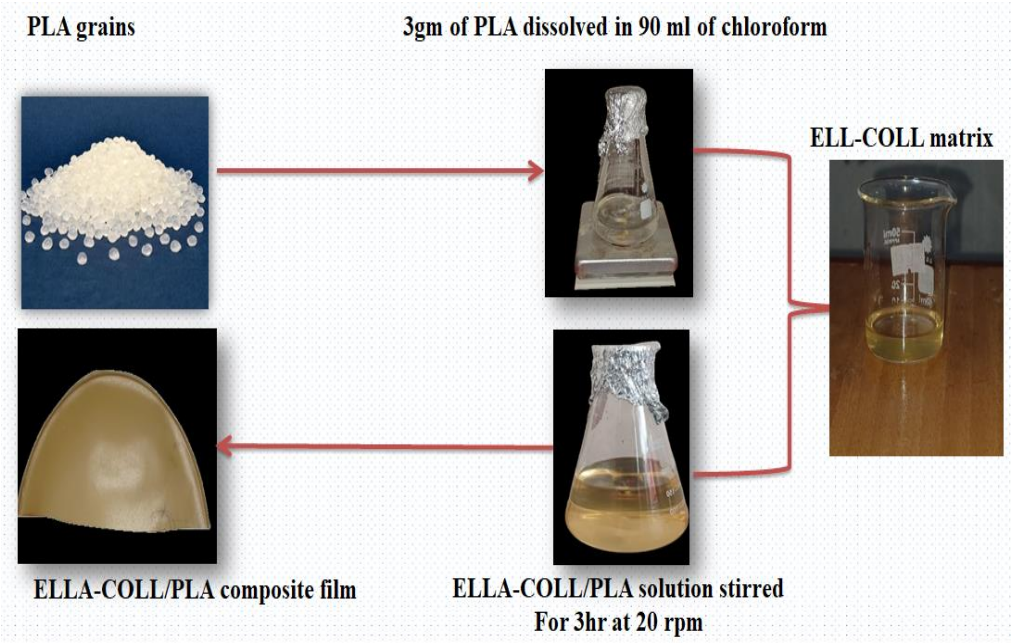

Figure 3.6: Preparation of m-ELL-COLL/PLA composite film

B. PLA-Ag/ZnO-m-ELL-COLL matrix composite film was prepared using solution casting method with different loading of Ag/ZnO NCs (1%, 3%, 5%, 10%, wt.%) based on the mass of PLA grains. Before the addition of m-ELL-COLL matrix, 3 gm of PLA grain was dissolved in 70 ml of chloroform and was stirred for 1 h. While the PLA grains being dissolved different samples of m-ELL-COLL matrix with 10% weight percentage was dissolved in 20 ml of chloroform which was followed by filtration. The filterd solution of m-ELL-COLL served as carrier to incorporate the Ag/ZnO NCs with PLA solution.This mixture (PLA-Ag/ZnO-m-ELL-COLL matrix) was stirred for additional of 2 h at room temperature and then was casted on a Petri

dish to obtain pre-films. After being casted the solution was left to be slowly dryed for 48 h then prepared films were stored in a desiccator.

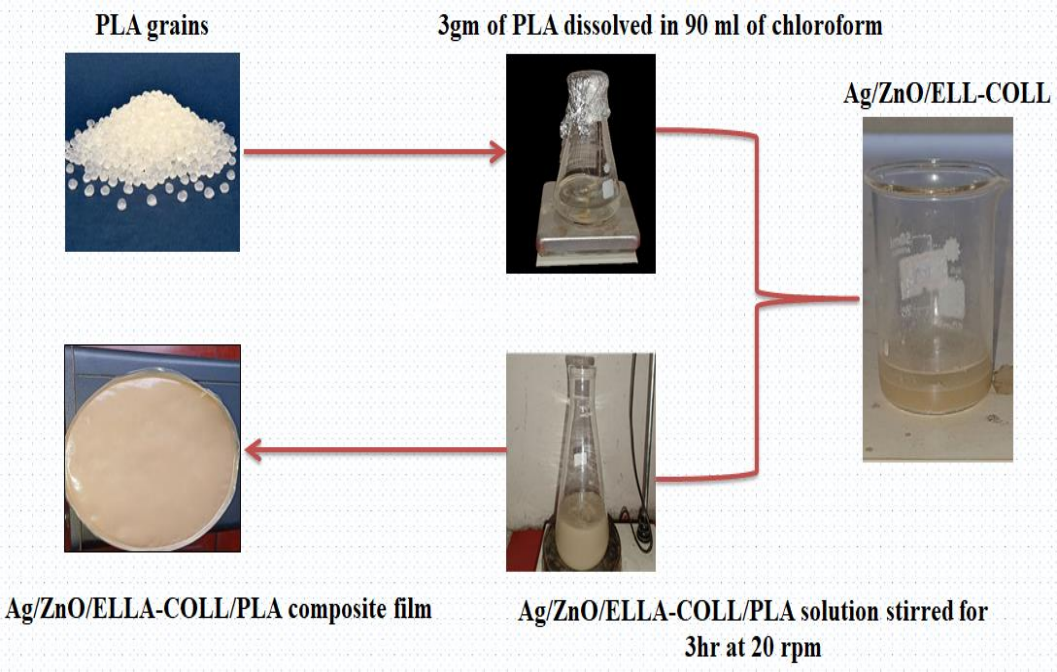

Figure 3.7: Preparation of Ag/ZnO/m-ELL-COLL/PLA composite film

3.3. Characterization of extracted ELL-COLL and m-ELL-COLL matrix

3.3.1. Functional Group Analysis (FTIR) of extracted and modified elastin collagen matrix

The extracted ELL-COLL and m-ELL-COLL matrix was monitored using Fourier transferred infrared radiation (FTIR with Model name FTIR-6600 type A and Serial number A013861790 to know the functional group. And this FTIR was attenuated with total reflectance (ATR) mode in the range of 4000 to 400 cm^{-1} with 4 cm^{-1} resolution and 64 scan rates.

3.4. Characterization of NPs(Ag, ZnO) and Ag/ZnO Nanocomposite

3.4.1. Crystallographic structural analysis

The powder X-ray diffraction (XRD) patterns of the Ag, ZnO, and Ag-ZnO nanomaterial were recorded by a SHIZMADZU XRD-7000 at a scanning rate of 3 °/min for 2Θ ranging from 10°

to 80°. The relation between the distance between two planes (D-spacing) *(d)* and the angle of diffraction (2θ) was calculated by Bragg's equation (equation 3.2).

Bragg's equation

$$2dsin\,\theta = n\lambda \dots\dots\dots\dots\dots\dots\dots\dots\dots\dots\dots\dots\dots\dots\dots\dots\dots\dots\dots\dots\dots\dots\dots\dots\dots\dots\dots\dots.\, equ.(3.2)$$

$$d = \frac{n\lambda}{2sin\theta} \dots\dots\dots\dots\dots\dots\dots\dots\dots\dots\dots\dots\dots\dots\dots\dots\dots\dots\dots\dots\dots\dots\dots\dots\dots\dots\dots\dots\dots\dots\dots\, equ.(3.3)$$

Where: d= Spacing, n= order of diffraction, λ= wave length of incident X-ray (0.15406 nm), n= order of diffraction (1) and θ= diffraction angle

Scherrer equation

The average crystalline or grain size of nanoparticle were calculated using scherrer equation (3.4)

$$D = \frac{K\lambda}{\beta cos\theta} \dots\dots\dots\dots\dots\dots\dots\dots\dots\dots\dots\dots\dots\dots\dots\dots\dots\dots\dots\dots\dots\dots\dots\dots\dots\dots\dots\dots\dots..\, equ.(3.4)$$

Where, D= Crystallite size, K= shape factor (Scherrer constant) (0.9), λ= wave length of X-ray (0.15406 nm), β= Full width half maxima (FWHM), θ= diffraction angle

3.4.2. Functional groups analysis (FTIR) of Ag, ZnO, and Ag/ZnO Nano composite

The chemical structures of the Ag, ZnO, and Ag/ZnO Nano composite were analyzed using FTIR (FTIR with Model name FTIR-6600 type A and Serial number A013861790) this FTIR attenuated with total reflectance (ATR) mode in the range of 4000 to 500 cm -1 with 4 cm-1 resolution and 64 scan rates.

3.4.3. Ultraviolet-visible Spectroscopy

The synthesized Ag, ZnO, and Ag/ZnO Nano composites were analyzed using VASCO UV-VIS Spectrophotometer (UV-770). The UV-VIS absorbance and reflectance spectra of the samples were recorded in the range of 200-800 nm using VASCO's UV-770, UV-VIS Spectrophotometer.

3.4.4. Particle size analysis by PSDA

The zeta-sizer nano series performs measurements using a process called dynamic light scattering (DLS). Particle size distribution analyzer (PSDA) was determined from the distribution of the scattered light energy using the rigorous Mie light scattering theory. Zetasizer Nano instrument (Nano ZS (Red badge)) with a model number of ZEN 3600 (Malvern Instrument Ltd, UK). Zetasizer Nano range options for particle size measurements size range with maximum diameter 0.3 nm to 10 µm.

3.5.Characterization of poly (lactic acid)/Elastin collagen matrix blend (film) and poly (lactic acid)/ Ag/ZnO dispersed protein matrix blend (film)

3.5.1. Thermal analysis

3.5.1.1. Differential scanning calorimeter (DSC)

Thermal and crystallization behavior of poly (lactic acid)/m-ELL-COLL matrix blend (film) and poly (lactic acid)/ Ag/ZnO dispersed m-ELL-COLL matrix blend (film) was analyzed using a differential scanning calorimeter (DSC). Samples weighing ~8.1 mg was sealed in a crucible and scanned for a cycle of heat/cool at a rate of 10 ºC/min for the temperature range of 26 to 200 ºC performed under a nitrogen atmosphere. Isothermal conditions were maintained at 200 ºC for 3 min to erase the thermal history after the first heating cycle. Data from the second heating cycle was considered for further analysis. Glass transition temperature (T_g), melting temperature (T_m), degree of crystallization (*Xc*), and heat of fusion (H_m) was estimated.

$$Xc\ (\%) = {}^{Hf}\big/_{Hf^0} * 100 \ldots\ldots\ldots\ldots\ldots \text{equation 3.5}$$

Hf- Heat of fusion of the composite films
Hf^O- Standard heat of fusionof PLA

3.5.1.2.Thermogravimetric analysis (TGA)

Thermal analysis of poly (lactic acid)/ Ag/ZnO dispersed m-ELL-COLL matrix blend (film) was carried out on TGA equipment. Samples weighing 8-10 mg was heated from 30°C to 800 °C at the heating rates of 10 °C/min under a nitrogen (N_2) atmosphere.

3.5.2. Mechanical properties analysis

Before preparing the sample for the test, poly (lactic acid)/ m-ELL-COLL matrix blend (film) was conditioned overnight, under a conditioning oven at 20 °C and 65.78% humidity. After this step sample was prepared in 100 cm in length by 13cm in width using a ruler, pen (marker), and scissors. This test was performed By the Ethiopian Conformity Assessment Enterprise, following the ASTM D638 tensile strength measuring procedure using universal tensile strength testing machine. The force at break, young modulus, and tensile strength were done simultaneously.

3.5.3. Antibacterial activity

As we have been working on before *in vitro* antibacterial susceptibility test for the prepared film was determined by the disc diffusion method (Iconaru et al., 2014). The agar medium was prepared by dissolving 38 g of Mueller Hinton agar medium (MHA) in 1000 mL of distilled water autoclaved at 121 °C for 15 min. The autoclaved medium was poured into sterile plates (20-25 mL/plate) and the plates were allowed to solidify under the sterile condition at room temperature. After solidification, the plates were seeded with overnight grown culture approximately 1.5 X 108 CFU/mL by swabbing evenly onto the surface of the medium with a sterile cotton swab. According to the methods described by CLSI with slight modification the neat PLA, PLA- m-ELL-COLL matrix 10Wt% , PLA- m-ELL-COLL-Ag/ZnO-1Wt%, PLA- m-ELL-COLL-Ag/ZnO-5Wt%, PLA-m-ELL-COLL-Ag/ZnO-10Wt% , PLA- m-ELL-COLL-Ag-10 Wt% and PLA-m-ELL-COLL-ZnO-10Wt% films were cut in the diameter of approximately 6 mm (as discs) using puncher. The 6mm FS biofilm was placed and positioned on the surface of the medium with sterile forceps. gently pressed down to ensure contact with the MHA. Ampicillin was used as standard antibiotics and then plates were inverted and then incubated at 37 ℃ for 24 hrs. After incubation, the inhibition of the zones of growth inhibition around each of the antibiotic disks against *E.coli* , *S.pyogen, P. aeruginosa* and *S.aureus* were measured to the nearest millimeter.

CHAPTER FOUR

4. RESULTS AND DISCUSSIONS

4.1. Functional groups analysis of ELL-COLL matrix

Through FTIR, the chemical bond of the materials as-prepared was examined. The FT-IR spectra of the examined protein revealed N-H stretching at a wavelength of about 3440 cm^{-1}. The isolated elastin and collagen matrix contains amide I, amide II, and amide III groups, according to the functional groups examined by FTIR (Figure 4.1). These functional groups are each represented by a peak at 1632 cm^{-1} where this specific peak is a good representative of the β sheet structure elastin matrix (Baird et al., 2020) and Amide II has shown characteristic absorption bands at 1461 cm^{-1} this finding aligned with other research work (Bazrafshan et al.,2019). The characteristic peaks of the amide III band appeared at 1279 which is attributed to C-N stretching of the ELL-COLL matrix this phenomenon was supported by Ding et al., 2021 and also the proline side chain's CH_3 wagging vibration, which frequently occurs for both collagen and elastin and α- helix of collagen was indicated by the peak measured at 1383 cm-1 and 978 cm^{-1} (Sanden et al.,2011).

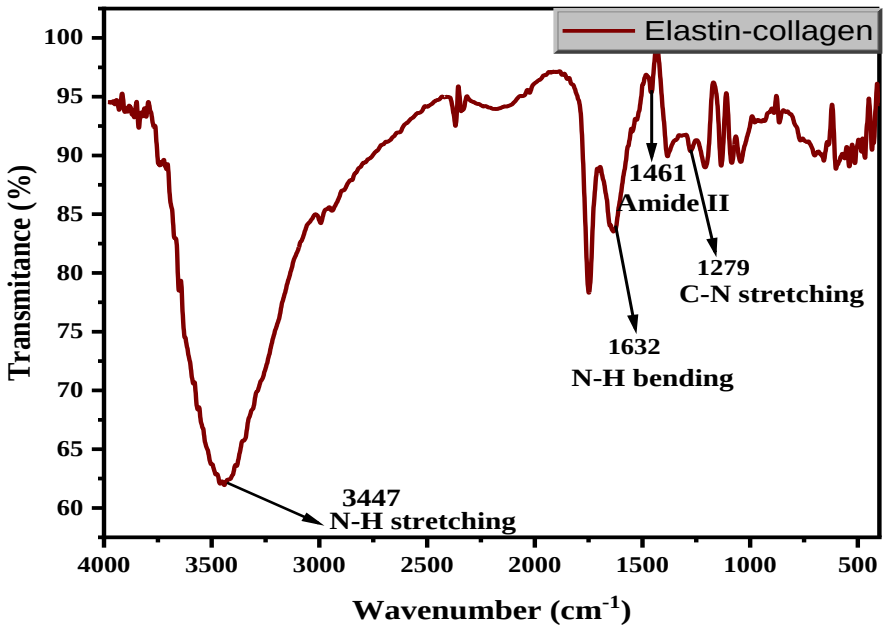

Figure 4.1: FTIR spectra of ELL-COLL matrix

4.2.Grafting Efficiency of ELL-COLL matrix

In this research the ELL-COLL matrix was utilized as a carrier (dispersant) for NPs and NCs dispersion into PLA polymer and also as a composite film forming polymer.in the preliminary investigation the dispersion of ELL-COLL matrix was not good, so that o address these issues, it was crucial to modify the ELL-COLL matrix.the grafting was done using lactic acid and one-variable-at-a-time strategy, which is a way of designing experiments including the testing of factors, or causes, one at a time instead of several factors concurrently, was used to examine the grafting effectiveness of the ELL-COLL matrix on the lactic acid monomer. Three separate parameters, including reaction time, temperature, and mixing ratio, were used in this analysis of the efficacy of grafting. A consistent volume of lactic acid was used to dissolve various amounts of the ELL-COLL matrix, which was then grafted at different temperatures and reaction times. All the parameters and their several grafting efficiencies were shown in Table 4.1.

Table 4.1: Grafting efficiency of ELL-COLL matrix using oligomerized lactic acid (OLAC)

Sample	***Time(hr)***	***Temperature(^{o}C)***	***Mixing ratio(gm/100ml)***	***Grafting efficiency (%)***
ELL-COLL/OLAC	1	150	20	50
ELL-COLL/OLAC	3	150	20	52
ELL-COLL/OLAC	5	150	20	**72.8**
ELL-COLL/OLAC	7	150	20	58
ELL-COLL/OLAC	5	150	30	44
ELL-COLL/OLAC	5	150	10	60
ELL-COLL/OLAC	5	120	20	32
ELL-COLL/OLAC	5	180	20	52.18

4.2.1. Effect of ELL-COLL Concentration

The effect of the weight ratio of ELL-COLL: LA was examined in the range of 10 – 30 gm of ELL-COLL per 100 ml LA, and as shown in the previous table (Table 4.1), the pattern of grafting effectiveness was increasing, but when more concentration of the matrix was added, it started to fall. The ELL-COLL: LA weight ratio of 1:5 had the highest observed grafting efficiency of 72.8%. This finding may be explained by the fact that LA molecules are readily available on the ELL-COLL backbone, allowing for more efficient chain propagation with LA. As a result, LA used up all of the ELL-COLL molecules' active sites. On the other hand, the decline in grafting efficiency that occurred when the weight ratio was 30 gm:100 ml is attributable to the presence of active ELL-COLL sites that were not grafted or interacted with LA. This is in agreement with the results obtained for the grafting of styrene onto carboxymethyl chitosan (Abdel Gawad et al.,2020)

4.2.2. Effect of reaction temperature

While response time and the weight ratio of ELL-COLL: LA were held constant, grafting was done at various temperatures (120-180 °C). Grafting efficiency (GE%) was seen to rise when the temperature rose from 120 to 150 °C. the temperature increament resulted inreduction of reaction medium's viscosity, causing in more frequent collisions between the reactants and enhanced monomer mobility (Abdel Gawad et al., 2020). However, raising the temperature above 150 °C caused the GE% to decrease, most likely as a result of the protein matrix's degradation whereas at lower temperature the lowest grafting efficiency was observed, this might be due to there was no enough activation energy to start up the grafting or might be the temperature was not enough for the reactant to be reacted to each other.

4.2.3. Effect of reaction time

At a constant weight ratio of ELL-COLL: LA and reaction temperature, the impact of reaction time was studied. The grafting effectiveness rises from 1 to 5 hours before beginning to decrease off yet when compared to each other the grafting efficiency at 1 and 3 h was lower whuch might be Attributed to the reaction between ELL-COLL matrix and LA was not completed. The rise in homopolymerization of LA was caused by the decrease in GE% over 5 hours. In general terms**,** new compatible film-forming materials were successfully prepared by

grafting LA onto the ELL-COLL backbone which is confirmed by the analytical techniques used. The optimum grafting parameters were found to be at 1:5 ELL-COLL:LA weight ratio, 150 °C, and 5 h reaction time.

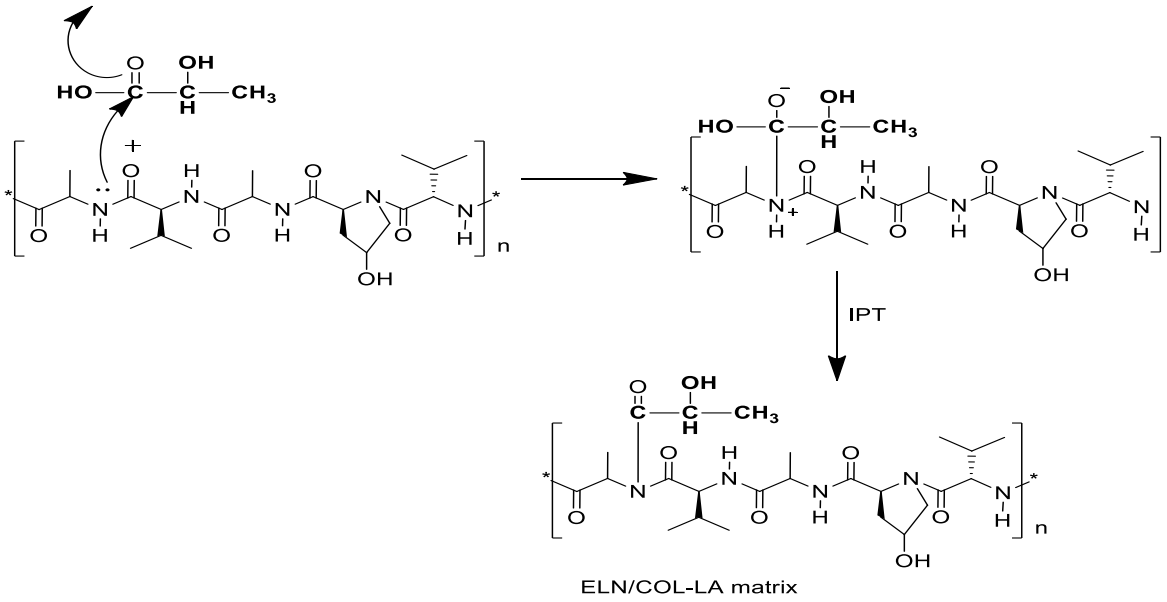

Figure 4.2: Reaction scheme of grafting of ELL-COLL matrix

As shown in Figure 4.2 the possible reaction that can occur during the grafting modification process would be internal proton transfer (IPT) in which the amine group of the ELL-COLL matrix would react with the C=O group of lactic acid which ended up by amide formation. yet as explained earlier there was no 100% grafting efficiency which led us to consider the ungrafted parts of the protein matrix. The aforementioned reaction and phenomena were supported by FTIR analysis of the grafted and ungrafted protein matrix.

4.2.4. Functional groups analysis of grafted and ungrafted ELL-COLL

To analyze how the grafting of LA on the backbone of the ELL-COLL matrix brought a structural and functional change to pristine ELL-COLL matrix FTIR analysis of grafted and ungrafted ELL-COLL matrix was conducted, here the FTIR of LA and pristine ELL-COLL were served as reference to show how the changes happened in the protein matrix when it was grafted.

The FTIR spectra of pristine ELL-COLL, LA, grafted, and ungrafted ELL-COLL are shown in Figure 4.3. grafted and ungrafted ELL-COLL matrix showed a broad peak at 3334.34 cm^{-1} due to free OH that came from unreacted lactic acid and NH groups that are formed when the amine group of the ELL-COLL reacted with that of the C=O group the lactic acid. This phenomenon was reported by (Kaithet al.,2011) when soy protein graft copolymerization with ethyl methacrylate.

Whereas the N-H stretching that was found on the pristine ELL-COLL matrix was around 1640 cm^{-1}, this specific peak has shown a broad peak when it is grafted and shifted to 1692 cm^{-1} this shift in wavenumber and broadening of the peak have proven that the amide group formation in another word the grafting of LA on the ELL-COLL backbone (Ding et al.,2021,), comparing the grafted with the ungrafted one, the peak broadening of the grafted ELL-COLL was higher than that of ungrafted ELL-COLL which indicated the favored formation (bending) of an amide group. The peak attributed to Amide II in the pristine ELL-COLL matrix was found at 1461 and 1546 cm^{-1} where as the grafted ELL-COLL matrix showed a broadening peak at 1457 and 1547 which showed that the formation of an amide bond.

In general the modification process was done and confirmed by the FTIR, in which the peak broadening and the formation of new peaks were detected for modified ELL-COLL matrix which proved that the formation of amide group. Yet the difference between the grafted and ungrafed ELL-COLL matrix was the newly formed peaks have higher intensity in the grafed ELL-COLL matrix thn that of ungrafted one.

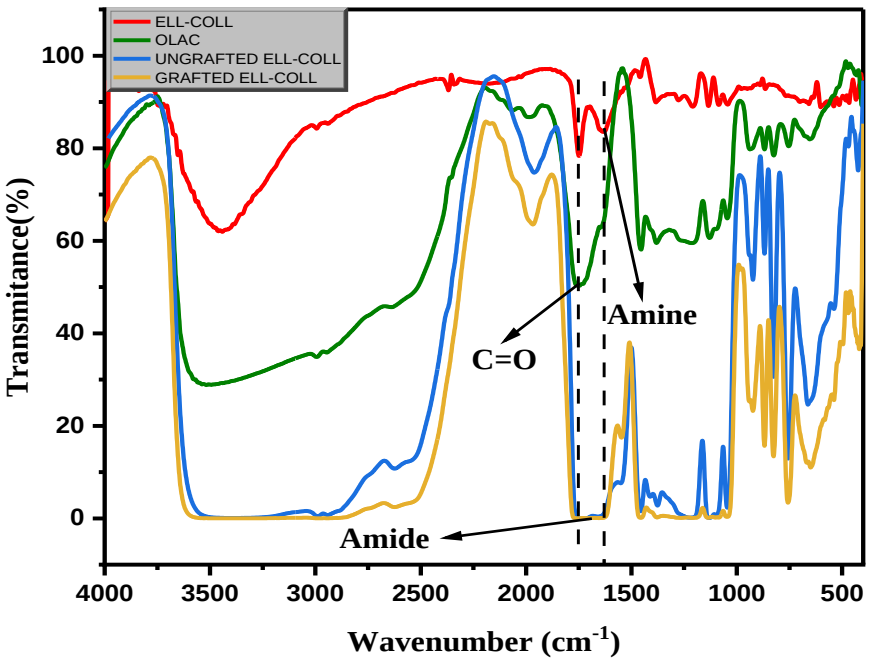

Figure 4.3: FTIR spectrum of ELL-COLL, LA, grafted and ungrafted m-ELL-COLL

4.3.Characterization of synthesized Ag NPs, ZnO NPs and Ag/ZnO NCs

4.3.1. Functional groups analysis of Ag NPs, ZnO NPs and Ag/ZnO NCs

To determine the presence of different structural units in the examined single nanoparticles and Nanocomposites, the FTIR spectra were taken in the spectral range of 400–4000 cm^{-1}. FTIR spectra of ZnO are shown in Figure 4.4. Pure ZnO NPs and the Zn-O bond stretching vibration can both be detected as a strong peak at 452 cm^{-1} and 574 cm^{-1}(Handore et al.,2014; Guo et al.,2022). Due to the Zn-O bond's stretching mode, a sharp peak was also seen at 1104 cm-1 (Hoseinpour et al.,2017). The O-H bond stretching and bending vibrations are responsible for the peaks at wavenumbers of 3556 and 1624 cm-1, respectively (Stan et al.,2016). The physically adsorbed water can be given the O-H bond. Only C-H bending caused by the oxalic acid which was responsible for the peak at wavenumber 1385 cm-1.

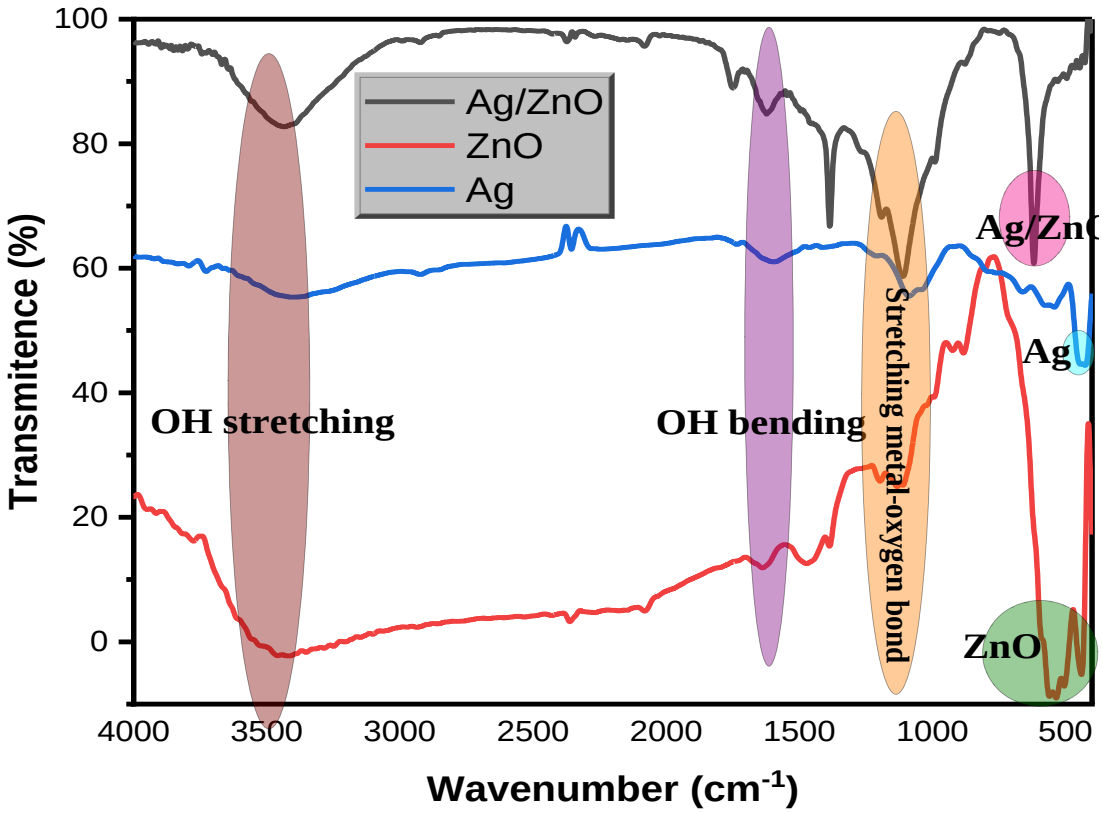

Figure 4.4: FTIR spectra of a) Ag, ZnO and Ag-ZnO b) ZnO c) Ag d) Ag-ZnO NCs

In Figure 4.4 five large absorption bands at 3407, 1600, 1090, 545, and 427 were found in the FTIR spectra of the Ag NPs. Ag NPs are capable of absorbing atmospheric water molecules because of the OH stretching and bending vibrations, which are represented by a broad band with a center at 3407 cm^{-1} and a sharp band at 1600 cm^{-1}. The stretching vibrations of the silver-oxygen connection also form two distinct bands. The first one is attributed to the vibration of Ag-O-Ag bonds and was at a frequency of 1082 cm^{-1} (Mazumder et al.,2019). Furthermore, the second one, which is related to Ag-O stretching, is at 545 cm^{-1} (Awwad et al.,2012). At 432 cm^{-1}, pure metal AgNPs appeared.

The FTIR spectra of Ag/ZnO were shown in Figure 4.4, and it was discovered that a large absorption band at 3457 cm^{-1} and 1627 cm^{-1} was seen due to the stretching and bending mode of O-H groups present in the sample, which may be caused by moisture (hygroscopic characteristics of the composite). According to Qamar et al. (2021), the absorption band around 1110 cm^{-1} is due to the metal-O bond's stretching mode, while the band around 1747 and 1385 cm^{-1} is solely attributed to C=O and C-H bending that results from the reducing

agent (oxalic acid). Nevertheless, the band of about 618 cm^{-1} showed the Metal-Oxide-Metal modes of Zn–O–Ag stretching vibration which confirms the presence of Ag/ZnO Nanocomposite (Vivek et al.,2019). The characteristic bands support the formation of the Ag, ZnO, and Ag/ZnO phases as claimed in the XRD analysis. The FTIR spectra of the Ag/ZnO composite only contain bands related to the corresponding Ag and ZnO functional groups, respectively, which confirms the effective formation of the Ag/ZnO composite as illustrated in Figure 4.4.

4.3.2. Crystallographic structural analysis of Ag-ZnO and NCs NPs (Ag, ZnO)

The XRD pattern of an Ag/ZnO nanocomposite synthesized by sol-gel technique with ZnO labeled peaks is shown in Figure 4.5 the peaks reflect the very pure wurtzite structure of ZnO NPs. Diffraction peaks 31.78°, 34.38°, 36.37°, 47.51°, 56.6°, 62.68°, 66.49°, 67.91°, 69.11°, 72.66°, 77.16° are in good accord with the literature (Tran Thi et al., 2019; Iqbal et al., 2021). The crystalline structure of AgNPs synthesized using $NaBH_4$ as a reducing agent was identified by using powder X-ray diffraction (XRD). The diffraction pattern occurred at 2Ɵ 38.17°, 44.44°, 64.62°, and 77.71°, respectively, corresponding to the crystallographic planes of (111), (200), (220), and (311). This is consistent with prior patterns of silver structure (JCPDS no. 03e0921) (Mostafa et al.,2020).

The presence of these four characteristic peaks (38.17, 44.44, 64.62, and 77.71) in the 25% Ag- 75% ZnO, 50% Ag- 50% ZnO , 75% Ag- 25% ZnO composite samples indicated the formation of highly polycrystalline AgNPs. Furthermore, no other peaks were visible in the diffraction pattern, confirming that no other structural form was formed. From Figure 4.5 the peaks that represented the presence of Ag NPs along with the crystalline structure of ZnO showed the formation of Ag/ZnO NCs. The charcterstics diffraction peaks of Ag NPs at 38.19°, 44.27°, 64.43°, and 77.39°, showed the presence of Ag NPs which is aligned with different literature reported on Ag/ZnO NCs (Shahid et al., 2020). It can be concluded that the XRD patterns showed the formation of Ag/ZnO Nanocomposite. The intensity of the diffraction peaks for ZnO NPs. decreased significantly with the increase in the concentration of Ag NPs and these phenomena were reported (S. Shet et al., 2010).

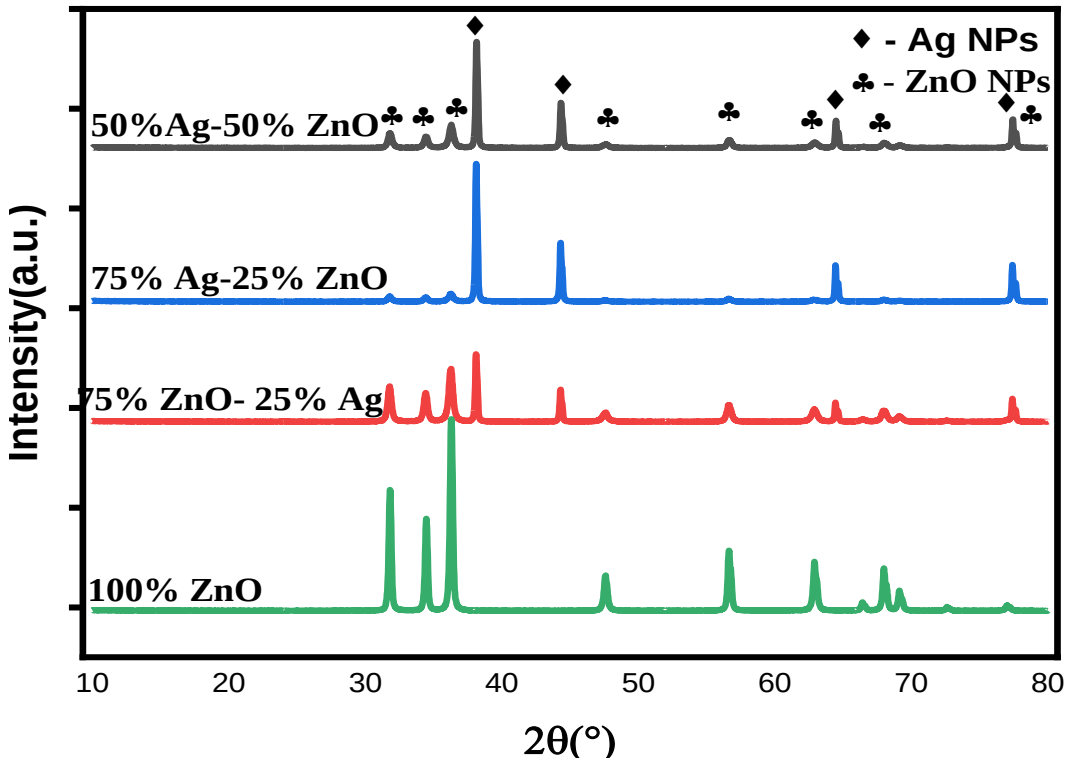

Figure 4.5: XRD pattern of ZnO and Ag-ZnO NCs

The formation of Ag/ZnO composite was studied from the XRD patterns and the fundamentals of detecting the formation of composite particles were comparing the crystallite size and the space between the planes of the pure (single) nanoparticle and the composites formed by changing the concentration of silver (Ag NPs) and zinc oxide (ZnO) nanoparticles. The values for each Peak position were obtained using Scherrer and Bragg's equation referring to equation 3.2 up to 3.4. Using the above equations the calculated values for crystallite size and the space between the planes were obtained. In Table 4.2 the values of crystallite size and the space between the planes for each peak position of 100% ZnO, 25% Ag-75% ZnO, 50% Ag-50% ZnO, and 75% Ag-25% ZnO were listed and the values for 100% ZnO were taken as a reference to see the effect of the concentration of Ag on crystalline size and D-spacing of Ag/ZnO nanocomposite (on the formation of nanocomposite).

Table 4.2. Average Crystalline size and D-spacing for a)100% ZnO b) 25% Ag-75% ZnO c)50% Ag-50% ZnO and d) 75% Ag-25% ZnO

Sample	Average crystal size (nm)	Average D-spacing (nm)
100% ZnO	29.3796	1.7659
75% ZnO – 25% Ag	25.8818	2.0154
50% Ag – 50% ZnO	24.9644	2.0139
75% Ag – 25% ZnO	27.5506	1.9444

In the 25% Ag-75% ZnO composition, the concentration of silver was much smaller than that of ZnO yet its effect in lowering the crystalline size and increasing the D-spacing values for each peak position of ZnO was significant (around 4 and 0.3 nm on average) and also there was the formation of a new peak with high value of crystalline size, these phenomena explain the formation of Ag/ZnO nanocomposite. The effect of an equal amount (concentration) of Ag and ZnO on the formation of the expected nanocomposite was explained by the crystalline size and D-spacing values of each peak position, each value explained how the existence of Ag nanoparticle shifted the crystalline behavior of ZnO nanoparticles. In comparing the crystalline size of the first peak position (31.8^{O}) of pure ZnO which was estimated to be around 35.128 nm and when the composition of Ag/ZnO shifted to 1:1 (50%Ag/50%ZnO) the crystalline size of the first peak position (31.8^{O}) ZnO was estimated to be around 22.33 nm in which the change in the crystalline size was brought from the existence of Ag. These phenomena can be explained as the existence of Ag with this composition changing the crystalline property of ZnO at a high level.

By following the same pattern the concentration of each particle was shifted to 75%Ag/25%ZnO in which the expected effect of Ag on the crystalline behavior of ZnO was analyzed considering Ag nanoparticle as host particle. In the third peak position (36.29^{O}) the crystalline size of ZnO (100%) was estimated to be 32.5 nm which explains how strong crystalline characteristics were possessed by ZnO, however when the composition becomes as explained earlier its value lowered to 15.58 nm. This change explains how the highly crystalline particles affect the other particle which with lower crystalline characteristics

compared to the previous one. In all compositions, the values for the crystalline size of the emerged peak(38.1^{O}) while forming the composite were in the range between 41 – 43 nm. These larger values of crystalline size explained the existence and the formation of another particle with a high degree of crystallinity that could determine the characteristics of the synthesized nanocomposite. The detailed crystalline size values for each peaks is reported in **Appendix 4.**

The formation of nanocomposite with different compositions of specific particles (Ag and ZnO) can also be explained by following the average values of crystalline size and the space between the planes. The average values of 100% ZnO NPs for crystalline size and the space between the planes were taken as reference and the values were 29.37 and 1.7. For different compositions of Ag and ZnO, the trend for the average crystalline size showed a decrement pattern relative to the values of pure ZnO which directed us in considering the effect of Ag NPs on the crystalline characteristics of ZnO, but in the composition (75%Ag/25%ZnO) the decrement pattern in crystalline size shifted to increment pattern.This phenomena can be explained when the concentration of highly crystalline particle dominates the crystalline characteristics of Ag/ZnO nanocomposites in a good way.

In general, the crystalline size of nanocomposites with different concentrations showed a decrement pattern when compared to single nanoparticles (ZnO). This decrement pattern explains the effect of Ag NPs on the crystalline size of pure ZnO and also as the concentration of Ag increases the crystalline size of the composite started to increase.These calculated values are in agreement with different research reports (Mote et al., 2012; Jia et al., 2013).

Comparing the d-spacing values of the ZnO NPs with the synthesized composite the minimum d-spacing was obtained for ZnO which explains crystallinie property of ZnO NPs. Same results of d-spacing for the particles and composite were reported (Saad et al., 2021; Abbas et al., 2021; Pandey et al., 2021) and this confirms also the synthesis of the ZnO NP and Ag/ZnO was successful

The crystalline structure of AgNPs synthesized using $NaBH_4$ as a reducing agent was identified using powder X-ray diffraction (XRD). The diffraction pattern occurred at 38.17°, 44.44°, 64.62°, and 77.71°, respectively, corresponding to the crystallographic planes of (111),

(200), (220), and (311). This is consistent with prior patterns of silver structure (JCPDS no. 03e0921) (Mostafa et al.,2020). The presence of these four characteristic peaks indicates the formation of highly polycrystalline AgNPs. Furthermore, no other peaks were visible in the diffraction pattern, confirming that no other structural form was formed.

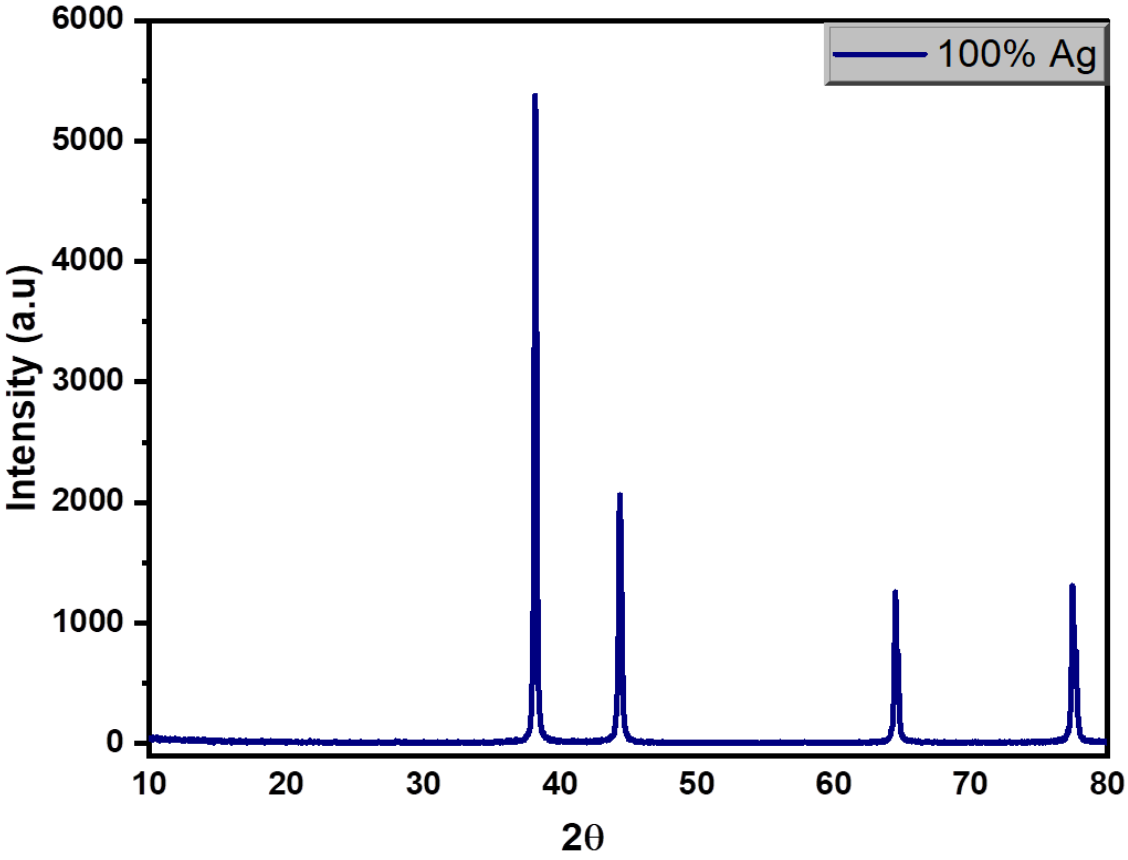

Figure 4.6: XRD pattern of Ag nanoparticle

From the XRD pattern, the peak position of 38.19 and 44.38 showed a sharp peak which can be an alternative way of confirming the crystalline characteristics of the particle. The aforementioned analysis (crystalline characteristics) from the XRD pattern can be proved by analyzing the values obtained from the calculation using Scherrer and Bragg's equation. In Table 4.3 the values of crystallite size and the space between the planes for each peak position of Ag NPs were listed and these values were taken as a reference to confirm the formation of Ag NPs. For the peak position of 38.19°, 44.38°, 64.55°, and 77.51° the values for crystalline size are 37.57 nm, 31.14 nm, 27.89 nm and 24.73 nm which indicates that the crystaligopheric property of the nanoparticle and these values are in good agreement with different research

works (Saad et al., 2021;Abbas et al., 2021; Pandey et al., 2021). In addition to this, the average d-spacing has lower values when compared to both ZnO and Ag/ZnO which confirms that the crystalline property of Ag NPs is higher than that of ZnO and Ag/ZnO.

Table 4.3: Crystalline size and average D-spacing of 100% Ag

100% Ag				
Peak position	**FWHM**	**Crystalline size D (nm)**	**Average crystalline size (D)**	**Average D-spacing**
38.19012	0.22372	37.57759062		
44.38328	0.27546	31.14729607	**30.3375**	**1.76**
64.55086	0.33685	27.89391967		
77.51559	0.41193	24.7314034		

4.3.3. UV-VIS analysis of Ag, ZnO, and Ag-ZnO NCs

UV-VIS absorption spectra of pure ZnO, Ag and Ag-ZnO NCs are shown in Figure 4.7. ZnO exhibited a UV absorption band in the range of 370-382 nm, which is a characteristic absorption peak of ZnO (Kadam et al.,2018). Because of their tiny size and larger surface area, Ag NPs showed a surface plasmon resonance (SPR) peak at 426 nm, whereas the characterstic absorption peak of Ag NPs failed in between 390 - 430 nm, indicating the existence of silver nanoparticles in our sample (Barbir et al., 2019). Ag-ZnO NCs showed an absorption peak around 388 which confirms that the absorption of this composite is in between the absorption band range of ZnO and Ag NPs. In other word the absorption of Ag-ZnO NCs was not a simple superposition of individual single component materials. The surface plasmon band of Ag-ZnO NCs was distinctly broadened and red-shifted by 16 nm compared to that of the pure ZnO NPs probably due to strong electronic coupling between the Ag core and ZnO shell. The formation of these phenomena aligned with different literature (Zare et al., 2019)

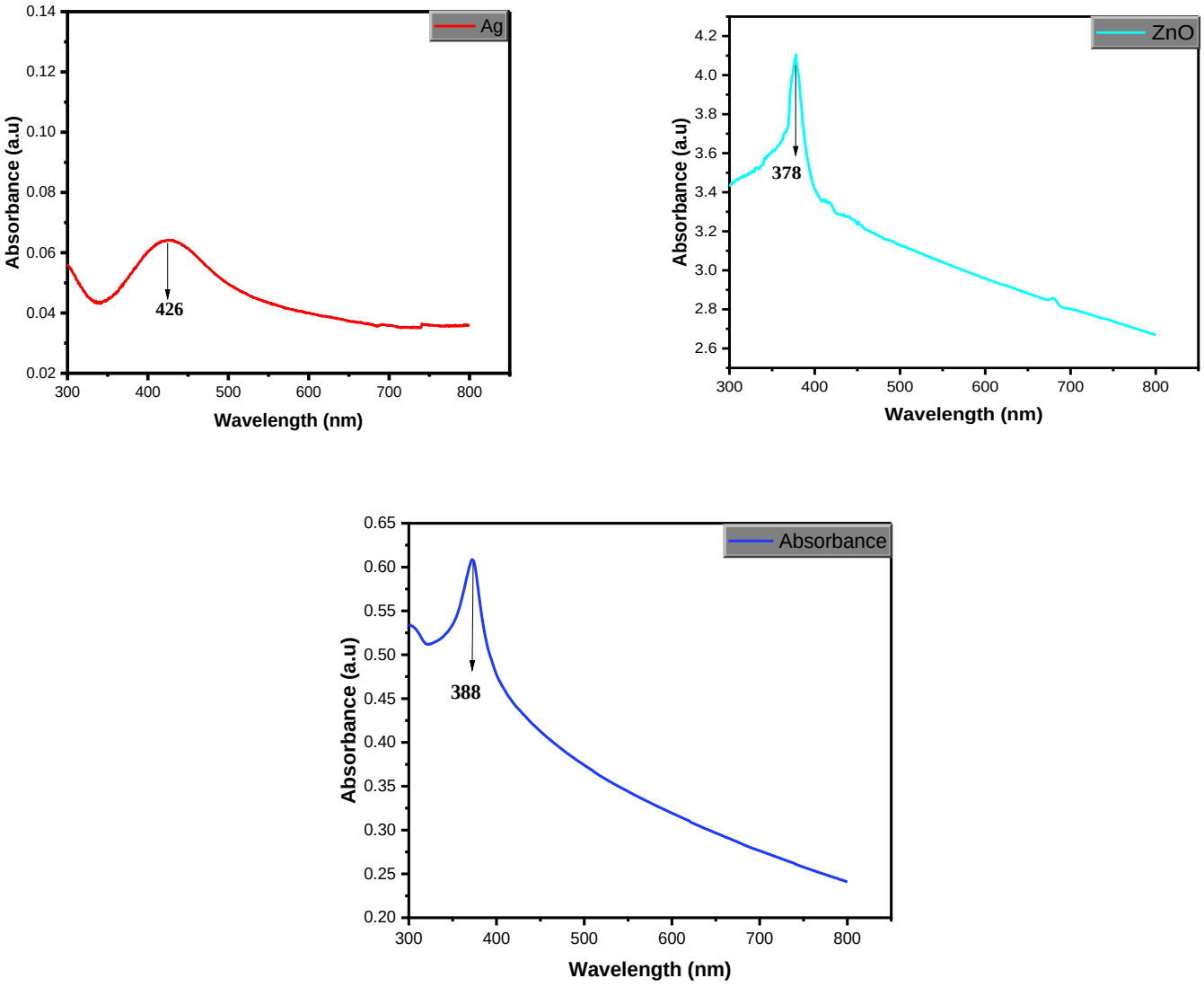

Figure 4.7: UV-VIS absorption spectra of a) Ag b)ZnO c) Ag-ZnO NCs

4.3.4. Particle size analysis for Ag/ZnO, Ag, and ZnO

The distinctive qualities that each metal or metal oxide particle possesses—properties that give the particle its multifunctionality—are determined by its particle size. In this way, the synthesis and analytical processes have an impact on the size of metal particles. Zetasizer Nano (PSDA) was used to measure the particle sizes of the two samples (NPs and NCs), and the effects of the particle size analysis (solvents and sonication time) were investigated. Three different sonication times and two different dispersant solvents were chosen to study how

solvents and sonication times affected the size of metal nanoparticles. Their effects are discussed below for Ag/ZnO and ZnO nanoparticles, and the size of silver nanoparticles was only determined by one parameter (45 min and ethanol).

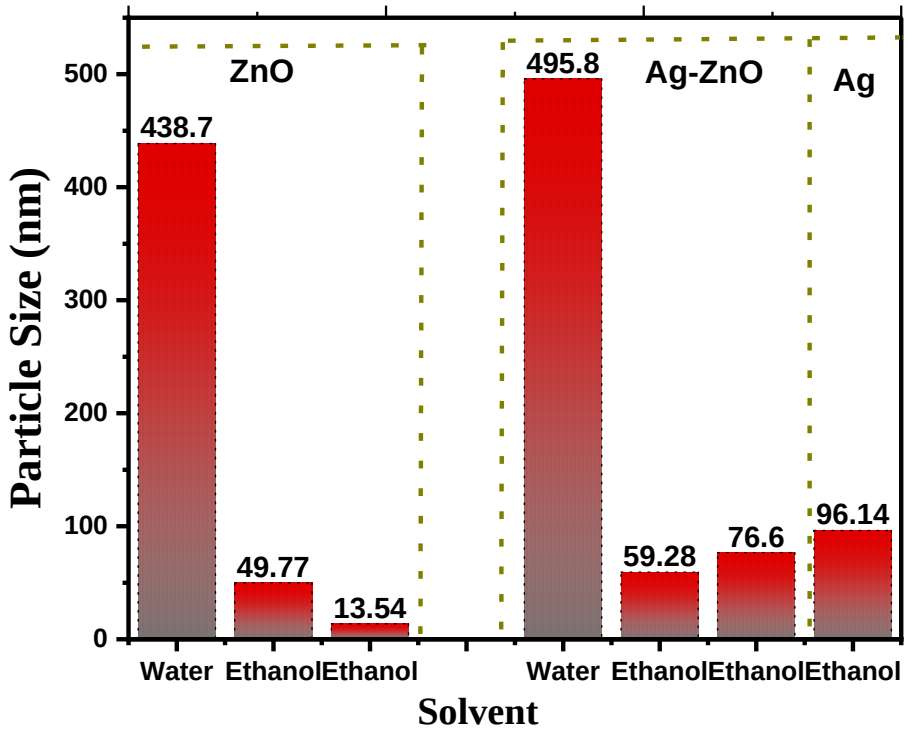

Figure 4.8: Particle size of ZnO, Ag/ZnO, and Ag analyzed by PSDA

To prevent particle agglomeration, ZnO and Ag/ZnO were dissolved in water and subjected to a 15-minute sonication process in the first run. However, the results of this run revealed that the highest particle sizes were 438.7 nm for ZnO and 495.8 nm for Ag/ZnO, and all of the particles were in the monophase region. As can be observed from the results, neither the solvent nor the duration of the sonication had a substantial impact in solving the agglomeration-related issues. According to the aforementioned findings, it was crucial to alter the solvent and extend the sonication period.

Table 4.4: Particle size of ZnO, Ag/ZnO, and Ag analyzed by PSDA

Sample name	Solvent	Sonication time (min)	Size (nm)	phase
ZnO	Water	15	438.7	Monophase
	Ethanol	30	49.77	Monophase
		45	13.54	
Ag/ZnO	Water	15	495.8	Monophase
	Ethanol	30	59.28	Polyphase
			4505	
		45	76.6	Monophase
Ag	Ethanol	45	96.1	Monophase

The second test employed ethanol as the solvent and 30 minutes of sonication. The obtained results demonstrated a polydispersity of two peaks for Ag/ZnO, peak-1 having 59.28 nm particle size with 62.3 % intensity, and peak-2 being recorded with a very higher particle size of 4505 nm with 37.7 % intensity. For ZnO, a single peak was detected with a particle size of 49.77 nm, indicating a monodispersity. The results showed that the solvent and sonication period had a considerable impact on the agglomerated particles, which was highly important information.

The third and final run was carried out by sticking to the same pattern but changing or lengthening the sonication time. Here, results were obtained at 13.3 nm for ZnO, 76.6 nm for Ag/ZnO, and 96.14 nm for Ag NPs using the same solvent (ethanol) with a longer sonication

period of 45 minutes. These outcomes provided a strong cue that the composites and manufactured particles were in the nano-size range. Finally, 45 minutes and ethanol were found to be the ideal sonication time and solvent for resolving agglomeration issues and obtaining the proper particle size.

4.4. Image analysis for dispersion of m-ELL-COLL matrix into PLA

The optical microscope image analysis was used to study the dispersion of the ELL-COLL matrix into the poly (lactic acid) matrix. The investigation was done for PLA/protein matrix with loading rates ranging from (0%, 10%, 20%, 30%, 40%) and all films were annealed at 110 ^{O}C for 150 min. By exposing some grain size structures across the film, Figure 4.9(A) demonstrated the neat-semi-crystalline PLA's structure. These structures may be more significant than they appear to be due to the influence of the annealing process. The neat-PLA biofilm was used as a baseline in this image analysis to show how the protein matrix diffused and developed some additional structure. The formation of additional structures is directly related to the change in structural as well as different characteristics of PLA.

With the addition of 10% wt% of the ELL-COLL matrix, there was change in the structure of PLA as it can be detected. The grain-like structures that were observed in neat-PLA films were somehow decreased in size yet the dispersion of the protein matrix into the PLA was favored. As the loading of the protein matrix increased additional honeycomb-like structures were identified which might be attributed to the structure of the ELL-COLL matrix. The formation of additional structure on the surface of the PLA films might be indicated that the intermolecular mixing between the ELL-COLL matrix and PLA was not favored as the loading rate of the ELL-COLL matrix increased. These phenomena might lead us to conclude that the intermolecular mixing between two polymers is the key factor in providing different properties to the host polymer, in this study the protein matrix served as filler and PLA served as the host polymer. The formation of additional structure on the surface of PLA matrix was due to high concentration of filler compromises the intermolecular mixing of these two polymers. This assumption was approved by crystallization and mechanical property analysis.

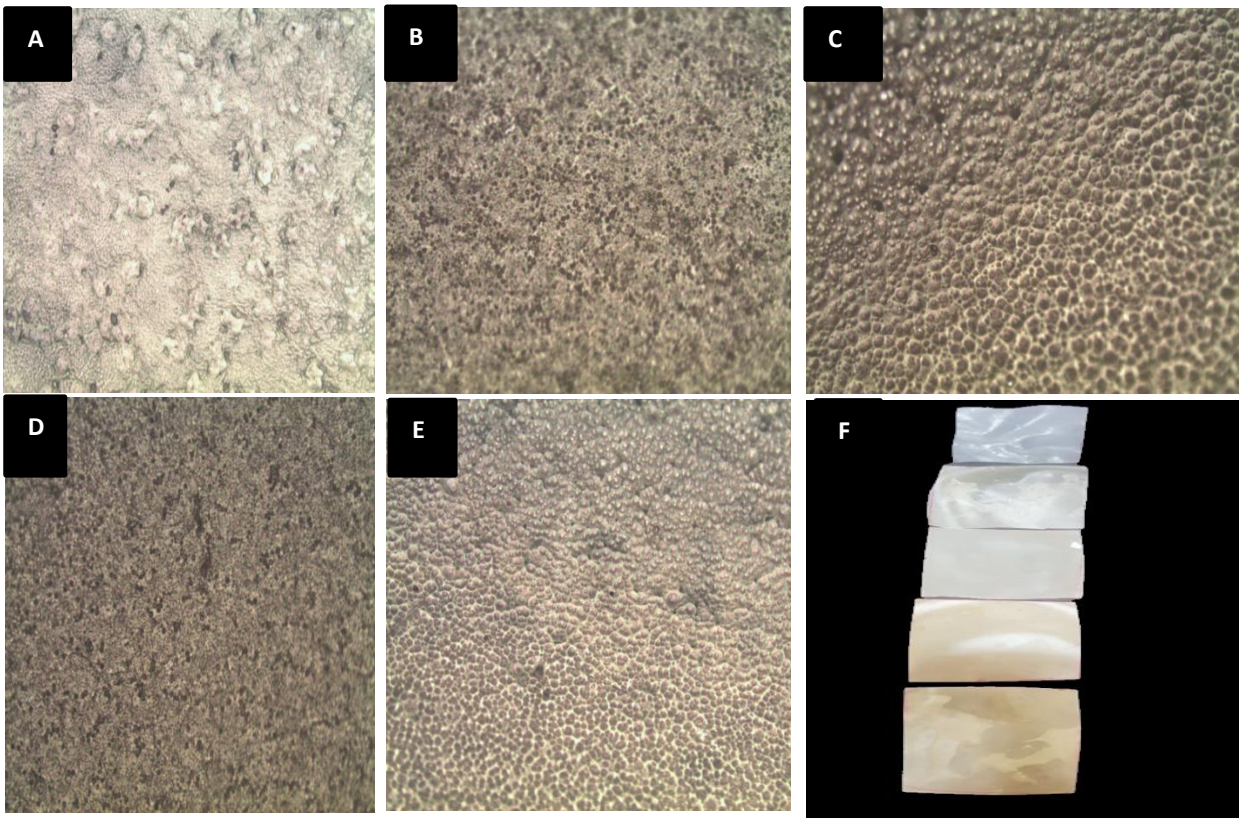

Figure 4.9: Optical microscope analysis neat PLA(A) and PLA/m-ELL-COLL(10%(B), 20% (C),30%(D),40%(E), images of prepared films (F))

4.5. Thermal property study of PLA

4.5.1. Nucleation effect of ELL-COLL matrix (as filler) on Crystallization of PLA

The crystallization kinetics of the PLA-based films were evaluated. Figure 4.10 shows the first heating cycle for the crystallization behaviors of the PLA and PLA/m-ELL-COLL composite films. To investigate how nucleating agents (m-ELL-COLL) affects the PLA crystallization property, DSC analysis was used .The effect of different loading of the m-ELL-COLL (1%, 3%, 5%, 10% and 20% wt%) on the crystallization property of PLA was investigated. Table 4.5 summarizes the thermal properties of composite films estimated from the DSC curves. The melting temperature (T_m), the heat of fusion (H_f), degree of crystallization (X_c), and the glass transition temperature (Tg) were determined from the DSC plot.The degree of crystallization (X_c) was calculated based on the following equation.

When elastin-collagen content increased, a slight decrease in T_m was observed as it can be seen in Table 4.5. This is due to the presence of elastin-collagen in the PLA matrix, which helps to improve chain mobility (motion) in the crystalline area and also the increasing entanglements of ELL-COLL, which prevented the matrix chains from developing larger crystalline domains. After that there was an increment in T_m which revealed that the PLA matrix started to fold on the m-ELL-COLL nucleating agent yet the T_m of the composite films upto 10% loading of m-ELL-COLL lower than the T_m of neat PLA fim, this phenomena confirms that the chain mobility around crystalline area of PLA film prevented the composite film to develop larger crystalline domains (Baheti et al., 2013). Considering 20% loading of m-ELL-COLL matrix the T_m of the composite film decreased upto 150.74 ^{O}C which was the lowest T_m from the DSC analysis. The decrement phenomena in T_m confirmed that instead of serving as nucleating agent, the m-ELL-COLL matrix was acting as plasticiszer which resulted in lower degree of crystallinity.

Intermolecular interactions, steric effects, chain flexibility, molecular weight, branching, and crosslinking density are all factors that affect the Tg, making it a complicated phenomenon (Baheti et al., 2013). The T_g from DSC analysis started to fall between 58.79 ^{O}C and 51.9 ^{O}C when the m-ELL-COLL matrix content rose from 0 wt% to 1 wt%, which can be attributed to the matrix causing a decrease in the total crosslinking density of PLA. In other words the interaction between m-ELL-COLL and PLA molecular chains, which took the place of the interaction between the original PLA molecular chains, weakens the force between the molecular chain segments.This was the cause of the blend's slightly lower glass transition temperature than that of pure PLA (Qian et al., 2018; Wang et al.,2021) and also it might be the plasticizing effect (chain flexibility) of the ELL-COLL matrix that protruding in the PLA phase (Goffin et al., 2011). These phenomena can be concluded as, the weak interaction between the PLA and elastin-collagen matrix may have increased free volume which, in turn, increases molecular mobility facilitating the process of thermal relaxing.

The major scientific fact behind this shift is when PLA and m-ELL-COLL dissolved in a solvent the m-ELL-COLL would lose its secondary structures and also the entagled PLAs would somehow separated and forms number of a single chains. Due to this the interactions might be changed to PLA-m-ELL-COLL-PLA instead of PLA-PLA which is suronded by

solvents. When the composite film was casted the solvent would evaporate thorough slow drying. Throughout the slow drying process the m-ELL-COLL started to regain its secondary structure without changing position, as the protein started to regain its secondary structures the PLA started to fold on the surface of m-ELL-COLL matrix.when the PLA started to fold on the m-ELL-COLL matrix it started to crystallize.Yet the m-ELL-COLL matrix have synergetic properties that would make it to serve as plasticizer and crystallizer (nucleating agent). As the loading of m-ELL-COLL increases the interaction between PLA and m-ELL-COLL started to being compromised and m-ELL-COLL/m-ELL-COLL interaction favoured due to formation of localized protiens. The above-mentioned incident occurred when the m-ELL-COLL loading exceeded 10% as it shown in fig 4.10, which leads the PLA/m-ELL-COLL matrix to be relaxed and the crystalinity started to drop.

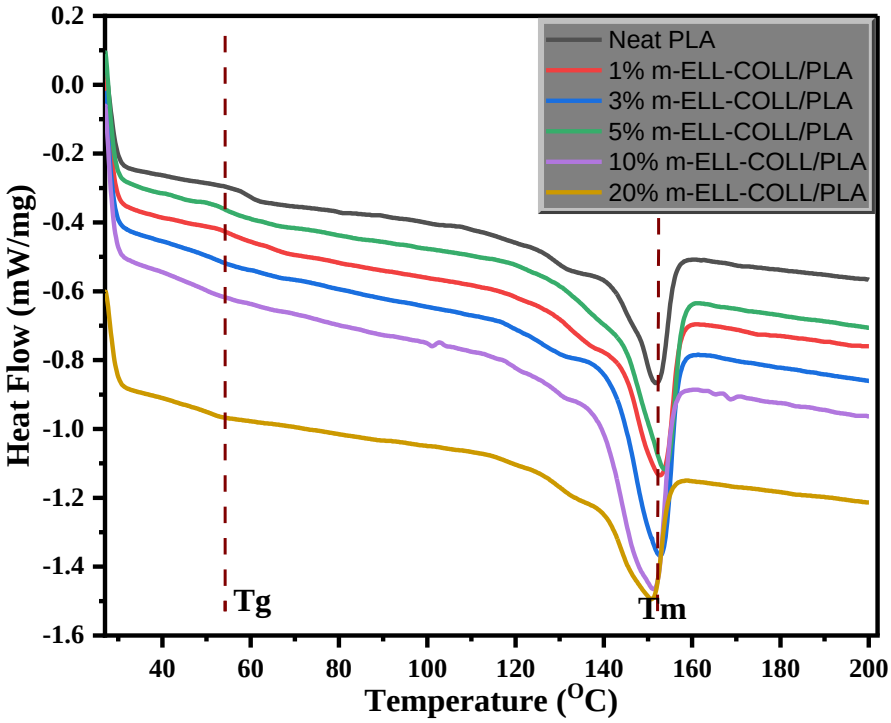

Figure 4.10. First heating DSC curves at 10 °C/min for neat PLA and PLA/ELL-COLL composite films

Naturally, the nucleating agent that has been used to enhance the crystallization properties of PLA which were m-ELL-COLL matrix which possesses two properties which are elasticity from elastin and rigidity from collagen, therefore these synergetic properties of the nucleating

agent play a vital role in the enhancing process. The neat PLA was used as a reference in this study to examine the crystallization impact of varying the loadings of an m-ELL-COLL matrix, and the composite films were developed with loadings rates of (1%, 3%, 5%,10% and 20%) Because of the matrix's synergetic impact, it is anticipated that loading the matrix will improve PLA's crystallinity up to a certain loading rate then an increase in loading rate could change the material's intended usage from a nucleating agent to a plasticizer.

Table 4.5: Tg, Tm, Hf and Calculated degree of Crystallinity of neat PLA and PLA/m-ELL-COLL (1%,3%, 5%, 10%, 20%)

FILMS	***Tg(^{O}C)***	***Tm(^{O}C)***	***H_f (J/g)***	***Xc(%)***
Neat PLA	58.79	151.76	29.98	32.04
PLA-m-ELL/COLL-1%	51.99	150.83	35.78	38.22
PLA-m-ELL/COLL-3%	51.17	151.68	43.33	46.3
PLA-m-ELL/COLL-5%	46.514	151.33	47.17	50.6
PLA-m-ELL/COLL-10%	51.2	151.13	48.01	51.3
PLA-m-ELL/COLL-20%	46.15	150.74	35.84	36.9

From Table 4.5 the degree of crystallinity of the neat PLA film was 32.04 % which was in good agreement with (de Azevedo Gonçalves Mota et a., 2021), and with 1% loading of the m-ELL-COLL matrix, it has shifted to 38.22 % which indicated that the matrix exhibited nucleating characteristics on the PLA by raising its crystallinity. This increment trend continued up to a certain level of loading rate. There was a shift in crystallinity of the composite film when the loading rate was 20% (51.3% to 36.9%) this might be due to the weak surface interaction between polymer chains and the m-ELL-COLL matrix when the loading rate exceeded the right amount of concentration.

The crystallinity of PLA film which was incorporated with 20% of the m-ELL-COLL matrix was less than that of PLA film which was incorporated with 1% of the m-ELL-COLL matrix which might be the indication that the interaction between the PLA and the m-ELL-COLL matrix was favored at lower loading rate. This shift in the degree of crystallinity of the PLA/m-ELL-COLL composite film was also supported by the mechanical test analysis in which the shift in tensile strength has dcreased from 60.202 ± 1.657 to 34.472 ± 0.985 as the loading rate changed from 10% to 20%. The relationship between crystallinity and tensile strength is somehow direct so the decrement pattern of crystallinity has been also identified in the change of tensile strength. The nucleation caused by the addition of the m-ELL-COLL matrix led to the binding of numerous small crystal grains, which increased the crystal grain size (Chou et al.,2021).

4.5.2. Nucleation effect of Ag/ZnO nanocomposite (as filler) on Crystallization of PLA

Because it influenced morphology, crystalline structure, and macroscopic characteristics of the material, investigation on the crystallization and melting behavior of polymer nanocomposites films has always been an interesting area. The thermal transitions of PLA nanocomposites were examined using DSC. The effects of Ag NPs, ZnO NPs, and Ag/ZnO Ncs as nucleating agents were examined using DSC in the following section. Based on the results of the previously mentioned DSC analysis, the weight percentage of the m-ELL-COLL matrix that demonstrated a high degree of crystallinity was 10 wt %. However, in this analysis, the role of the 10 wt % m-ELL-COLL matrix was limited to that of a carrier for introducing the nanoparticles and nanocomposite into the PLA matrix. To study the impact of Ag/ZnO on the PLA's crystallinity properties, different loadings of Ag/ZnO NCs (0, 1, 3, 5%) were dispersed

into the m-ELL-COLL-10 matrix and incorporated to the pre-dissolved PLA matrix. A summary of the melting temperature (Tm), heat of fusion (Hf), degree of crystallization (Xc), and glass transition temperature (Tg) described in Table 4.6.

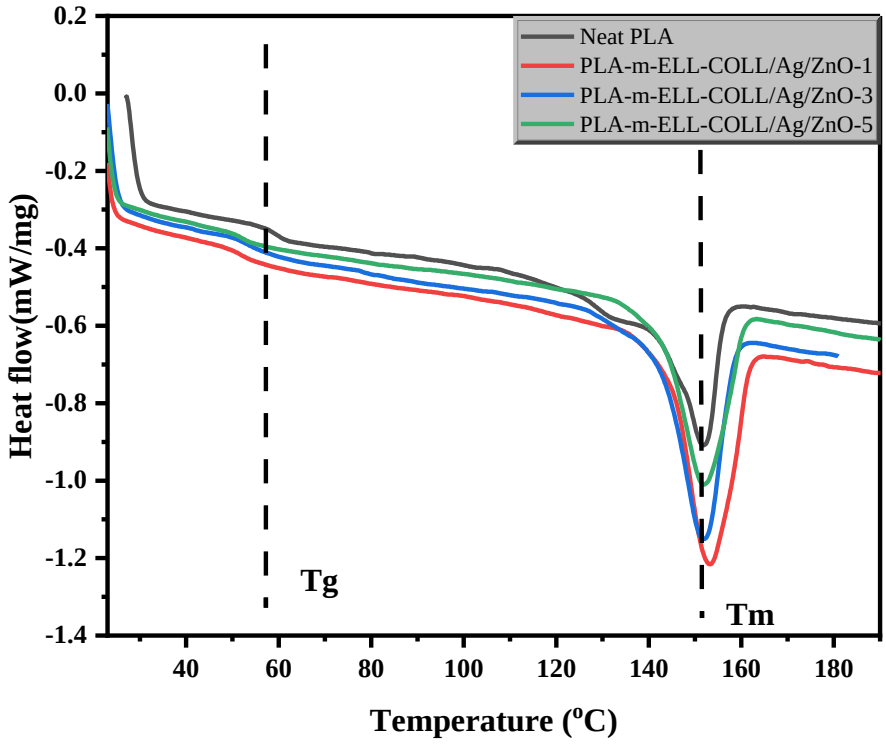

Figure 4.11: First heating DSC curves at 10 °C/min for neat PLA and PLA and PLA/ELL-COLL-Ag/ZnO (1%,3%, 5%,) composite films

The order of arrangement and crystalline properties of the PLA/m-ELL-COLL-Ag/ZnO nanocomposite films was presumably increased by the presence of these specific NCs, as shown in Table 4.6. Comparing the values of T_m of PLA composite films with different loadings of Ag/ZnO nanocomposite without considering the T_m value of neat PLA which showed a decreasing pattern. The decrement in T_m can be related to the initiation of chain mobility that resulted in the formation of entanglement. The key issues that inhibited the matrix chains from generating bigger crystalline domains were the occurrence of chain mobility and chain entanglement.

Table 4.6: Tg, Tm, Hf, and Calculated degree of Crystallinity of neat PLA and PLA/ELL-COLL-Ag/ZnO (1%,3%, 5%,)

Films	$T_g(^OC)$	$T_m(^OC)$	***Hf (J/g)***	X_c **(%)**
Neat PLA	58.79	151.76	29.98	32.04
PLA-m-ELL/COLL-Ag/ZnO-1%	51.75	153.06	40.55	43.3
PLA-m-ELL/COLL-Ag/ZnO-3%	53.19	151.73	38.12	40.7
PLA-m-ELL/COLL-Ag/ZnO-5%	51.96	151.84	32.3	34.5

As shown in Table 4.6, the degree of crystalinity was shifted from 32.04 to 43.3% with 1% loading of Ag/ZnO nanocomposite this shift indicated that the dispersion of Ag/ZnO in to the polymer matrix was good which leads the nanocomposite to paly a great role as nucleating effect.The same results were obtained at lower weight percentage of different metal and metal oxide nanoparticles and composites (Bautista-Del-Ángel et al., 2020). In contrast, as the loding of the Ag/ZnO nanocomposite increased the degree of crystalinity of nanocomposite films started to decline. This phenomena can be expressed as the crystallinity of PLA-m-ELL/COLL-Ag/ZnO-3% and PLA-m-ELL/COLL-Ag/ZnO-5% has decreased, owing to the agglomeration of the large amount of Ag/ZnO NCs existing in the PLA matrix. The same result were reported by different scholars (Zhang, et al.,2018; Yu et al.,2021) Generally, the electrostatic interaction between the NCs and polymer can increase the crystallinity and Tg value. Unexpectedly, on increasing the Ag/ZnO NCs content, our as-prepared bio-nanocomposite films showed a decrease in the Tg value as a result of poor dispersion and the interaction between the Ag/ZnO and PLA polymer matrix.

4.5.3. Comparision of the nucleating effect of of Ag, ZnO and Ag/ZnO nanoparticles

To determine the effectiveness of our main product, Ag/ZnO NCs, as a good nucleating agent, it is important to compare the single nanoparticles that make up the composite, Ag and ZnO NPs with the Ag/ZnO NCs. The thermal characteristics of the nanocomposite film were examined using the same loading, solvent casting method, and DSC measurements. Figure 4.12 shows the first heating curves for neat PLA, PLA/m-ELL-COLL/Ag-10, PLA/m-ELL-COLL/ZnO-10, and PLA/m-ELL-COLL/Ag-ZnO-10. Here, the neat PLA was compared to each nanoparticle (single and composite) based on its degree of crystallinity, as well as to Ag, ZnO, and the nucleating impact of Ag/ZnO NCs.

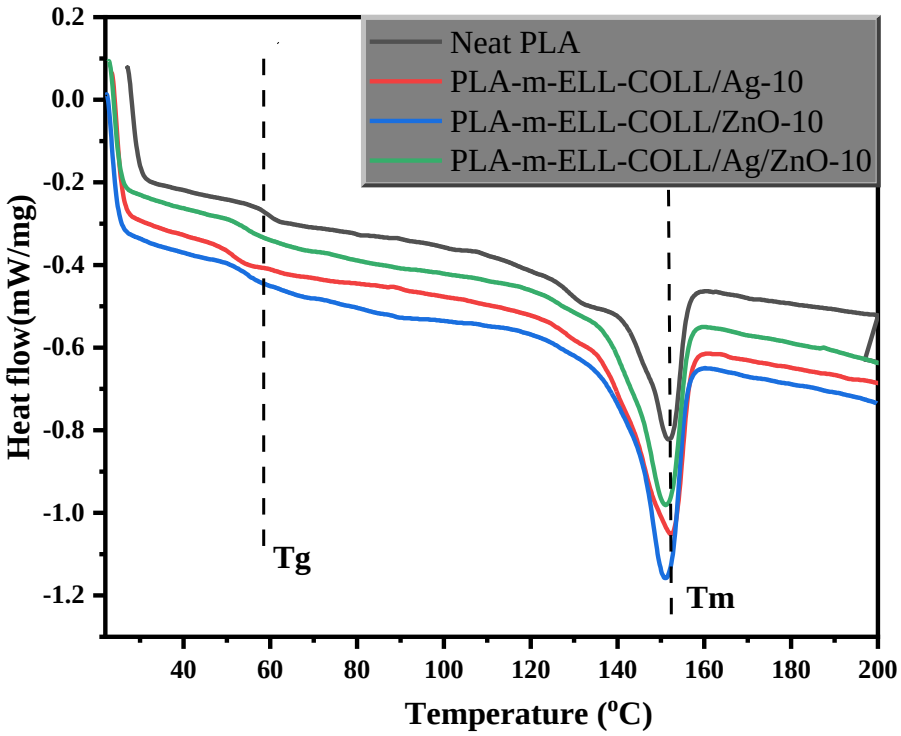

Figure 4.12: First heating DSC curves at 10 °C/min for neat PLA and PLA/m-ELL-COLL-Ag/ZnO,Ag and ZnO (10%) composite films

The dgree of crystalinity (*Xc*), T_g, T_m and H_f are the comparison parameters which all can be drived from the first heating curve thermogram. Yet the *Xc* is calculated using the same formula that was used earlier.

Table 4.7: Tg, Tm, Hf, and Calculated degree of Crystallinity of neat PLA and PLA/ELL-COLL-Ag/ZnO,Ag and ZnO (10%) composite films

Films	$T_g(^OC)$	$T_m(^OC)$	*Hf (J/g)*	X_c *(%)*
Neat PLA	58.79	151.76	29.98	32.04
PLA-m-ELL/COLL-Ag -10%	51.5	151.52	38.32	40.94
PLA-m-ELL/COLL-ZnO-10%	54.68	150.88	36.56	39.1
PLA-m-ELL/COLL-Ag/ZnO-10%	54.12	151.02	31.7	33.9

According to Table 4.7, all of the nanocomposite films displayed a pattern of decreasing in Tg values when compared to neat PLA, which is a strong indication that PLA has begun to crystallize or that the nucleation impact of the nanoparticles has caused the polymer matrix to begin to crystallize. The PLA-m-ELL/COLL-Ag -10% with lower Tg, which was around 51.5 ^oC, has proved right the previous fact by demonstrating that its degree of crystalinity was greater than that of neat PLA, PLA/m-ELL-COLL-ZnO, and PLA/m-ELL-COLL-Ag/ZnO based nanocomposite. In light of Tm, chain mobility is encouraged around the crystalline region of the PLA-based nanocomposite with lower T_m. The lower the Tm, the lower the degree of crystallinity of the PLA.

The PLA-m-ELL/COLL-Ag -10 percent calculation of the *Xc* yielded the highest value. This might be attributable to the nucleation effect of Ag NP was higher than ZnO and Ag/ZnO, which resulted from the particle's excellent dispersion into the PLA matrix. In actuality, PLA matrix crystals that form at higher heats of fusion tend to be smaller and less dense. (Cacciotti et al., 2014). This phenomenon was noted in the X-ray diffraction data of Ag, ZnO, and

Ag/ZnO, which demonstrated that the Ag NPs had a higher crystalline size as compared to other nano composite. This suggests that when the Ag NPs were dispersed into the PLA matrix, they brought their crystalline properties with them.

4.6. Thermogravimetric Analysis study

4.6.1. Thermal stability of PLA/ELL-COLL composite film

To determine the weight percentage of m-ELL-COLL that was required for the best possible dispersion of single and composite nanoparticles, thermogravimetric analysis of PLA/m-ELL-COLL composite films was conducted. m-ELL-COLL matrix plays a significant role in introducing nanomaterials into the PLA matrix as a carrier. The TGA curves of neat PLA, PLA/m-ELL-COLL-10%, and PLA/m-ELL-COLL-40% were shown in Figure 4.13. the curve showed that dehydration (moisture loss) occurred in all samples between 90 and 95 ^{o}C in the following order of mass loss: 9.95 %, 7.53 %, and 9.23 %. For neat PLA, a single-step total weight loss was observed with a maximum degradation temperature of 361.5 ^{o}C. While a drop of around 55.5 ^{o}C was identified for the PLA/m-ELL-COLL-40 binary composite, a shift to lower temperatures of about 15 ^{o}C and in T_{max} value were seen in the PLA/m-ELL-COLL-10 binary composites, indicating that the presence of protein matrix alters the thermal degradation process.

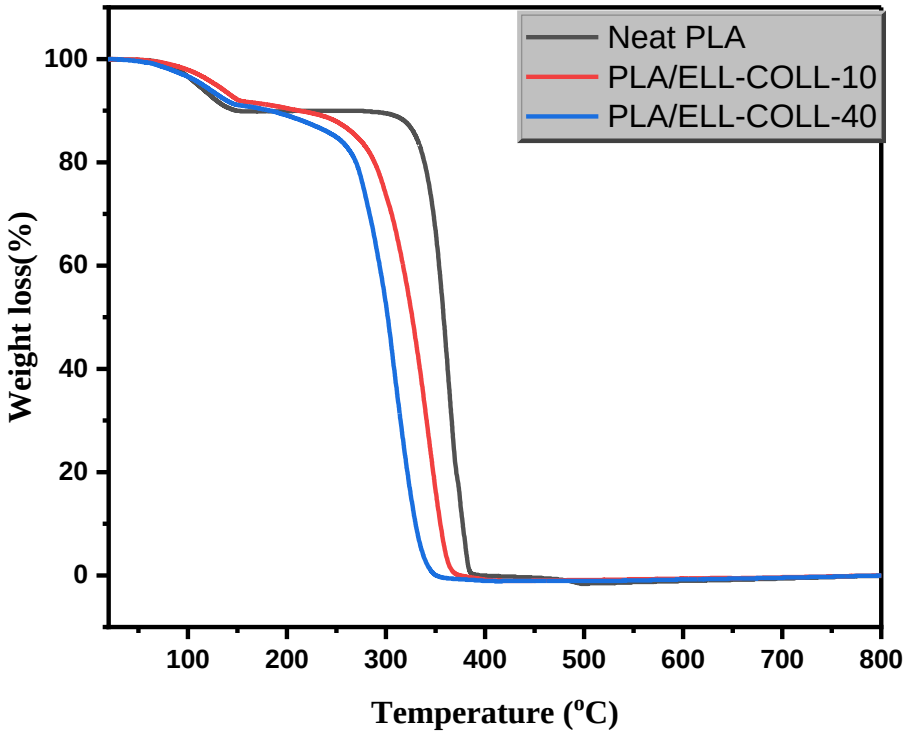

Figure 4.13: TGA curves of Neat PLA and PLA/m-ELL-COLL composite films

Additionally, a multi-stage decomposition process for PLA/m-ELL-COLL-10(10 wt% m-ELL-COLL matrix dispersed PLA film) was seen in the binary composite films DTG curve, with the major peak occurring at 345.9 ^{o}C and a second stage occurring at 288.9 ^{o}C. In the case of PLA/m-ELL-COLL-40(40 wt% m-ELL-COLL matrix dispersed PLA film) the multi stage degradation occurred at 306 ^{o}C and 278.22^{o}C.These multi-stage degradations proved that the degradation of m-ELL-COLL occurs at a lower temperature than the PLA matrix these phenomena was supported by other research work (Fortunati et al.,2010).The TGA investigation was primarily done to select the optimal carrier among the two weight percentages m-ELL-COLL-10 and m-ELL-COLL-40 based on their thermal stability when dispersed in the PLA matrix. Based on the T_{10}, $T_{90,}$ and T_{max} values for neat PLA, PLA/m-ELL-COLL-10 and PLA/m-ELL-COLL-40 which are listed in Table 4.8, PLA/ELL-COLL-10 demonstrated greater thermal stability than PLA/m-ELL-COLL-40, with a maximum degradation temperature of 345.9 ^{o}C, making it the best candidate to act as the carrier for the dispersion of single and composite NPs into PLA matrix.this phenomena is attributed to the formation of localaized protein in the PLA/m-ELL-COLL-40 composite film, which resulted

in thermal relaxing. The other reason might be as the concentration of m-ELL-COLL increased the matrix started to act as plastiscizer which might also made the PLA/m-ELL-COLL-40 composite film to degrade rapidly than the other composite films.

Table 4.8: Thermal characteristics of neat PLA, PLA/ELL-COLL-10, and PLA/ELL-COLL-40

Films	T_{10} (^{o}C)	T_{90} (^{o}C)	T_{max} (^{o}C)
Neat PLA	141.7	376.1	361.05
PLA/m-ELL-COLL-10	200	355.76	345.9
PLA/m-ELL-COLL-40	174	331.2	306

4.6.2. Effect of Ag/ZnO nanocomposite (as filler) on the thermal stability of PLA

The effect of Ag NPs, ZnO NPs, and Ag/ZnO NCs, as well as m-ELL-COLL, on the thermal properties of the PLA matrix in a nitrogen atmosphere, was investigated using TGA) measurement, and Figures 4.14a and 4.14b depict weight loss versus elevated temperature curves for PLA and its corresponding nanocomposites films. Thermal stabilities can be assessed by comparing temperatures at 10% mass loss (T_{10}), 90% mass loss (T_{90}), and maximum degradation temperature (T_{max}). From Figure 4.14a all the film samples showed a two-step thermal degradation pattern where the initial slight weight loss located at around 115-145 ◦C which was attributed to the evaporation of the absorbed water in the film. The second and major weight loss was observed at 281–385.28°C for the pure PLA, 232.5–307.21°C for PLA/m-ELL-COLL/Ag/ZnO-1, 212-290 °C for PLA/-ELL-COLL/Ag/ZnO-5, 211.83-291.77 °C for PLA/m-ELL-COLL/Ag/ZnO-10, 233-355°C for PLA/m-ELL-COLL/Ag-10, 208.42-291.77°C for PLA/m-ELL-COLL-ZnO-10 composite films.

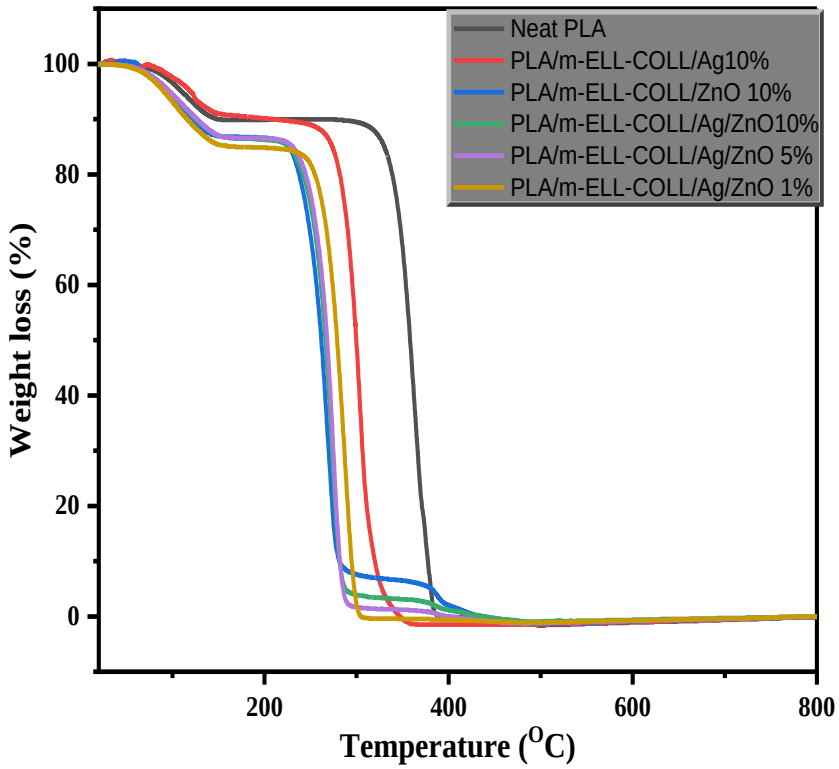

Figure 4.14a: TGA curves of Neat PLA and PLA/m-ELL-COLL/Nanoparticles composite films

The TGA results (T_{onset} and T_{endset}) revealed that, compared to neat PLA, all single and composite nanoparticles lowered the on-set and end-set temperatures of ternary films; however, the PLA/m-ELL-COLL/Ag-10 ternary film displayed better thermal stability among the single and composite nanoparticles; this may be explained by the dispersion of Ag into the PLA matrix or by the presence of more thermally stable Ag nanoparticles in the matrix. For neat-PLA and five distinct PLA-based composite films, the temperature at 10% mass loss (T_{10}) and the temperature at 90% mass loss (T_{90}) were determined from the TGA curve analysis. The T_{10} and T_{90} for PLA-based composite films, with the exception of PLA/ELL-COLL/Ag-10, displayed a declining pattern when compared with plain PLA, as shown in Table 4.9. This can be supported with the analysis of the thermal conductivity of the nanocomposite films which showed that the most stable nanocomposite film (PLA/m-ELL-COLL/Ag-10) showed the lowest thermal conductivity. The nanocomposite film with highest thermal conductivity was PLA/m-ELL-COLL/ZnO-10, this implied the catalytic activity of

ZnO.In the case of PLA/m-ELL-COLL/Ag/ZnO-5 and PLA/m-ELL-COLL/Ag/ZnO-10, the thermal conductivity analysis revealed that the former composite film had higher value than the latter. This can be related to lower value of T_{10} (◦C) for PLA/m-ELL-COLL/Ag/ZnO-5 film. Generally the thermal conductivity of the films showed that thermally stable films would have lower thermal conductivity than the films with lower thermal stability, detailed explanation of thermal conductivity can be found in **Appendix** 12.

Table 4.9: TGA analysis for selected weight loss and maximum degradation

FILMS	**T_{10} (◦C)**	**T_{90}(◦C)**	**T_{max}(◦C)**
Neat PLA	141.7	376.1	361.05
PLA/m-ELL-COLL/Ag-10	144.2	320.16	302.7
PLA/m-ELL-COLL/ZnO-10	114.2	279.73	269.3
PLA/m-ELL-COLL/Ag/ZnO-10	126.3	298.4	271.49
PLA/m-ELL-COLL/Ag/ZnO-5	124.4	281.73	274.5
PLA/m-ELL-COLL/Ag/ZnO-1	116	294.6	280.2

Form Figure 4.14b (DTG curve) the maximum degradation temperature for neat PLA and PLA/m-ELL-COLL/Ag, ZnO, Ag/ZnO ternary composite films were obtained. The results showed that the incorporation of the single and composite nanoparticles shifted the degradation of PLA to lower temperatures, the maximum degradation temperature ranged from 361.5 °C to 269.3 °C. The maximum degradation temperature has shown a decreasing pattern especially comparing the maximum degradation temperature of neat PLA and PLA/m-ELL-COLL-ZnO-10 there was a significant difference which was around 91.75 °C, and a similar decrease in thermal stability with the addition of metal oxides like MgO was reported in other studies (Swaroop et al., 2019).

The lower maximum degradation rate of this PLA/m-ELL-COLL-ZnO-10 ternary film implied the catalytic activity of ZnO NP was higher when compared to Ag and Ag/ZnO single

and composite nanoparticles (Tarani et al.,2021). Furthermore, at high-temperature settings, zinc compounds catalyze the intermolecular transesterification processes that result in PLA with smaller molecular weights as well as the "unzipping" depolymerization that, in the end, results in the selective production of lactic acid (yu et al., 2021).The other incident observed from the DTG curve is the occurrence of two degradation peaks which might be attributed to the degradation of the m-ELL-COLL and PLA matrix, respectively.

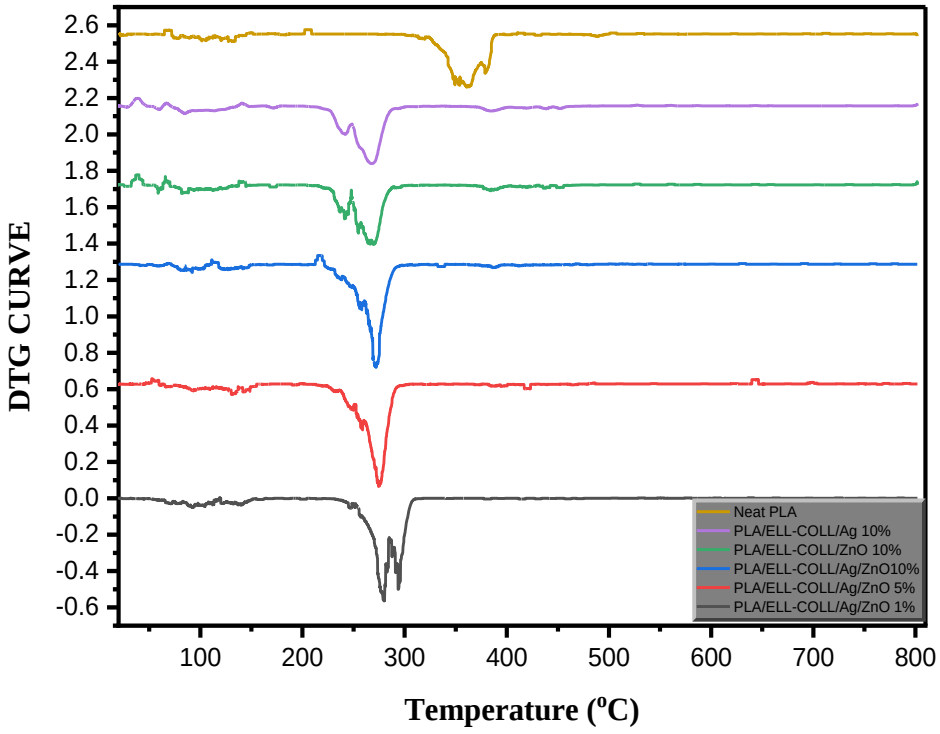

Figure 4.14b: DTG curves of Neat PLA and PLA/m-ELL-COLL/Nanoparticles composite films

4.7. Mechanical properties of PLA/ELL-COLL films

The intermolecular forces of the polymerizing chains, the ratio of constituent makeup, the additives added to the film, and environmental factors all affect the mechanical properties of the films. Tensile strength, elongation at break, and Young's modulus are the three most crucial metrics for assessing mechanical qualities. Due to the following factors, it is crucial to enhance the mechanical characteristics of biodegradable films.

- Due to the tension of the film, the high mechanical strength of the film makes it more difficult to cause mechanical damages like perforation and maintains the film's resistance to gases and moisture.
- The film's high degree of elasticity makes it possible for it to readily serve as a packaging material and fit the shape of the food without breaking.

Mechanical testing was done to see how the addition of m-ELL-COLL could affect the mechanical properties of the PLA polymer matrix. Table 4.10 displays the mechanical characteristics of PLA/m-ELL-COLL composite films made of polylactic acid at four levels of 0 %., 10 %., 20 %., 30 %., and 40 %. For mechanical characteristics like tensile strength, elongation at break, and Young's modulus, sample values were taken into account.

The tensile strength is depicted in Figure 4.15 according to the graph, poly-lactic acid films with a 30% elastin/collagen matrix have a tensile strength of 32.25 MPa, whereas pure poly-lactic acid films have a tensile strength of 67 MPa. Tensile strength of the neat and composite films was trending downward (from 67 MPa to 33.7 MPa), which may be related to the protein matrix's impact on the elongation of the film, which causes a drop in tensile strength as protein matrix loading increases This trend was the same until the loading reaches 40%, here the trend shifted to the increasing pattern yet the increment was not significant. For maximum loading of the protein matrix, the TS significantly decreased up to 98.8% compared to neat PLA

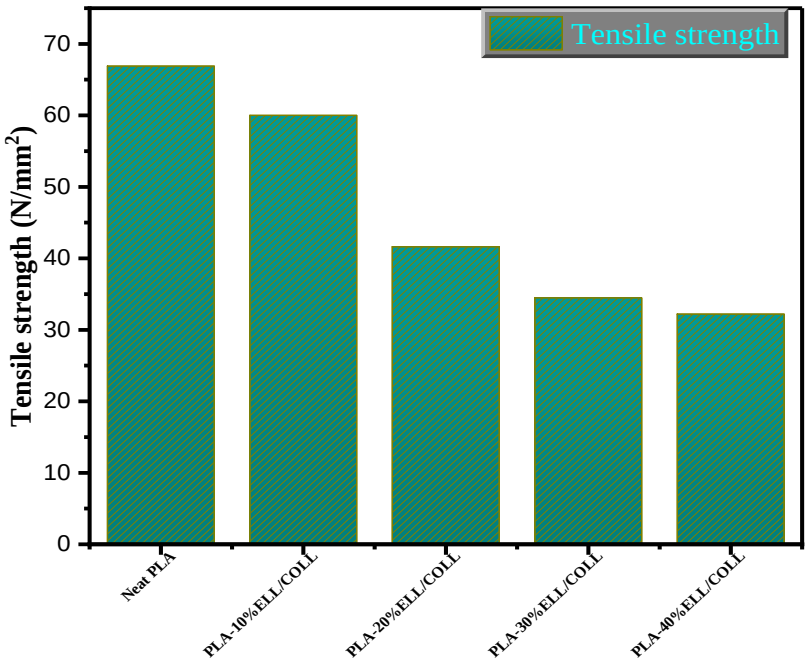

Figure 4.15: Tensile strength for neat PLA and PLA/m-ELL-COLL (10%, 20%,30%,40%) with annealing

The intermolecular mixing between the PLA and protein matrix was found to be reduced as the concentration of the additive (m-ELL-COLL) tended to be increased, and the other factor was that, because the additive was identified as an plasticsizer because it is composed from elastin as well, it was obvious that as the concentration of the additive was increasing the tensile strength would be decreased. These two factors were the crucial reasons why the tensile strength of the film was decreasing.

Díez-Pascual et al.,(2014), stated that the degree of crystallization can be directly related to the tensile strength of particular composite films. From the composite films (neglecting neat PLA) the tensile strength of the poly-lactic acid films with a 10% elastin/collagen matrix was higher. For this phenomenon the possible reason behind this its highest degree of crystallinity compared to the othercomposite films. These phenomena can be seen from DSC analysis.

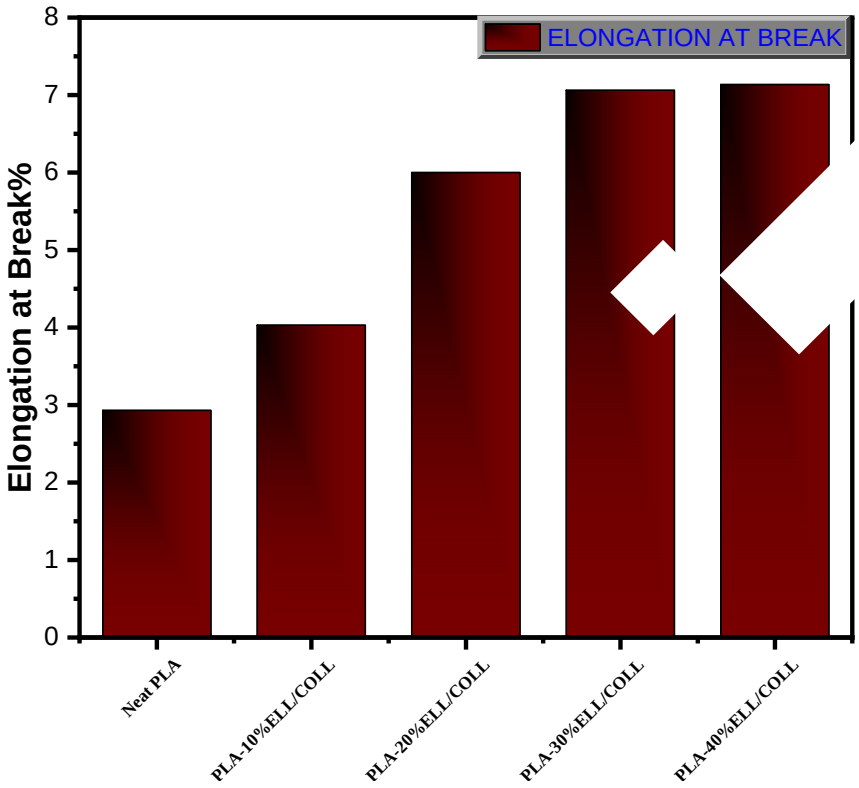

Figure 4.16: Elongation at the break for neat PLA and PLA/m-ELL-COLL (10%, 20%,30%,40%) with annealing

In Figure 4.16, for these various composite films, elongation at the breakpoint was preferred over tensile strength. The composite films with different protein loading rates (10% - 40%) showed a significant improvement in elongation at break, which ranged from 36.7% for PLA-/m-ELL-COLL 10% to 143.1% for PLA-/m-ELL-COLL 40% compared to neat PLA. As the rate at which the protein matrix loading increased, so did the elongation at the breaking point. This could be due to the m-ELL-COLL matrix's plasticizing effect, which facilitated the PLA film's chain mobility. According to this, hydrogen bonds were formed between the amino groups of m-ELL-COLL and the OH groups of PLA. The natively ordered hydrogen bond connections of the PLA chains were disrupted by these m-ELL-COLL hydrogen interactions. The improvement in elongation at the breakpoint of the PLA-/m-ELL-COLL composite films makes it more promising for practical application

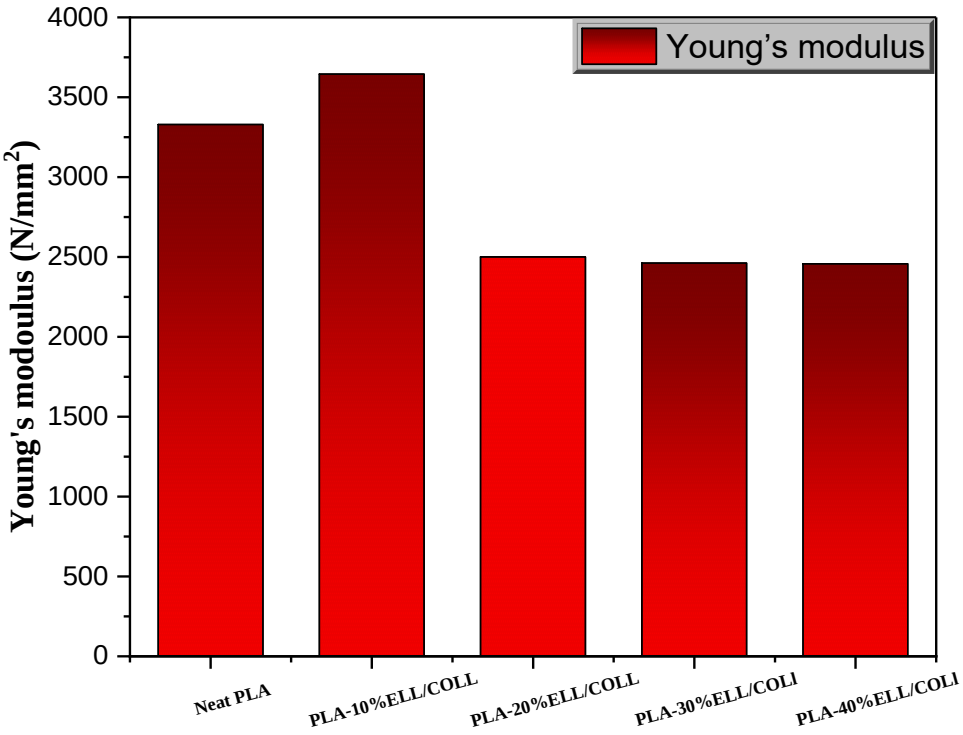

Figure 4.17: Young's modulus break for neat PLA and PLA/m-ELL-COLL (10%, 20%,30%,40%) with annealing

The young's modulus for the neat PLA and PLA/m-ELL-COLL composite film is shown in Figure 4.17, from the mechanical property analysis, the young's modulus increased by 9.5% when the PLA was incorporated with 10% of m-ELL-COLL matrix, this increment was due to the increased interaction area between PLA and protein matrix along with higher crystallinity of PLA in nanocomposites. But as the loading rate of the ELL-COLL matrix increases, there was a significant reduction in modulus. The significant fall in modulus value at 20 - 40 wt% m-ELL-COLL loading explained the possibility of agglomerations of localized protein molecules which reduces the intermolecular mixing between PLA and ELL-COLL matrix and entanglements of ELL-COLL at higher loading (Baheti et al., 2013). This phenomenon is directly related to the decrement pattern in crystallization and tensile strength of the composite film as the loading rate increases.

Table 4.10: Elongation at break, tensile strength, and young's modulus of neat PLA and PLA/m-ELL-COLL composite film with different loading

Sample name	Elongation at break (%)	Young's Modulus ($N/mm^{2)}$	Stress at break (N/mm^2)
Neat PLA	2.935 ± 0.827	3328.817	66.958 ± 7.917
PLA/m-ELL-COLL-10%	36.7 ± 0.436	3644.383	60.202 ± 1.657
PLA/m-ELL-COLL-20%	105.9 ± 0.803	2499.455	34.472 ± 0.985
PLA/m-ELL-COLL-30%	140.6 ± 2.952	2461.604	32.252 ± 3.328
PLA/m-ELL-COLL-40%	143.1	2456.595	33.757 ± 4.16

In general, the effect of the ELL-COLL matrix on the mechanical properties of PLA was analyzed by computing tensile strength, elongation at break, and young's modulus of the composite film. It can be concluded that the protein matrix favored the elongation at the break of composite film on the contrary the tensile strength and young's modulus decreased as the loading rate of the protein matrix increased.

4.7.1. Effect of annealing temperature on the mechanical property of PLA/ELL-COLL composite film

The effect of temperature on the mechanical property of m-ELL-COLL dispersed PLA biofilms were studied in terms of how the biofilm's mechanical properties were affected and what would be the possible reason behind these phenomena. As it is shown below in Figure 4.18 the elongation at break for PLA/10%-ELL-COLL composite film was higher for the film

analyzed under no thermal effect (without annealing) this might be due to the intermolecular interaction between m-ELL-COLL and PLA might be favored i.e no localized protein was there that halt the effect of the m-ELL-COLL matrix, which facilitated the elasticity properties of m-ELL-COLL on the PLA. Whereas the other possibility might be since there was no thermal effect, the nucleation effect of m-ELL-COLL was not facilitated, this nucleation effect is the main factor in enhancing tensile strength but here the tensile strength was lower than that of elongation at break.

On contrary in case of the tensile strength of the composite films, it was favored when the film was annealed, this might be due to the favored nucleation effect of the m-ELL-COLL matrix on the PLA these phenomena were supported with a high degree of crystallinity, while the film that was not annealed showed lower tensile strength. The presence of stable nucleation sites and an increase in chain mobility upon annealing facilitated crystallization which leads up to higher tensile strength (Ghassemi et al.,2017; Simmons et al.,2019).

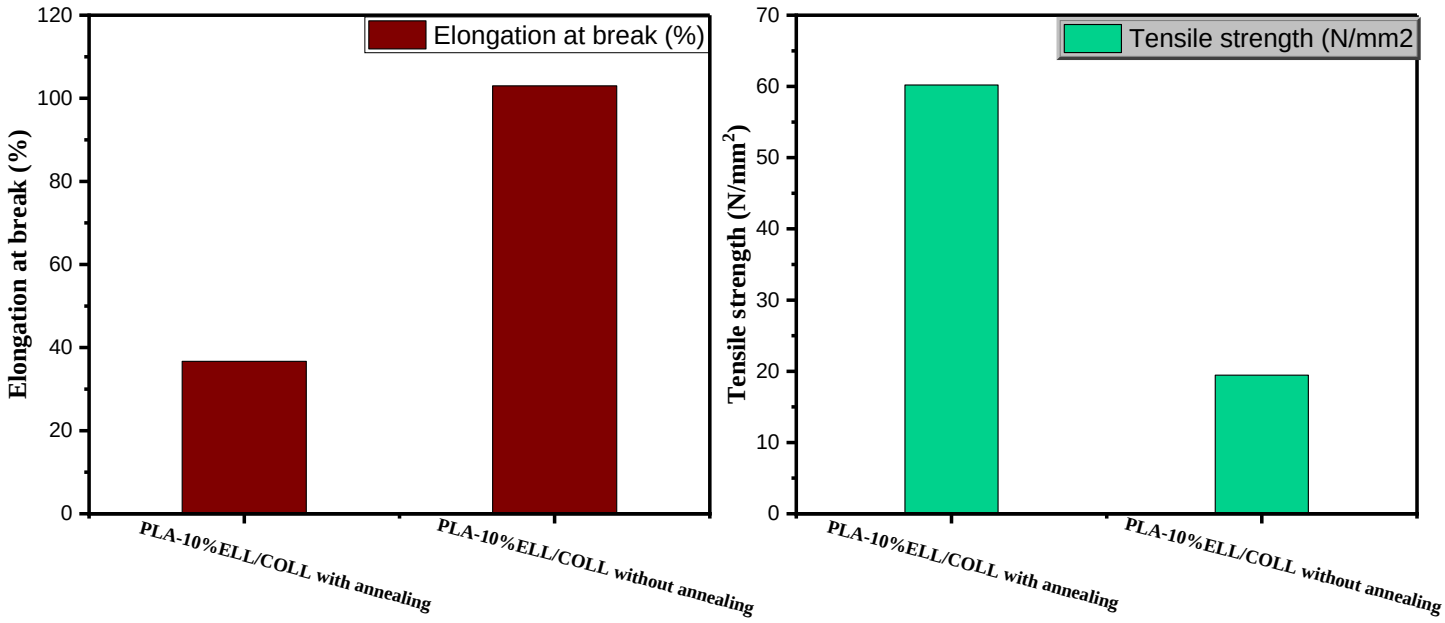

Figure 4.18: Elongation at break and Tensile strength for PLA/10%-m-ELL-COLL with and without annealing

In the same manner, the effect of annealing temperature for the PLA/40%-m-ELL was studied which resulted in higher elongation at break and higher stress at the break were observed for the bio-film that was annealed. As it is shown in Figure 4.19 the elongation at break of annealed PLA/40%-m-ELL-COLL composite film was favored over that of the unannealed PLA/40%-m-ELL-COLL composite film, this might be due to the localized proteins were gone through some thermal relaxing due to the effect of temperature and played as a plasticizer. In the case of tensile strength, the effect of annealing temperature is always related to a higher degree of crystallinity. As the films passed through some thermal process the nucleation effect of the m-ELL-COLL might be favored which resulted in higher tensile strength.

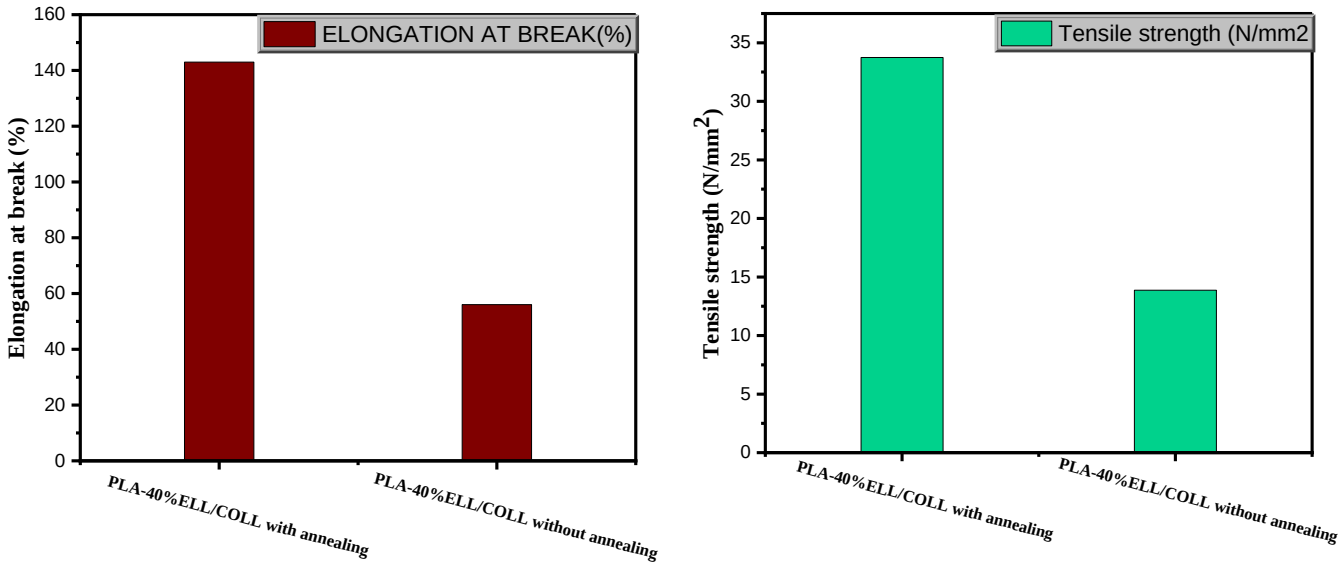

Figure 4.19: Tensile strength and elongation at break for PLA/40%-m-ELL-COLL/OLLA with and without annealing

In general, comparing PLA/10%-m-ELL-COLL and PLA/40%-m-ELL-COLL composite film with and without annealing, there was a significant difference in tensile strength as well as in elongation at the breakpoint. The tensile strength of both bio-films was favored with annealing process due to formation of more crystalline sites in the matrix due to nucleating activity of m-ELL-COLL matrix, but in the case of elongation at break point, PLA/10%-m-ELL-COLL

shown higher elongation at the break while it was analyzed without the application of thermal process (without annealing) due to favored intermolecular interaction between PLA and ELL-COLL matrix. On the contrary PLA/40%-m-ELL-COLL terinary films elongation at break were higher when it is annealed, hereby among PLA/10%-m-ELL-COLL and PLA/40%-m-ELL-COLL composite films, a higher tensile and elongation were possessed by PLA/10%-ELL-COLL when with and without annealing,respectively.

4.8. Antibacterial activity

In recent years, there has been a lot of discussion about the inclusion of antibacterial chemicals in food packaging materials. In this regard, neat PLA, m-ELL-COLL/PLA, and Ag/ZnO NCs and Ag and ZnO NPs dispersed m-ELL-COLL/PLA nanocomposite films' antibacterial properties were assessed against two gram-negative *E. coli*, *P. aeruginosa,* and two gram-positive bacterias *S. aureus, S. payogen* at different percentages of Ag/ZnO NCs in the m-ELL-COLL/PLA matrix, and Ag and ZnO NPs were used as a comparison against the antimicrobial effect of Ag/ZnO. As shown in Figure 4.20 the inhibition zone around neat PLA film was 8 mm for *E. coli,* 8.5 mm against *S. aureus,* 8 mm *against P. aeruginosa,* and 9 mm against *S. payogen,* and also in the same manner 10 wt%-m-ELL-COLL/PLA showed an inhibition zone around 7 mm, 8 mm, 7 mm and 8 mm against *E. coli, S. aureus, P. aeruginosa,* and *S. payogen* respectively.

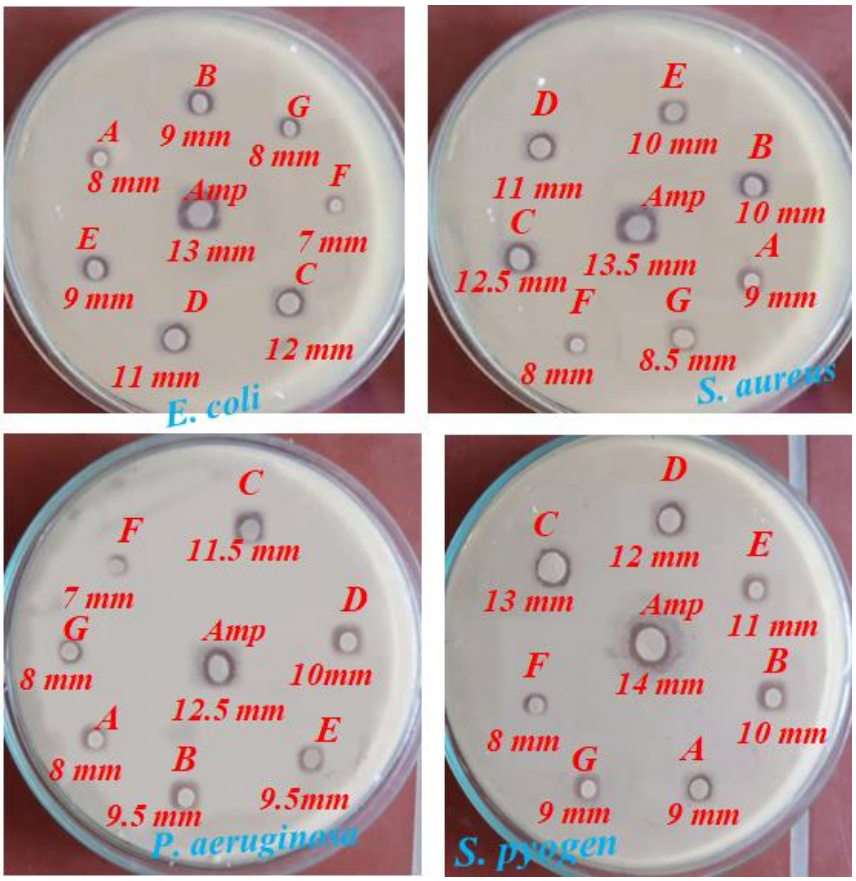

Figure 4.20: Inhibition zone of neat PLA(G), ELL-COLL/PLA film (F), and nanocomposite films (A-E)

The antibacterial activity of nanoparticles and nanocomposites against bacteria is analyzed by considering the cell wall structure of bacteria and the surface structure (modification) of PLA-NPs composite films. And also the percentage of loading NPs to the PLA polymermatrix is the crucial factor. The inhibition zones around the PLA/m-ELL-COLL-Ag/ZnO NCs films squares were formed, and they ranged from 9 to 12 mm against *E. coli*, from 10 to 12.5 mm against *S. aureus*, from 9.5 to 11.5 mm against *P. aeruginosa*, and 11 to 13 mm against *S. payogen*, respectively for 1, 5 and 10 wt% of Ag/ZnO. This suggests that the PLA/m-ELL-COLL-Ag/ZnO NCs films have good antibacterial activity which might arise from synergetic effect of Ag and ZnO NPs in the composite.

From Table 4.11, the antibacterial activity of the Ag/ZnO was higher for gram-positive bacterias than that of gram-negative bacterias this result aligned with the previous study

(Charoensri et al., 2021).When NCs (at a total of 10% weight) was integrated into the m-ELL-COLL/PLA matrix, the development of both S. payogen and S. aureus was more effectively slowed (i.e. 92-93 %) than when solo NP at the same weight did (66-74 % reduction). The result revealed that antibacterial activity by utilizing Ag and ZnO combinations will have synergistic antibacterial effects when compared to the individual components' effects. These nanocomposites' antibacteria activities might include the breakdown of the lipopolysaccharide cell wall, resulting in enhanced cell permeability, as well as attachment to receptors and respiratory enzymes in the lipopolysaccharide membrane.

Most bacteria's cell membranes include polymers with electronegative chemical groups, allowing them to absorb metallic cations. Thus, it has been proposed that the membrane is the place where certain metals exhibit bactericidal toxicity and, another explanation is that DNA damage stops the bacterium from reproducing and interferes with the activity of the ribosome, preventing the generation of energy cycle enzymes that aligned with various types of literature proposed ideas (Peighambardoust et al.,2019; Seth et al.,2021).

Certainly, both ZnO and Ag are responsible for the antibacterial activity in polymer nanocomposites. The antibacterial activity increases as Ag^{+} and Zn^{+2} are gradually released from the Ag/ZnO NCs. Generally, differences in cell surface structure and composition were thought to be the cause of the variable behavior against the various species of bacteria in which these released ions (Ag^{+} and Zn^{+2}) reacted with the cell wall, membrane, and intracellular components and as a result, they could oxidize proteins, lipids in which the cell wall of the bacterias was built and result in antibactericidal effect.

Table 4.11: Antimicrobial activity of Neat PLA and composite films

Bacteria type	**Bacteria name**	**The concentration of Ag/ZnO (%Wt)**	**Ag/ZnO NCs zone of Inhibition zone (mm)***	**% Activity of Ag/ZnO compared with that of Ampicillin**	**Concentration (%Wt)**	**Ag, ZnO and Ag/ZnO zone of Inhibition zone (mm)***	**% Activity of Ag, ZnO and Ag/ZnO compared with that of Amoxicillin**
Gram-negative	Escherichia coli ATCC25922	Ampicillin**	13	-	Ampicillin**	13	-
		Neat PLA (G)	8	61.5	10 wt%-m-ELL-COLL/PLA (F)	7	53.8
		Ag/ZnO-1 %(E)	9	69.23.	Ag -10 wt% (A)	9	69.2
		Ag/ZnO-5 % (D)	11	84.6	ZnO-10 wt% (B)	8	61.5
		Ag/ZnO-10 % (C)	12	92.3	Ag/ZnO-10 wt% (C)	12	92.3
	Pseudomonas aeruginosa	Ampicillin**	12.5	-	Ampicillin**	12.5	-
		Neat PLA (G)	8	64	10 wt%-m-ELL-COLL/PLA (F)	7	56
		Ag/ZnO-1 % (E)	9.5	76	Ag -10 wt% (A)	9.5	76
		Ag/ZnO -5 % (D)	10	80	ZnO-10 wt% (B)	8	64

	ATCC27853	Ag/ZnO -10 % (C)	11.5	92	Ag/ZnO-10 wt% (C)	11.5	92
Gram-positive	Staphylococcus aureus ATCC25923	Ampicillin**	13.5	-	Ampicillin**	13.5	-
		Neat PLA (G)	8.5	65.4	10 wt%-m-ELL-COLL/PLA (F)	8	59.25
		Ag/ZnO-1 % (E)	10	74.4	Ag -10 wt%	10	74.3
		Ag/ZnO-5 % (D)	11	81.48	ZnO-10 wt% (B)	9	66.6
		Ag/ZnO-10 % (C)	12.5	92.6	Ag/ZnO-10 wt% (C)	12.5	92.6
	Streptococcus pyogenes ATCC19615	Ampicillin**	14	-	Ampicillin**	14	-
		Neat PLA (G)	9	64.3	10 wt%-m-ELL-COLL/PLA (F)	8	57.14
		Ag/ZnO-1 % (E)	11	78.5	Ag -10 wt% (A)	9	64.3
		Ag/ZnO-5 % (D)	12	85.7	ZnO-10 wt% (B)	10	74.3
		Ag/ZnO-10 % (C)	13	92.85	Ag/ZnO-10 wt% (C)	13	92.85

5. CONCLUSIONS AND RECOMMENDATIONS

5.1. Conclusions

Extra-cellular protiens which are found in broiler skin was extracted and modified through grafting using lactic acid (LA). In order to analyze the formation of ELL-COLL matrix and how it was modified, FTIR analysis was performed. The ananlysis results revealed that the formation of ELL-COLL matrix was confirmed by the Amide I, II and III characterstics peaks. While dealing with the grafted and ungrafted ELL-COLL matrix the formation of broad peaks have proved that the polycondensation reaction resulted in the formation of amide bond.

The synthesis of Ag NPs, ZnO NPs and Ag/ZnO NCs was performed through chemical method and the formation and characterstics of the above-mentioned NPs and NCs was confirmed by using XRD, UV-VIS, FTIR and also the size of the nanomaterials confirmed by PSDA.The XRD results revealed that there was no shift on the characterstics peaks of ZnO when Ag/ZnO formed where as the average crystalline size of Ag, ZnO and Ag/ZnO NCs are 30.34 nm, 29.38 nm, 24.96 nm, respectively. The particle size distribution was 96.14 nm, 13.54 nm and 76.6 nm for Ag, ZnO and Ag/ZnO NCs, respectively.Binary(PLA/m-ELL-COLL) and ternary (PLA/m-ELL-COLL-Ag/ZnO) composite films were prepared using solution casting method and the films were characterized using DSC, TGA, UTM and disc fusion method for antimicrobial activity of the films. For PLA/m-ELL-COLL composite films the crystalization effect of m-ELL-COLL matrix was studied and resulted in 51.3% degree of crystalinity with 10% wt loading rate where as the elongation at break point was improved by 143.1% with 40% wt loading rate compared to neat PLA. In the same manner for PLA/m-ELL-COLL-Ag/ZnO ternary composite films the effect of dispersed nanomaterials on crystallization, thermal properties and antimicrobial activity of the terinary films were alalyzed. The result showed 35.14% improvement in crystallization property with 1% loading of Ag/ZnO NCs when compared to neat PLA. All ternary composite films had lower thermal stability than neat PLA due to thermal conductivity of the fillers where as the inhibition zone of PLA/m-ELL-COLL-Ag/ZnO-10 was 13 and 12.5 mm for Streptococcus pyogenes and Staphylococcus aureus respectively . From this study it can be concluded that both m-ELL-

COLL and Ag/ZnO were a good candidate in enahancing crystallization, mechanical and antimicrobial activity of PLA.

5.2. Recommendation

In this study, both products, the Ag/ZnO NCs and the ELL-COLL matrix, were successfully produced. The degradability and compatibility of the ELL-COLL matrix, which was created from organic materials, allowed it to be used as a carrier matrix dispersion of Ag/ZnO NCs into PLA matrix and a nucleating agent for the crystallization property of PLA matrix. Ag/ZnO NCs dispersed PLA composite films have shown great improvement when compared to neat PLA. Considering the afformentioned effect of ELL-COLL matrix and Ag/ZnO NCs the following reccomendations will be a good research areas to focus on.

- The effect of NCs on the mechanical property of PLA will be a good research area.
- Even though these NCs posses an attractive antimicrobial activity their migration have to be controlled, so studying the migration/release kinetics of these NCs would also be a good task to do.
- With the obtained mechanical , thermal and antimicrobial properties of the film, it can be a good candidate for packaging application, so water-vapour ,air permeability and degradiability should be studied.
- The dispersion of m-ELL-COLL and Ag/ZnO into the PLA matrix should be analysed and studied using SEM and TEM.
- Thermal conductivity of the ELL-COLL/Ag/ZnO, Ag and ZnO-PLA Nano composite have shown good results but detailed study on thermal conductivity is required.

REFERENCES

Abay, A. K., Gebeyehu, M. B., Lin, H. K., Lin, P. C., Lee, J. Y., Wu, C. M., ... & Chiang, T. C. (2016). Preparation and characterization of poly (lactic acid)/recycled polypropylene blends with and without the coupling agent, n-(6-aminohexyl) aminomethyltriethoxysilane. *Journal of Polymer Research*, *23*(9), 1-12.

Abdel Gawad, O. F. (2020). Graft modification of carboxymethyl chitosan with styrene and its biological applications. *Beni-Suef University Journal of Basic and Applied Sciences*, *9*(1), 1-15.

Ahmed, D. S., Mohammed, M. R., & Mohammed, M. K. (2020). Synthesis of multi-walled carbon nanotubes decorated with ZnO/Ag nanoparticles by co-precipitation method. *Nanoscience & Nanotechnology-Asia*, *10*(2), 127-133.

Al-Ajlouni, K., Fleming, P. D., & Pekarovicova, A. (2021). *Glucomannan for Food Packaging Biofilms: Faceting of the Polymer Film* (No. 6135). EasyChair.

Andrzejewski, J., & Nowakowski, M. (2021). Development of Toughened Flax Fiber Reinforced Composites. Modification of Poly (lactic acid)/Poly (butylene adipate-co-terephthalate) Blends by Reactive Extrusion Process. *Materials*, *14*(6), 1523.

Asadi, S., & Pirsa, S. (2020). Production of biodegradable film based on polylactic acid, modified with lycopene pigment and TiO 2 and studying its physicochemical properties. *Journal of Polymers and the Environment*, *28*(2), 433-444.

Atta, O. M., Manan, S., Ahmed, A. A. Q., Awad, M. F., Ul-Islam, M., Subhan, F., ... & Yang, G. (2021). Development and characterization of yeast-incorporated antimicrobial cellulose biofilms for edible food packaging application. *Polymers*, *13*(14), 2310.

Atta, O. M., Manan, S., Ahmed, A. A. Q., Awad, M. F., Ul-Islam, M., Subhan, F., ... & Yang, G. (2021). Development and characterization of yeast-incorporated antimicrobial cellulose biofilms for edible food packaging application. *Polymers*, *13*(14), 2310.

Baek, N., Kim, Y. T., Marcy, J. E., Duncan, S. E., & O'Keefe, S. F. (2018). Physical properties of nanocomposite polylactic acid films prepared with oleic acid modified titanium dioxide. *Food packaging and shelf life*, *17*, 30-38.

Baheti, V., Militky, J., & Marsalkova, M. (2013). Mechanical properties of poly lactic acid composite films reinforced with wet milled jute nanofibers. *Polymer composites*, *34*(12), 2133-2141.

Baird, G., Farrell, C., Cheung, J., Semple, A., Blue, J., & Ahl, P. L. (2020). FTIR Spectroscopy Detects Intermolecular β-Sheet Formation Above the High Temperature Tm for Two Monoclonal Antibodies. *The Protein Journal*, *39*(4), 318-327.

Bajwa, D. S., Shojaeiarani, J., Liaw, J. D., & Bajwa, S. G. (2021). Role of hybrid nano-zinc oxide and cellulose nanocrystals on the mechanical, thermal, and flammability properties of poly (lactic acid) polymer. *Journal of Composites Science*, *5*(2), 43.

Bangar, S. P., Kumar, M., & Whiteside, W. S. (2021). Mango seed starch: A sustainable and eco-friendly alternative to increasing industrial requirements. *International Journal of Biological Macromolecules*.

Bautista-Del-Ángel, J. E., Morales-Cepeda, A. B., & Wood-Adams, P. M. (2020). Compatibility, crystalinity and mechanical properties of poly (lactic acid)-poly (ether-block-amide) based copper nano-composites. *Polymer International*, *69*(10), 1024-1037.

Bax, D. V., Smalley, H. E., Farndale, R. W., Best, S. M., & Cameron, R. E. (2019). Cellular response to collagen-elastin composite materials. *Acta biomaterialia*, *86*, 158-170.

Bazrafshan, Z., & Stylios, G. K. (2019). A novel approach to enhance the spinnability of collagen fibers by graft polymerization. *Materials Science and Engineering: C*, *94*, 108-116.

Bednarek, M., Borska, K., & Kubisa, P. (2021). New polylactide-based materials by chemical crosslinking of PLA. *Polymer Reviews*, *61*(3), 493-519.

Bindhu, B., Renisha, R., Roberts, L., & Varghese, T. O. (2018). Boron Nitride reinforced polylactic acid composites film for packaging: Preparation and properties. *Polymer Testing*, *66*, 172-177.

Cacciotti, I., Fortunati, E., Puglia, D., Kenny, J. M., & Nanni, F. (2014). Effect of silver nanoparticles and cellulose nanocrystals on electrospun poly (lactic) acid mats: Morphology, thermal properties and mechanical behavior. *Carbohydrate polymers*, *103*, 22-31.

Chai, B., Wang, X., Cheng, S., Zhou, H., & Zhang, F. (2014). One-pot triethanolamine-assisted hydrothermal synthesis of Ag/ZnO heterostructure microspheres with enhanced photocatalytic activity. *Ceramics International*, *40*(1), 429-435.

Chan, L. J., Feeney, O. M., Leong, N. J., McLeod, V. M., Porter, C. J., Williams, C. C., & Kaminskas, L. M. (2017). An evaluation of optimal PEGylation strategies for maximizing the lymphatic exposure and antiviral activity of interferon after subcutaneous administration. *Biomacromolecules*, *18*(9), 2866-2875.

Chen, H., Wang, J., Cheng, Y., Wang, C., Liu, H., Bian, H., ... & Han, W. (2019). Application of protein-based films and coatings for food packaging: A review. *Polymers*, *11*(12), 2039

Chen, X., Fan, M., Tan, H., Ren, B., Yuan, G., Jia, Y., ... & Hu, X. (2019). Magnetic and self-healing chitosan-alginate hydrogel encapsulated gelatin microspheres via covalent cross-linking for drug delivery. *Materials Science and Engineering: C, 101*, 619-629.

Chou, C. T., Shi, S. C., & Chen, C. K. (2021). Sandwich-Structured, Hydrophobic, Nanocellulose-Reinforced Polyvinyl Alcohol as an Alternative Straw Material. *Polymers*, *13*(24), 4447.

Ciarfaglia, N., Laezza, A., Lods, L., Lonjon, A., Dandurand, J., Pepe, A., & Bochicchio, B. (2021). Thermal and dynamic mechanical behavior of poly (lactic acid)(PLA)-based electrospun scaffolds for tissue engineering. *Journal of Applied Polymer Science*, *138*(44), 51313.

Collazo-Bigliardi, S., Ortega-Toro, R., & Chiralt, A. (2019). Using grafted poly (ε-caprolactone) for the compatibilization of thermoplastic starch-polylactic acid blends. *Reactive and Functional Polymers*, *142*, 25-35.

Cui, C., Ji, N., Wang, Y., Xiong, L., & Sun, Q. (2021). Bioactive and intelligent starch-based films: A review. *Trends in Food Science & Technology*, *116*, 854-869.

de Azevedo Gonçalves Mota, R. C., de Menezes, L. R., & da Silva, E. O. (2021). Poly (lactic acid) polymers containing silver and titanium dioxide nanoparticles to be used as scaffolds for bioengineering. *Journal of Materials Research*, *36*(2), 406-419.

de Moraes, J. O., Scheibe, A. S., Augusto, B., Carciofi, M., & Laurindo, J. B. (2015). Conductive drying of starch-fiber films prepared by tape casting: Drying rates and film properties. *LWT-Food Science and Technology*, *64*(1), 356-366.

Di Lorenzo, M. L., & Androsch, R. (Eds.). (2018). *Synthesis, Structure and Properties of Poly (lactic acid)* (Vol. 279, pp. 1-343). Cham, Switzerland: Springer International Publishing.

Díez-Pascual, A. M., & Diez-Vicente, A. L. (2014). ZnO-reinforced poly (3-hydroxybutyrate-co-3-hydroxyvalerate) bionanocomposites with antimicrobial function for food packaging. *ACS applied materials & interfaces*, *6*(12), 9822-9834.

Ding, W., Jahani, D., Chang, E., Alemdar, A., Park, C. B., & Sain, M. (2016). Development of PLA/cellulosic fiber composite foams using injection molding: Crystallization and foaming behaviors. *Composites Part A: Applied Science and Manufacturing*, *83*, 130-139.

Ding, X., Ye, B., Dai, R., Chen, H., & Shan, Z. (2021). A graft copolymer of collagen hydrolysate obtained from chrome leather scraps for retardation in Portland cement. *Journal of Cleaner Production*, *284*, 125408.

Dogan, S. K., Boyacioglu, S., Kodal, M., Gokce, O., & Ozkoc, G. (2017). Thermally induced shape memory behavior, enzymatic degradation and biocompatibility of PLA/TPU blends:"Effects of compatibilization". *Journal of the mechanical behavior of biomedical materials*, *71*, 349-361.

Domene-López, D., García-Quesada, J. C., Martin-Gullon, I., & Montalbán, M. G. (2019). Influence of starch composition and molecular weight on physicochemical properties of biodegradable films. *Polymers*, *11*(7), 1084

Elolimy, A. A., Arroyo, J. M., Batistel, F., Iakiviak, M. A., & Loor, J. J. (2018). Association of residual feed intake with abundance of ruminal bacteria and biopolymer hydrolyzing enzyme activities during the peripartal period and early lactation in Holstein dairy cows. *Journal of animal science and biotechnology*, *9*(1), 1-10

Fadakar Sarkandi, A., Montazer, M., Harifi, T., & Mahmoudi Rad, M. (2021). Innovative preparation of bacterial cellulose/silver nanocomposite hydrogels: In situ green

synthesis, characterization, and antibacterial properties. *Journal of Applied Polymer Science*, *138*(6), 49824.

Fan, C., Chi, H., Zhang, C., Cui, R., Lu, W., Yuan, M., & Qin, Y. (2019). Effect of multiscale structure on the gas barrier properties of poly (lactic acid)/Ag nanocomposite films. *Polymers for Advanced Technologies*, *30*(7), 1709-1715.

Fan, Z., Xu, Z., Niu, H., Gao, N., Guan, Y., Li, C., ... & Guan, J. (2018). An injectable oxygen release system to augment cell survival and promote cardiac repair following myocardial infarction. *Scientific reports*, *8*(1), 1-22.

Farbod, M., Sharif, L., & Ahangarpour, A. (2021). A novel synthesis of Ag@ ZnO yolk-shell and ZnO hollow sphere nanostructures and comparison of their photocatalytic performances. *Physica B: Condensed Matter*, *613*, 412729.

Ferrández-Montero, A., Lieblich, M., González-Carrasco, J. L., Benavente, R., Lorenzo, V., Detsch, R., ... & Ferrari, B. (2019). Development of biocompatible and fully bioabsorbable PLA/Mg films for tissue regeneration applications. *Acta biomaterialia*, *98*, 114-124.

Fortunati, E., Armentano, I., Iannoni, A., & Kenny, J. M. (2010). Development and thermal behaviour of ternary PLA matrix composites. *Polymer Degradation and Stability*, *95*(11), 2200-2206.

García-Guzmán, L., Cabrera-Barjas, G., Soria-Hernández, C. G., Castaño, J., Guadarrama-Lezama, A. Y., & Rodríguez Llamazares, S. (2022). Progress in Starch-Based Materials for Food Packaging Applications. *Polysaccharides*, *3*(1), 136-177.

Garcia-Valdez, O., Champagne, P., & Cunningham, M. F. (2018). Graft modification of natural polysaccharides via reversible deactivation radical polymerization. *Progress in Polymer Science*, *76*, 151-173.

Getme, A. S., & Patel, B. (2020). A review: Bio-fiber's as reinforcement in composites of polylactic acid (PLA). *Materials Today: Proceedings*, *26*, 2116-2122.

Ghassemi, A., Moghaddamzadeh, S., Duchesne, C., & Rodrigue, D. (2017). Effect of annealing on gas permeability and mechanical properties of polylactic acid/talc composite films. *Journal of Plastic Film & Sheeting*, *33*(4), 361-383.

Girdthep, S., Limwanich, W., & Punyodom, W. (2022). Non-isothermal cold crystallization, melting, and moisture barrier properties of silver-loaded kaolinite filled poly (lactic acid) films. *Materials Chemistry and Physics*, *276*, 125227.

Goffin, A. L., Raquez, J. M., Duquesne, E., Siqueira, G., Habibi, Y., Dufresne, A., & Dubois, P. (2011). From interfacial ring-opening polymerization to melt processing of cellulose nanowhisker-filled polylactide-based nanocomposites. *Biomacromolecules*, *12*(7), 2456- 2465.

Gong, J., Li, J., Xu, J., Xiang, Z., & Mo, L. (2017). Research on cellulose nanocrystals produced from cellulose sources with various polymorphs. *RSC advances*, *7*(53), 33486-33493.

Groh, K. J., Backhaus, T., Carney-Almroth, B., Geueke, B., Inostroza, P. A., Lennquist, A. ... & Muncke, J. (2019). Overview of known plastic packaging-associated chemicals and their hazards. *Science of the total environment*, *651*, 3253-3268

Gutiérrez, T. J., Mendieta, J. R., & Ortega-Toro, R. (2021). In-depth study from gluten/PCL-based food packaging films obtained under reactive extrusion conditions using chrome octanoate as a potential food grade catalyst. *Food Hydrocolloids*, *111*, 106255.

Guzman, A., Gnutek, N., & Janik, H. (2011). Biodegradable polymers for food packaging–factors influencing their degradation and certification types–a comprehensive review.

Haghighi, H., Licciardello, F., Fava, P., Siesler, H. W., & Pulvirenti, A. (2020). Recent advances on chitosan-based films for sustainable food packaging applications. *Food Packaging and Shelf Life*, *26*, 100551

Hajizadeh, H., Peighambardoust, S. J., Peighambardoust, S. H., & Peressini, D. (2020). Physical, mechanical, and antibacterial characteristics of bio-nanocomposite films loaded with Ag-modified SiO2 and TiO2 nanoparticles. *Journal of food science*, *85*(4), 1193-1202.

Hamad, K., Kaseem, M., Yang, H. W., Deri, F., & Ko, Y. G. (2015). Properties and medical applications of polylactic acid: A review. *Express Polymer Letters*, *9*(5).

Hasan, I., Wang, J., & Tajvidi, M. (2021). Tuning physical, mechanical and barrier properties of cellulose nanofibril films through film drying techniques coupled with thermal compression. *Cellulose*, *28*(18), 11345-11366.

He, X., Lu, W., Sun, C., Khalesi, H., Mata, A., Andaleeb, R., & Fang, Y. (2021). Cellulose and cellulose derivatives: Different colloidal states and food-related applications. *Carbohydrate Polymers*, *255*, 117334.

Heydarkhan-Hagvall, S., Schenke-Layland, K., Dhanasopon, A. P., Rofail, F., Smith, H., Wu, B. M., ... & MacLellan, W. R. (2008). Three-dimensional electrospun ECM-based hybrid scaffolds for cardiovascular tissue engineering. *Biomaterials*, *29*(19), 2907-2914.

Hsueh, Y. H., Hsieh, C. T., Chiu, S. T., Tsai, P. H., Liu, C. Y., & Ke, W. J. (2019). Antibacterial property of composites of reduced graphene oxide with nano-silver and zinc oxide nanoparticles synthesized using a microwave-assisted approach. *International journal of molecular sciences*, *20*(21), 5394.

Huang, Y., Wang, T., Zhao, X., Wang, X., Zhou, L., Yang, Y., ... & Ju, Y. (2015). Poly (lactic acid)/graphene oxide–ZnO nanocomposite films with good mechanical, dynamic mechanical, anti-UV and antibacterial properties. *Journal of Chemical Technology & Biotechnology*, *90*(9), 1677-1684.

Jamróz, E., Kulawik, P., & Kopel, P. (2019). The effect of nanofillers on the functional properties of biopolymer-based films: A review. *Polymers*, *11*(4), 675.

Jian, J., Xiangbin, Z., & Xianbo, H. (2020). An overview on synthesis, properties and applications of poly (butylene-adipate-co-terephthalate)–PBAT. *Advanced Industrial and Engineering Polymer Research*, *3*(1), 19-26.

Jilani, A., Ansari, M. O., ur Rehman, G., Shakoor, M. B., Hussain, S. Z., Othman, M. H. D., ... & Alshahrie, A. (2022). Phenol removal and hydrogen production from water: Silver nanoparticles decorated on polyaniline wrapped zinc oxide nanorods. *Journal of Industrial and Engineering Chemistry*, *109*, 347-358.

Jin, K., Tang, Y., Zhu, X., & Zhou, Y. (2020). Polylactic acid based biocomposite films reinforced with silanized nanocrystalline cellulose. *International Journal of Biological Macromolecules*, *162*, 1109-1117.

Kadam, A. N., Bhopate, D. P., Kondalkar, V. V., Majhi, S. M., Bathula, C. D., Tran, A. V., & Lee, S. W. (2018). Facile synthesis of Ag-ZnO core–shell nanostructures with enhanced photocatalytic activity. *Journal of industrial and engineering chemistry*, *61*, 78-86.

Kaith, B. S., Jindal, R., & Bhatia, J. K. (2011). Morphological and thermal evaluation of soy protein concentrate on graft copolymerization with ethylmethacrylate. *Journal of applied polymer science*, *120*(4), 2183-2190.

Kale, R. D., Gorade, V. G., Madye, N., Chaudhary, B., Bangde, P. S., & Dandekar, P. P. (2018). Preparation and characterization of biocomposite packaging film from poly (lactic acid) and acylated microcrystalline cellulose using rice bran oil. *International journal of biological macromolecules*, *118*, 1090-1102.

Kamthai, S., & Magaraphan, R. (2015, May). Thermal and mechanical properties of polylactic acid (PLA) and bagasse carboxymethyl cellulose (CMCB) composite by adding isosorbide diesters. In *AIP conference proceedings* (Vol. 1664, No. 1, p. 060006). AIP Publishing LLC.

Kedzior, S. A., Zoppe, J. O., Berry, R. M., & Cranston, E. D. (2019). Recent advances and an industrial perspective of cellulose nanocrystal functionalization through polymer grafting. *Current Opinion in Solid State and Materials Science*, *23*(2), 74-91.

Khan, H., Kadam, A., & Dutt, D. (2020). Studies on bacterial cellulose produced by a novel strain of Lactobacillus genus. *Carbohydrate polymers*, *229*, 115513.

Khoo, R. Z., Ismail, H., & Chow, W. S. (2016). Thermal and morphological properties of poly (lactic acid)/nanocellulose nanocomposites. *Procedia Chemistry*, *19*, 788-794.

Khosravi, A., Fereidoon, A., Khorasani, M. M., Naderi, G., Ganjali, M. R., Zarrintaj, P., ... & Gutiérrez, T. J. (2020). Soft and hard sections from cellulose-reinforced poly (lactic acid)-based food packaging films: A critical review. *Food Packaging and Shelf Life*, *23*, 100429.

Khouri, J., Penlidis, A., & Moresoli, C. (2019). Viscoelastic properties of crosslinked chitosan films. *Processes*, *7*(3), 157.

Kim, I., Viswanathan, K., Kasi, G., Sadeghi, K., Thanakkasaranee, S., & Seo, J. (2019). Poly (lactic acid)/ZnO bionanocomposite films with positively charged ZnO as potential antimicrobial food packaging materials. *Polymers*, *11*(9), 1427.

Koh, J. J., Zhang, X., & He, C. (2018). Fully biodegradable Poly (lactic acid)/Starch blends: A review of toughening strategies. *International Journal of biological macromolecules*, *109*, 99-113.

Kotlhao, K., Lawal, I. A., Moutloali, R. M., & Klink, M. J. (2019). Antifouling properties of silver-zinc oxide polyamide thin film composite membrane and rejection of 2-chlorophenol and 2, 4-dichlorophenol. *Membranes*, *9*(8), 96.

Kovalcik, A., Pérez-Camargo, R. A., Fürst, C., Kucharczyk, P., & Müller, A. J. (2017). Nucleating efficiency and thermal stability of industrial non-purified lignins and ultrafine talc in poly (lactic acid)(PLA). *Polymer Degradation and Stability*, *142*, 244-254.

Kubicek, C. P. (2016). Synthetic Biopolymers. In *Synthetic Biology* (pp. 307-335). Springer, Cham.

Kunene, K., Sabela, M., Kanchi, S., & Bisetty, K. (2020). High-performance electrochemical biosensor for bisphenol using screen-printed electrodes modified with multi-walled carbon nanotubes functionalized with silver-doped zinc oxide. *Waste and Biomass Valorization*, *11*(3), 1085-1096.

Kyomuhimbo, H. D., Michira, I. N., Mwaura, F. B., Derese, S., Feleni, U., & Iwuoha, E. I. (2019). Silver–zinc oxide nanocomposite antiseptic from the extract of bidens pilosa. *SN Applied Sciences*, *1*(7), 1-17.

Liang, F., Yuan, H., Shao, Q., & Song, W. (2018). Study of suspension grafting process of polypropylene. *Designed Monomers and Polymers*, *21*(1), 130-136.

Li, C. G., Peng, W. G., Li, Y. X., Xu, P. F., Tian, W., & Zhang, R. (2011). Thermal and mechanical properties of bagasse microcrystalline cellulose reinforced PLA composites. In *Advanced Materials Research* (Vol. 284, pp. 1786-1789). Trans Tech Publications Ltd.

Li, K., Mcgrady, D., Zhao, X., Ker, D., Tekinalp, H., He, X., ... & Ozcan, S. (2021). Surface-modified and oven-dried microfibrillated cellulose reinforced biocomposites: Cellulose network enabled high performance. *Carbohydrate Polymers*, *256*, 117525.

Li, M. X., Ren, Y., Lee, D., & Choi, S. W. (2022). Crystallization Behavior and Electrical Properties of Nanoparticle-Reinforced Poly (lactic Acid)-Based Films. *Polymers*, *14*(1), 177.

Li, S., Chen, G., Qiang, S., Yin, Z., Zhang, Z., & Chen, Y. (2020). Synthesis and evaluation of highly dispersible and efficient photocatalytic TiO2/poly lactic acid nanocomposite

films via sol-gel and casting processes. *International journal of food microbiology*, *331*, 108763.

Liu, Z., Lu, H., Zhang, H., & Li, L. (2021). Poly (vinyl alcohol)/polylactic acid blend film with enhanced processability, compatibility, and mechanical property fabricated via melt processing. *Journal of Applied Polymer Science*, 51204.

Luchese, C. L., Frick, J. M., Patzer, V. L., Spada, J. C., & Tessaro, I. C. (2015). Synthesis and characterization of biofilms using native and modified pinhão starch. *Food hydrocolloids*, *45*, 203-210.

Lv, S., Zhang, Y., Gu, J., & Tan, H. (2018). Physicochemical evolutions of starch/poly (lactic acid) composite biodegraded in real soil. *Journal of environmental management*, *228*, 223-231.

Mallegni, N., Phuong, T. V., Coltelli, M. B., Cinelli, P., & Lazzeri, A. (2018). Poly (lactic acid)(PLA) based tear resistant and biodegradable flexible films by blown film extrusion. *Materials*, *11*(1), 148.

Mallegni, N., Phuong, T. V., Coltelli, M. B., Cinelli, P., & Lazzeri, A. (2018). Poly (lactic acid)(PLA) based tear resistant and biodegradable flexible films by blown film extrusion. *Materials*, *11*(1), 148.

Mao, J., Tang, Y., Zhao, R., Zhou, Y., & Wang, Z. (2019). Preparation of nanofibrillated cellulose and application in reinforced PLA/starch nanocomposite film. *Journal of Polymers and the Environment*, *27*(4), 728-738.

Mazumder, M. A. J., Sheardown, H., & Al-Ahmed, A. (Eds.). (2019). *Functional Polymers*. Switzerland: Springer.

Mondal, K., Sakurai, S., Okahisa, Y., Goud, V. V., & Katiyar, V. (2021). Effect of cellulose nanocrystals derived from Dunaliella tertiolecta marine green algae residue on crystallization behaviour of poly (lactic acid). *Carbohydrate Polymers*, *261*, 117881.

Montes-Zavala, I., Pérez-González, M. J., Castrejón-González, E. O., Santamaría-Razo, D. A., Almendárez-Camarillo, A., Pérez, E., & Gonzalez-Calderon, J. A. (2022). Thermal and mechanical properties of poly (lactic acid) filled with modified silicon dioxide: importance of the surface area. *Polymer Bulletin*, *79*(3), 1409-1435.

Moura, J. M., Farias, B. S., Cadaval, T. R. S., & Pinto, L. A. A. (2021). Chitin/Chitosan Based Films for Packaging Applications. *Bio-based Packaging: Material, Environmental and Economic Aspects*, 69-83.

Mousavi-Kouhi, S. M., Beyk-Khormizi, A., Amiri, M. S., Mashreghi, M., & Yazdi, M. E. T. (2021). Silver-zinc oxide nanocomposite: From synthesis to antimicrobial and anticancer properties. *Ceramics International*, *47*(15), 21490-21497.

Nagasundari, S. M., Muthu, K., Kaviyarasu, K., Al Farraj, D. A., & Alkufeidy, R. M. (2021). Current trends of Silver doped Zinc oxide nanowires photocatalytic degradation for energy and environmental application. *Surfaces and Interfaces*, *23*, 100931.

Nallasamy, P., Ramalingam, T., Nooruddin, T., Shanmuganathan, R., Arivalagan, P., & Natarajan, S. (2020). Polyherbal drug loaded starch nanoparticles as promising drug delivery system: Antimicrobial, antibiofilm and neuroprotective studies. *Process Biochemistry*, *92*, 355-364.

Nazrin, A., Sapuan, S. M., Zuhri, M. Y. M., Ilyas, R. A., Syafiq, R. S. F. K. S., & Sherwani, S. F. K. (2020). Nanocellulose reinforced thermoplastic starch (TPS), polylactic acid (PLA), and polybutylene succinate (PBS) for food packaging applications. *Frontiers in chemistry*, *8*, 213.

Nilsuwan, K., Benjakul, S., & Prodpran, T. (2018). Properties and antioxidative activity of fish gelatin-based film incorporated with epigallocatechin gallate. *Food Hydrocolloids*, *80*, 212-221.

Nilsuwan, K., Guerrero, P., de la Caba, K., Benjakul, S., & Prodpran, T. (2020). Properties and application of bilayer films based on poly (lactic acid) and fish gelatin containing epigallocatechin gallate fabricated by thermo-compression molding. *Food Hydrocolloids*, *105*, 105792.

Nofar, M., Sacligil, D., Carreau, P. J., Kamal, M. R., & Heuzey, M. C. (2019). Poly (lactic acid) blends: Processing, properties and applications. *International journal of biological macromolecules*, *125*, 307-360.

Nofar, M., Salehiyan, R., & Sinha Ray, S. (2019). Rheology of poly (lactic acid)-based systems. *Polymer Reviews*, *59*(3), 465-509.

Nuruddin, M., Chowdhury, R. A., Szeto, R., Howarter, J. A., Erk, K. A., Szczepanski, C. R., & Youngblood, J. P. (2021). Structure–Property Relationship of Cellulose Nanocrystal–Polyvinyl Alcohol Thin Films for High Barrier Coating Applications. *ACS Applied Materials & Interfaces*, *13*(10), 12472-12482.

Ochoa, S., Durango-Zuleta, M. M., & Osorio-Tobón, J. F. (2021). Integrated process for obtaining anthocyanins rich-extract by ultrasound-assisted extraction and starch recovery from purple yam (Dioscorea alata): a techno-economic evaluation. *Biomass Conversion and Biorefinery*, 1-10.

Olayil, R., Prabu, V. A., DayaPrasad, S., Naresh, K., & Sreekanth, P. R. (2021). A review on the application of bio-nanocomposites for food packaging. *Materials Today: Proceedings*

Oyeyinka, S. A., Kayitesi, E., Diarra, S. S., Adedeji, A. A., Amonsou, E. O., & Singh, S. (2021). Bambara Groundnut Starch. In *Food and Potential Industrial Applications of Bambara Groundnut* (pp. 85-118). Springer, Cham.

Palai, B., Mohanty, S., & Nayak, S. K. (2021). A comparison on biodegradation behaviour of polylactic acid (PLA) based blown films by incorporating thermoplasticized starch (TPS) and poly (butylene succinate-co-adipate)(PBSA) biopolymer in soil. *Journal of Polymers and the Environment*, *29*(9), 2772-2788.

Patwa, R., Saha, N., Sáha, P., & Katiyar, V. (2019). Biocomposites of poly (lactic acid) and lactic acid oligomer-grafted bacterial cellulose: It's preparation and characterization. *Journal of Applied Polymer Science*, *136*(35), 47903.

Peighambardoust, S. J., Peighambardoust, S. H., Pournasir, N., & Pakdel, P. M. (2019). Properties of active starch-based films incorporating a combination of Ag, ZnO and CuO nanoparticles for potential use in food packaging applications. *Food packaging and shelf Life*, *22*, 100420.

Pena-Juarez, M. G., Robles-Martinez, M., Mendez-Rodriguez, K. B., Lopez-Esparza, R., Pérez, E., & Gonzalez-Calderon, J. A. (2021). Role of the chemical modification of titanium dioxide surface on the interaction with silver nanoparticles and the capability to enhance antimicrobial properties of poly (lactic acid) composites. *Polymer Bulletin*, *78*(5), 2765-2790.

Phuruangrat, A., Siri, S., Wadbua, P., Thongtem, S., & Thongtem, T. (2019). Microwave-assisted synthesis, photocatalysis and antibacterial activity of Ag nanoparticles supported on ZnO flowers. *Journal of Physics and Chemistry of Solids*, *126*, 170-177.

Puscaselu, R., Gutt, G., & Amariei, S. (2019). Biopolymer-based films enriched with stevia rebaudiana used for the development of edible and soluble packaging. *Coatings*, *9*(6), 360.

Qian, S., Zhang, H., Yao, W., & Sheng, K. (2018). Effects of bamboo cellulose nanowhisker content on the morphology, crystallization, mechanical, and thermal properties of PLA matrix biocomposites. *Composites Part B: Engineering*, *133*, 203-209.

Rajendran, R., & Mani, A. (2020). Photocatalytic, antibacterial and anticancer activity of silver-doped zinc oxide nanoparticles. *Journal of Saudi Chemical Society*, *24*(12), 1010-1024.

Ramji, V., & Vishnuvarthanan, M. (2020). Influence of NiO supported silica nanoparticles on mechanical, barrier, optical and antibacterial properties of polylactic acid (PLA) bio nanocomposite films for food packaging applications. *Silicon*, 1-8.

Rao, T. K. (2021). Synthesis and characterization of zinc oxide@ silver ferrite multiferroic nanocomposite. *Materials Today: Proceedings*, *46*, 10747-10751.

Rashidi, H., Najaf Oshani, B., Hejazi, I., & Seyfi, J. (2020). Tuning crystallization and hydrolytic degradation behaviors of poly (lactic acid) by using silver phosphate, zinc oxide and their nano-hybrids. *Polymer-Plastics Technology and Materials*, *59*(1), 72-82.

Reimer, M., & Zollfrank, C. (2021). Cellulose for light manipulation: methods, applications, and prospects. *Advanced Energy Materials*, 2003866.

Rihayat, T., Fitriyani, C. N., Siregar, J. P., Jaafar, J., & Cionita, T. (2020, April). Synthesis and characterization of PLA-Chitosan-ZnO composite for packaging biofilms. In *IOP Conference Series: Materials Science and Engineering* (Vol. 788, No. 1, p. 012045). IOP Publishing

Rodríguez-Cabello, J. C., de Torre, I. G., Ibañez-Fonseca, A., & Alonso, M. (2018). Bioactive scaffolds based on elastin-like materials for wound healing. *Advanced drug delivery reviews*, *129*, 118-133.

Rogovina, S. Z., Aleksanyan, K. V., Loginova, A. A., Ivanushkina, N. E., Vladimirov, L. V., Prut, E. V., & Berlin, A. A. (2018). Influence of PEG on mechanical properties and biodegradability of composites based on PLA and starch. *Starch-Stärke*, *70*(7-8), 1700268.

Rouf, T. B., & Kokini, J. L. (2018). Natural biopolymer-based nanocomposite films for packaging applications. In *Bionanocomposites for packaging applications* (pp. 149-177). Springer, Cham.

Salama, H. E., & Aziz, M. S. A. (2020). Optimized carboxy-methyl cellulose and guanidinylated chitosan enriched with titanium oxide nanoparticles of improved UV-barrier properties for the active packaging of green bell pepper. *International Journal of Biological Macromolecules*, *165*, 1187-1197.

Sanden, K. W., Böcker, U., Ofstad, R., Pedersen, M. E., Høst, V., Afseth, N. K., ... & Pleshko, N. (2021). Characterization of collagen structure in normal, wooden breast and spaghetti meat chicken fillets by FTIR microspectroscopy and histology. *Foods*, *10*(3), 548.

Santana, Á. L., Zabot, G. L., Osorio-Tobón, J. F., Johner, J. C., Coelho, A. S., Schmiele, M., ... & Meireles, M. A. A. (2017). Starch recovery from turmeric wastes using supercritical technology. *Journal of food engineering*, *214*, 266-276.

Schenke-Layland, K., Vasilevski, O., Opitz, F., König, K., Riemann, I., Halbhuber, K. J., ... & Stock, U. A. (2003). Impact of decellularization of xenogeneic tissue on extracellular matrix integrity for tissue engineering of heart valves. *Journal of structural biology*, *143*(3), 201-208.

Seth, M., Khan, H., & Jana, S. (2021). Antimicrobial activity study of Ag-ZnO nanoflowers synthesised from neem extract and application in cotton textiles. *International Journal of Nanotechnology*, *18*(5-8), 531-544.

Shafiee Nasab, M., Tabari, M., & Azizi, M. H. (2018). Morphological and mechanical properties of Poly (lactic Acid)/zinc oxide nanocomposite films. *Nanomedicine Research Journal*, *3*(2), 96-101.

Shankar, S., & Rhim, J. W. (2019). Effect of types of zinc oxide nanoparticles on structural, mechanical and antibacterial properties of poly (lactide)/poly (butylene adipate-co-terephthalate) composite films. *Food Packaging and Shelf Life*, *21*, 100327.

Shankar, S., Wang, L. F., & Rhim, J. W. (2018). Incorporation of zinc oxide nanoparticles improved the mechanical, water vapor barrier, UV-light barrier, and antibacterial properties of PLA-based nanocomposite films. *Materials Science and Engineering: C*, *93*, 289-298.

Sharif, S., Abbas, G., Hanif, M., Bernkop-Schnürch, A., Jalil, A., & Yaqoob, M. (2019). Mucoadhesive micro-composites: Chitosan coated halloysite nanotubes for sustained drug delivery. *Colloids and Surfaces B: Biointerfaces*, *184*, 110527.

Sharma, S., Majumdar, A., & Butola, B. S. (2021). Tailoring the biodegradability of polylactic acid (PLA) based films and ramie-PLA green composites by using selective additives. *International Journal of Biological Macromolecules*, *181*, 1092-1103

Shi, C., Zhang, L., Bian, H., Shi, Z., Ma, J., & Wang, Z. (2021). Construction of Ag–ZnO/cellulose nanocomposites via tunable cellulose size for improving photocatalytic performance. *Journal of Cleaner Production*, *288*, 125089.

Simmons, H., Tiwary, P., Colwell, J. E., & Kontopoulou, M. (2019). Improvements in the crystallinity and mechanical properties of PLA by nucleation and annealing. *Polymer Degradation and Stability*, *166*, 248-257.

Sirotkin, N. A., Gurina, D. L., Khlyustova, A. V., Costerin, D. Y., Naumova, I. K., Titov, V. A., & Agafonov, A. V. (2021). Experimental and computational investigation of polylactic acid/silver-NP nanocomposite with antimicrobial activity prepared by plasma in liquid. *Plasma Processes and Polymers*, *18*(2), 2000169.

Siva Vijayakumar, T., Karthikeyeni, S., Vasanth, S., Ganesh, A., Bupesh, G., Ramesh, R., ... & Subramanian, P. (2013). Synthesis of silver-doped zinc oxide nanocomposite by pulse mode ultrasonication and its characterization studies. *Journal of Nanoscience*, *2013*.

Suaduang, N., Ross, S., Ross, G. M., Pratumshat, S., & Mahasaranon, S. (2019). Effect of spent coffee grounds filler on the physical and mechanical properties of poly (lactic acid) bio-composite films. *Materials Today: Proceedings*, *17*, 2104-2110.

Subhan, M., Awal, M. R., Ahmed, T., & Younus, M. (2014). Photocatalytic and antibacterial activities of Ag/ZnO nanocomposities fabricated by co-precipitation method. *Acta Metallurgica Sinica (English Letters)*, *27*(2), 223-232.

Šumigin, D., Tarasova, E., Krumme, A., & Viikna, A. (2012). Influence of cellulose content on thermal properties of poly (lactic) acid/cellulose and low-density polyethylene/cellulose composites. *Proceedings of the Estonian Academy of Sciences*, *61*(3), 237-244.

Sun, C., Li, C., Li, H., Liu, M., Zheng, H., Tan, H., ... & Zhang, Y. (2022). Modified Cellulose Nanocrystals Enhanced the Compatibility Between PLA and PBAT to Prepare a Multifunctional Composite Film. *Journal of Polymers and the Environment*, 1-11.

Surya, I., Olaiya, N. G., Rizal, S., Zein, I., Sri Aprilia, N. A., Hasan, M., ... & Abdul Khalil, H. P. S. (2020). Plasticizer enhancement on the miscibility and thermomechanical properties of polylactic acid-chitin-starch composites. *Polymers*, *12*(1), 115.

Swaroop, C., & Shukla, M. (2018). Nano-magnesium oxide reinforced polylactic acid biofilms for food packaging applications. *International Journal of Biological Macromolecules*, *113*, 729-736.

Swaroop, C., & Shukla, M. (2019). Development of blown polylactic acid-MgO nanocomposite films for food packaging. *Composites Part A: Applied Science and Manufacturing*, *124*, 105482.

Tarani, E., Pušnik Črešnar, K., Zemljič, L. F., Chrissafis, K., Papageorgiou, G. Z., Lambropoulou, D., ... & Terzopoulou, Z. (2021). Cold crystallization kinetics and thermal degradation of pla composites with metal oxide nanofillers. *Applied Sciences*, *11*(7), 3004.

Tarique, J., Sapuan, S. M., & Khalina, A. (2021). Effect of glycerol plasticizer loading on the physical, mechanical, thermal, and barrier properties of arrowroot (Maranta arundinacea) starch biopolymers. *Scientific reports*, *11*(1), 1-17.

Thakur, R., Pristijono, P., Scarlett, C. J., Bowyer, M., Singh, S. P., & Vuong, Q. V. (2019). Starch-based films: Major factors affecting their properties. *International journal of biological macromolecules*, *132*, 1079-1089.

Thi, B. T. N., Ong, L. K., Thi, D. T. N., & Ju, Y. H. (2017). Effect of subcritical water pretreatment on cellulose recovery of water hyacinth (Eichhornia crassipe). *Journal of the Taiwan Institute of Chemical Engineers*, *71*, 55-61.

Tsuji, H. (2013). Poly (lactic acid). *Bio-based plastics: materials and applications*, 171-239.

Udoetok, I. A., Wilson, L. D., & Headley, J. V. (2018). Ultra-sonication assisted cross-linking of cellulose polymers. *Ultrasonics Sonochemistry*, *42*, 567-576.

Umer, M., & Abid, M. (2017). Economic practices in plastic industry from raw material to waste in Pakistan: a case study. *Asian Journal of Water, Environment and Pollution*, *14*(2), 81-90.

Vázquez, J. J., & Martínez, E. S. M. (2019). Collagen and elastin scaffold by electrospinning for skin tissue engineering applications. *Journal of Materials Research*, *34*(16), 2819-2827.

Wang, Q., He, H., Li, B., Lin, H., Zhang, Y., Zhang, J., & Wang, Z. (2017). UV–Vis and ATR– FTIR spectroscopic investigations of postmortem interval based on the changes in rabbit plasma. *PloS one*, *12*(7), e0182

Wang, S., Liu, B., Qin, Y., & Guo, H. (2021). Effects of Processing Conditions and Plasticizing-Reinforcing Modification on the Crystallization and Physical Properties of PLA Films. *Membranes*, *11*(8), 640.

Wang, W., Zhang, H., Jia, R., Dai, Y., Dong, H., Hou, H., & Guo, Q. (2018). High performance extrusion blown starch/polyvinyl alcohol/clay nanocomposite films. *Food Hydrocolloids*, *79*, 534-543.

Wang, X., Tang, Y., Zhu, X., Zhou, Y., & Hong, X. (2020). Preparation and characterization of polylactic acid/polyaniline/nanocrystalline cellulose nanocomposite films. *International journal of biological macromolecules*, *146*, 1069-1075.

Wu, D., & Hakkarainen, M. (2015). Recycling PLA to multifunctional oligomeric compatibilizers for PLA/starch composites. *European Polymer Journal*, *64*, 126-137.

Wu, S., Ning, D., Xu, D., Cheng, Y., Mondal, A. K., Zou, Q., ... & Huang, F. (2022). Preparation and characterization of super hydrophobic aerogels derived from tunicate cellulose nanocrystals. *Carbohydrate Research*, *511*, 108488.

Yang, W., Weng, Y., Puglia, D., Qi, G., Dong, W., Kenny, J. M., & Ma, P. (2020). Poly (lactic acid)/lignin films with enhanced toughness and anti-oxidation performance for active food packaging. *International journal of biological macromolecules*, *144*, 102-110.

Yu, F., Fei, X., He, Y., & Li, H. (2021). Poly (lactic acid)-based composite film reinforced with acetylated cellulose nanocrystals and ZnO nanoparticles for active food packaging. *International Journal of Biological Macromolecules*, *186*, 770-779.

Yu, M., Zheng, Y., & Tian, J. (2020). Study on the biodegradability of modified starch/polylactic acid (PLA) composite materials. *RSC Advances*, *10*(44), 26298-26307.

Yu, Z., Rao, G., Wei, Y., Yu, J., Wu, S., & Fang, Y. (2019). Preparation, characterization, and antibacterial properties of biofilms comprising chitosan and ε-polylysine. *International journal of biological macromolecules*, *141*, 545-552.

Zare, M., Namratha, K., Alghamdi, S., Mohammad, Y. H. E., Hezam, A., Zare, M., ... & Zhang, X. (2019). Novel green biomimetic approach for synthesis of ZnO-Ag nanocomposite; antimicrobial activity against food-borne pathogen, biocompatibility and solar photocatalysis. *Scientific reports*, *9*(1), 1-15.

Zarei, S., Niad, M., & Raanaei, H. (2018). The removal of mercury ion pollution by using Fe3O4-nanocellulose: Synthesis, characterizations and DFT studies. *Journal of hazardous materials*, *344*, 258-273.

Zhang, J., Cao, C., Zheng, S., Li, W., Li, B., & Xie, X. (2020). Poly (butylene adipate-co-terephthalate)/magnesium oxide/silver ternary composite biofilms for food packaging application. *Food Packaging and Shelf Life*, *24*, 100487.

Zhang, M., Shi, X., Dai, X., Huo, C., Xie, J., Li, X., & Wang, X. (2018). Improving the crystallization and fire resistance of poly (lactic acid) with nano-ZIF-8@ GO. *Journal of materials science*, *53*(9), 7083-7093.

Zhang, S., Chen, C., Duan, C., Hu, H., Li, H., Li, J., ... & Ni, Y. (2018). Regenerated cellulose by the lyocell process, a brief review of the process and properties. *BioResources*, *13*(2), 4577-4592.

Zhao, S. W., Guo, C. R., Hu, Y. Z., Guo, Y. R., & Pan, Q. J. (2018). The preparation and antibacterial activity of cellulose/ZnO composite: a review. *Open Chemistry*, *16*(1), 9-20.

Zhou, L., Ke, K., Yang, M. B., & Yang, W. (2021). Recent progress on chemical modification of cellulose for high mechanical-performance poly (lactic acid)/cellulose composite: A review. *Composites Communications*, *23*, 100548.

Zhu, L., Qiu, J., Liu, W., & Sakai, E. (2019). Mechanical and thermal properties of rice Straw/PLA modified by nano Attapulgite/PLA interfacial layer. *Composites Communications*, *13*, 18-21

APPENDIXES

Appendix -1: Particle size analyser (PSA), particle size distribution of Ag NPs

Sample Details

Sample Name:	AgNPs		
SOP Name:	CNC.sop		
General Notes:			
File Name:	goyp.dts	**Dispersant Name:**	Water
Record Number:	89	**Dispersant RI:**	1.330
Material RI:	1.59	**Viscosity (cP):**	0.8872
Material Absorbtion:	0.010	**Measurement Date and Time:**	Monday, March 21, 2022 5:03...

System

Temperature (°C):	25.0	**Duration Used (s):**	10
Count Rate (kcps):	24.1	**Measurement Position (mm):**	1.25
Cell Description:	Disposable sizing cuvette	**Attenuator:**	11

Results

			Size (d.nm):	**% Intensity:**	**St Dev (d.n...**
Z-Average (d.nm):	2361	**Peak 1:**	96.14	100.0	6.818
PdI:	1.000	**Peak 2:**	0.000	0.0	0.000
Intercept:	1.11	**Peak 3:**	0.000	0.0	0.000

Result quality : Refer to quality report

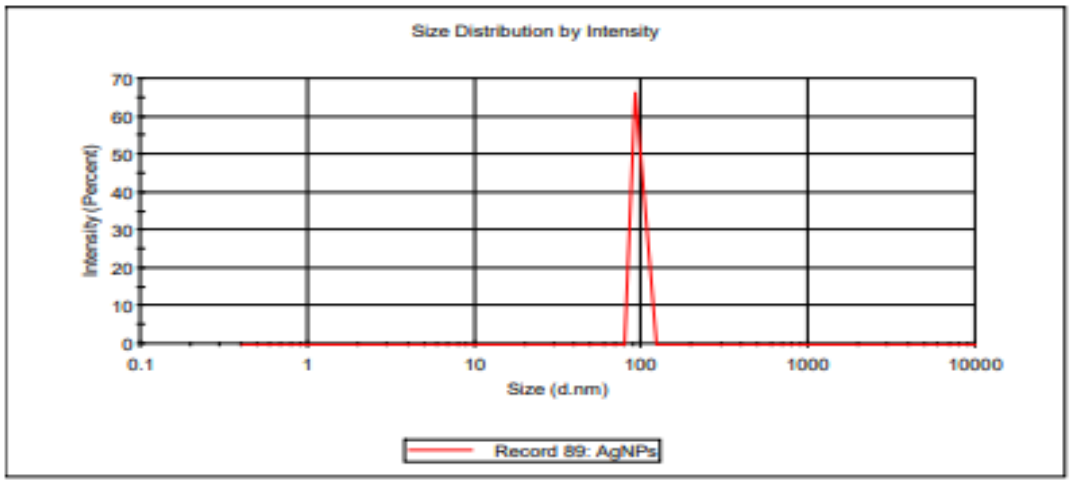

Appendix -2: Particle size analyser (PSA), particle size distribution of ZnO

Sample Name:	ZnO		
SOP Name:	CNC.sop		
General Notes:			
File Name:	Nano material.dts	**Dispersant Name:**	Water
Record Number:	284	**Dispersant RI:**	1.330
Material RI:	1.59	**Viscosity (cP):**	0.8872
Material Absorbtion:	0.010	**Measurement Date and Time:**	Wednesday, February 16, 2022.

System

Temperature (°C):	25.0	**Duration Used (s):**	450
Count Rate (kcps):	8.8	**Measurement Position (mm):**	1.25
Cell Description:	Disposable sizing cuvette	**Attenuator:**	11

Results

			Size (d.nm):	**% Intensity:**	**St Dev (d.n...**
		Peak 1:	438.7	100.0	30.66
PdI:	0.736	**Peak 2:**	0.000	0.0	0.000
Intercept:	1.07	**Peak 3:**	0.000	0.0	0.000

Result quality : Refer to quality report

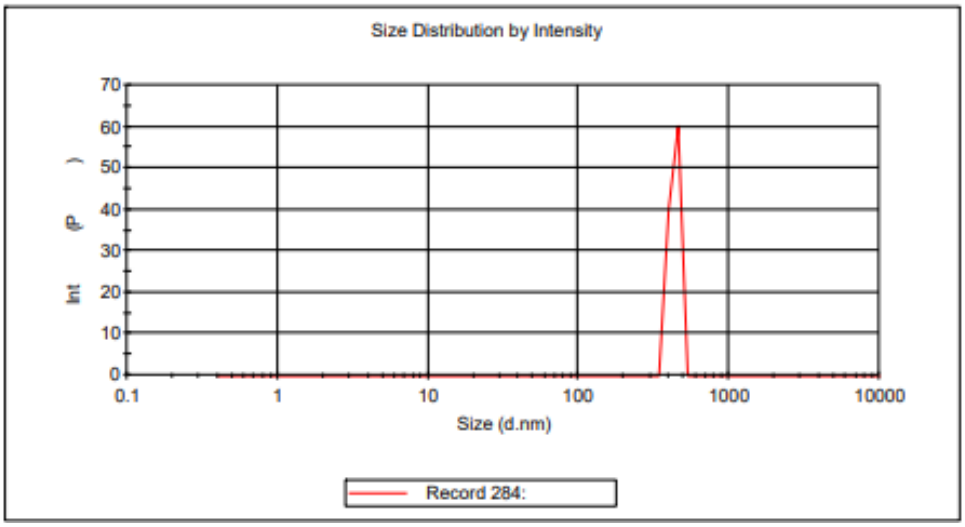

Sample Details

Sample Name: ZnO
SOP Name: mansettings.nano
General Notes:

File Name:	Nano material.dts	**Dispersant Name:**	Ethanol
Record Number:	361	**Dispersant RI:**	1.429
Material RI:	1.59	**Viscosity (cP):**	16.1118
Material Absorbtion:	0.010	**Measurement Date and Time:**	Monday, February 28, 2022 4...

System

Temperature (°C):	25.0	**Duration Used (s):**	10
Count Rate (kcps):	25.5	**Measurement Position (mm):**	3.00
Cell Description:	Disposable micro cuvette (40µl)	**Attenuator:**	11

Results

			Size (d.nm):	% Intensity:	St Dev (d.n...
Z-Average (d.nm):	79.30	**Peak 1:**	49.77	100.0	5.243
PdI:	0.602	**Peak 2:**	0.000	0.0	0.000
Intercept:	0.934	**Peak 3:**	0.000	0.0	0.000

Result quality : Refer to quality report

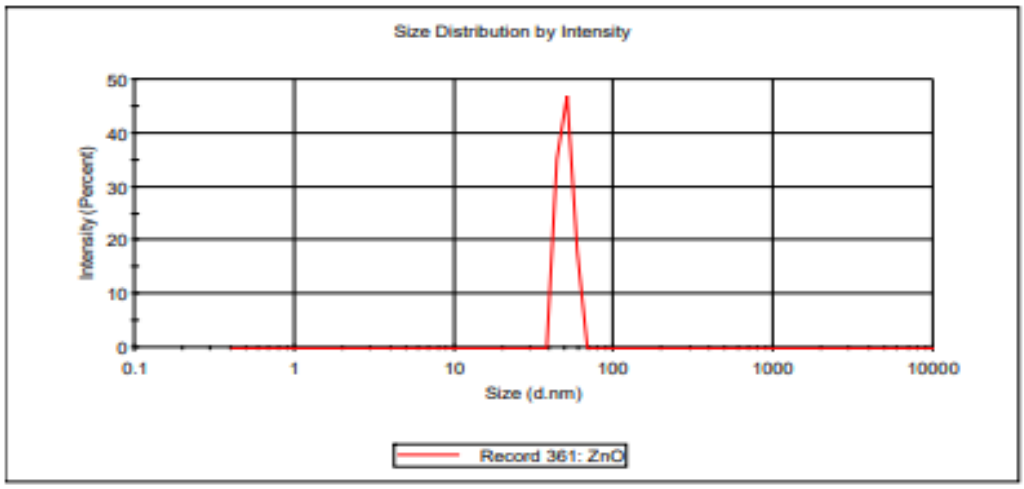

Sample Details

Sample Name: ZnO
SOP Name: mansettings.nano
General Notes:

File Name:	goyp.dls	**Dispersant Name:**	Ethanol
Record Number:	50	**Dispersant RI:**	1.390
Material RI:	1.59	**Viscosity (cP):**	2.3200
Material Absorbtion:	0.010	**Measurement Date and Time:**	Friday, March 18, 2022 2:05:...

System

Temperature (°C):	25.0	**Duration Used (s):**	20
Count Rate (kcps):	39.6	**Measurement Position (mm):**	3.00
Cell Description:	Disposable micro cuvette (40µl)	**Attenuator:**	11

Results

			Size (d.nm):	% Intensity:	St Dev (d.n...
Z-Average (d.nm):	1.663e4	**Peak 1:**	13.54	100.0	1.686e-7
PdI:	0.561	**Peak 2:**	0.000	0.0	0.000
Intercept:	1.60	**Peak 3:**	0.000	0.0	0.000

Result quality : Refer to quality report

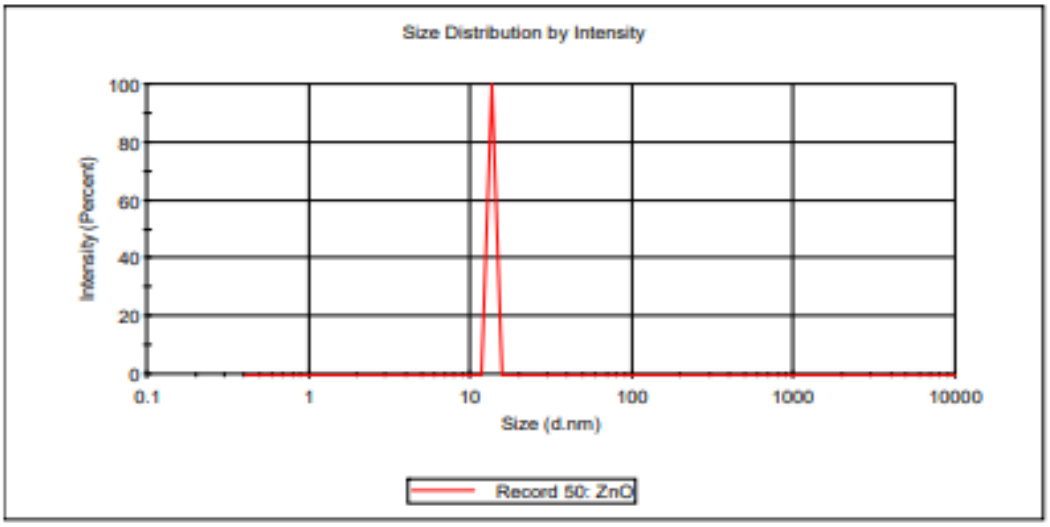

Appendix -3: Particle size analyser (PSA), particle size distribution of Ag/ZnO

Sample Details

Sample Name:	ZnO-AgNPs		
SOP Name:	CNC.sop		
General Notes:			
File Name:	Nano material.dts	**Dispersant Name:**	Water
Record Number:	285	**Dispersant RI:**	1.330
Material RI:	1.59	**Viscosity (cP):**	0.8872
Material Absorbtion:	0.010	**Measurement Date and Time:**	Wednesday, February 16, 2022.

System

Temperature (°C):	25.0	**Duration Used (s):**	450
Count Rate (kcps):	9.0	**Measurement Position (mm):**	1.25
Cell Description:	Disposable sizing cuvette	**Attenuator:**	11

Results

			Size (d.nm):	% Intensity:	St Dev (d.n...
		Peak 1:	495.8	100.0	46.58
PdI:	0.689	**Peak 2:**	0.000	0.0	0.000
Intercept:	1.03	**Peak 3:**	0.000	0.0	0.000

Result quality : Refer to quality report

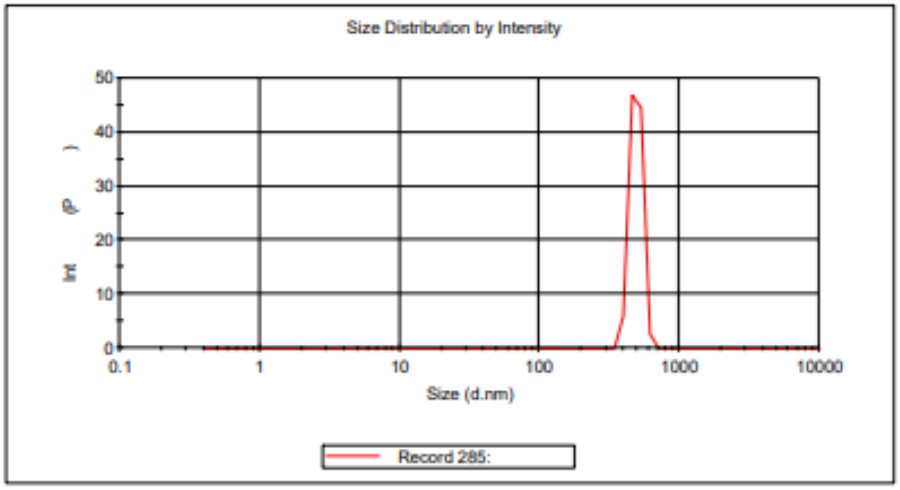

Sample Details

Sample Name: ZnO-AgNPs 1
SOP Name: mansettings.nano
General Notes:

File Name:	Nano material.dts	**Dispersant Name:**	Ethanol
Record Number:	357	**Dispersant RI:**	1.429
Material RI:	1.59	**Viscosity (cP):**	16.1118
Material Absorbtion:	0.010	**Measurement Date and Time:**	Monday, February 28, 2022 4...

System

Temperature (°C):	25.0	**Duration Used (s):**	30
Count Rate (kcps):	23.1	**Measurement Position (mm):**	3.00
Cell Description:	Disposable micro cuvette (40µl)	**Attenuator:**	11

Results

			Size (d.nm):	% Intensity:	St Dev (d.n...
Z-Average (d.nm):	102.7	**Peak 1:**	59.28	62.3	7.154
PdI:	0.718	**Peak 2:**	4505	37.7	782.4
Intercept:	0.968	**Peak 3:**	0.000	0.0	0.000

Result quality : Refer to quality report

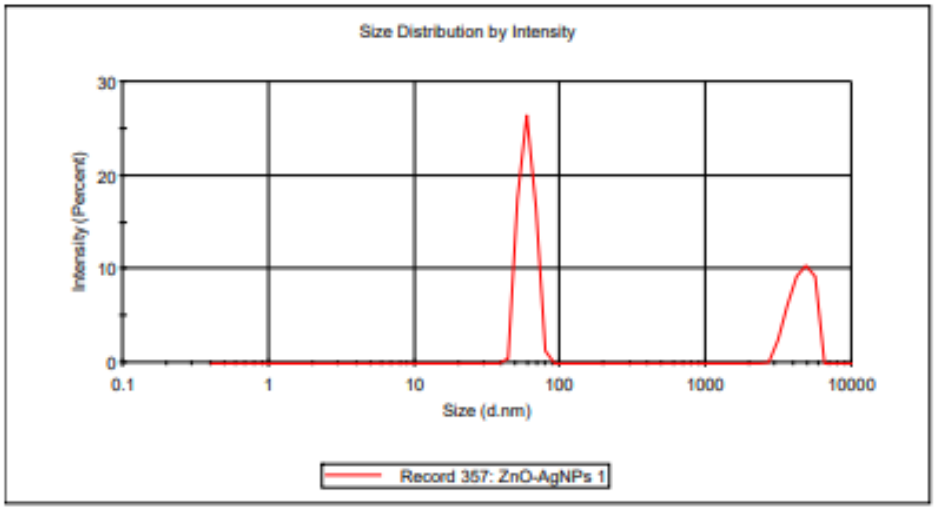

Sample Details

Sample Name: AgNPs-ZnO 1
SOP Name: mansettings.nano
General Notes:

File Name:	goyp.dts	**Dispersant Name:**	Ethanol
Record Number:	33	**Dispersant RI:**	1.390
Material RI:	1.59	**Viscosity (cP):**	2.3200
Material Absorbtion:	0.010	**Measurement Date and Time:**	Friday, March 18, 2022 2:41:...

System

Temperature (°C):	25.0	**Duration Used (s):**	10
Count Rate (kcps):	42.1	**Measurement Position (mm):**	3.00
Cell Description:	Disposable micro cuvette (40µl)	**Attenuator:**	11

Results

			Size (d.nm):	% Intensity:	St Dev (d.n...
Z-Average (d.nm):	8276	**Peak 1:**	76.76	100.0	4.233
PdI:	0.680	**Peak 2:**	0.000	0.0	0.000
Intercept:	1.55	**Peak 3:**	0.000	0.0	0.000

Result quality : Refer to quality report

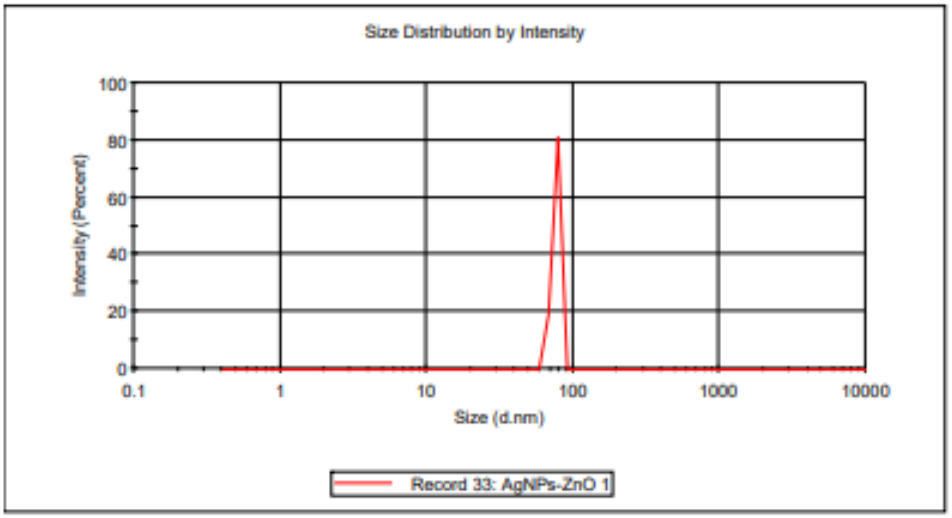

Appendix -4: Crystalline size of pure ZnO NPs and Ag/ZnO NCs with different concentration

100% ZnO			
Peak position	**FWHM**	**Crystalline size (nm)**	**Average crystalline size (nm)**
31.80632	0.23515	35.12841909	**29.37960683**
34.46574	0.23586	35.26533418	
36.29813	0.25699	32.53128631	
47.60003	0.32282	26.89631001	
56.66563	0.30662	29.43543017	
62.93839	0.35644	26.13122759	
68.031	0.3637	26.3521947	
66.46034	0.35092	27.06409428	
69.16798	0.37675	25.6121651	

25% Ag-75% ZnO			
Peak postion	**FWHM**	**Crystalline size (nm)**	**Average crystalline size (nm)**
31.77085	0.3525	23.43182896	**25.88186506**
34.41548	0.35225	23.60979728	
36.258786	0.39408	21.21212686	
38.12318	0.1989	42.25822147	
44.34584	0.22081	38.85100891	
47.56523	0.49942	17.38317324	
56.64367	0.41876	21.55067169	
62.89799	0.51502	18.08125101	
64.47706	0.28924	32.47216322	
68.00169	0.47989	19.96840801	
69.13582	0.53774	17.9408578	
77.43876	0.35794	28.4464678	

50%Ag/50%ZnO			
Peak position	**FWHM**	**Crystalline size (nm)**	**Average crystalline size (nm)**
31.80939	0.36983	22.33596735	**24.96440492**
34.44799	0.37684	22.07112357	
36.29236	0.42975	19.4533503	
38.15711	0.20043	41.93993234	
44.34981	0.22689	37.81044739	
47.59716	0.52665	16.48641582	
56.67222	0.41761	21.61291991	
62.93213	0.55167	16.88310648	
64.5123	0.28988	32.40675764	
68.04166	0.5141	18.64402845	
77.47545	0.35827	28.42756451	

75%Ag/25%ZnO			
Peak position	**FWHM**	**Crystalline size D (nm)**	**Average crystalline size (nm)**
31.78067	0.35693	23.14157167	**27.55062165**
34.4231	0.37001	22.47702058	
36.26408	0.44968	18.58966689	
38.12877	0.19409	43.30620814	
44.32	0.22343	38.39190437	
56.64411	0.38597	23.38155285	
64.48514	0.28449	33.01580442	
62.90671	0.5576	16.70129003	
77.45205	0.35174	28.95057591	

Appendix -5: Mechanical property Test for PLA/ELL-COLL-40% without annealing

TEST REPORT
PE BAG

SAMPL TYPE : protien despresed pl
LDS : 14283175
CUSTOMER : -
ANALIST : eyob
STANDARD : ES ISO 1184:2000

Test Name : BIOPLASTIC TEI
Test Type : Tensile
Test Date : 28/06/2022 10:2
Test Speed : 50.000 mm/mi
Pretension : Off
Width : 13.000 mm
Thickness : 0.317 mm
Sample Length : 100.000 mr

Comments :

Test No	Force @ Break (N)	Elong. @ Break (mm)	Force @ Break (N/mm)	Stress @ Break (N/mm²)	Youngs Modulus (N/mm²)
1	52.53	55.094	4.041	12.747	524.851
2	65.82	63.525	5.063	15.972	598.896
3	57.7	37.963	4.438	14.001	601.773
4	52.6	69.715	4.046	12.764	582.242
Mean	57.162	56.574	4.397	13.871	576.941
S.D.	6.259	13.779	0.481	1.519	35.778
C. of V.	10.949	24.355	10.949	10.949	6.201
Mean - SD	50.904	42.795	3.916	12.352	541.163
Mean + SD	63.421	70.353	4.879	15.39	612.718

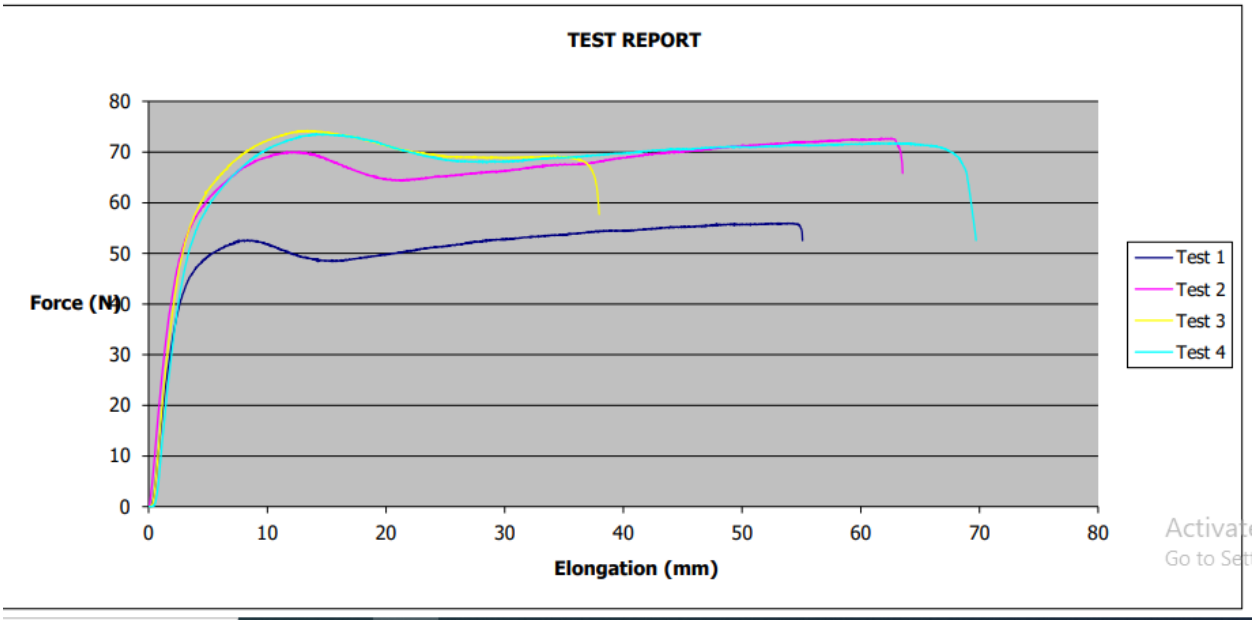

Appendix -6: Mechanical property Test for PLA/ELL-COLL-10% without annealing

TEST REPORT
PE BAG

SAMPL TYPE : protien despresed pl
LDS : 14283176
CUSTOMER : -
ANALIST : eyob
STANDARD : ES ISO 1184:2000

Test Name : BIOPLASTIC TEI
Test Type : Tensile
Test Date : 28/06/2022 10:!
Test Speed : 50.000 mm/mi
Pretension : Off
Width : 13.000 mm
Thickness : 0.305 mm
Sample Length : 100.000 mr

Comments :

Test No	Force @ Break (N)	Elong. @ Break (mm)	Force @ Break (N/mm)	Stress @ Break (N/mm²)	Youngs Modulus (N/mm²)
1	77.0	211.678	5.923	19.42	461.092
2	73.93	126.038	5.687	18.646	418.343
3	80.47	272.667	6.19	20.295	501.816
Mean	77.133	203.461	5.933	19.454	460.417
S.D.	3.272	73.659	0.252	0.825	41.74
C. of V.	4.242	36.203	4.242	4.242	9.066
Mean - SD	73.861	129.802	5.682	18.628	418.677
Mean + SD	80.405	277.12	6.185	20.279	502.157

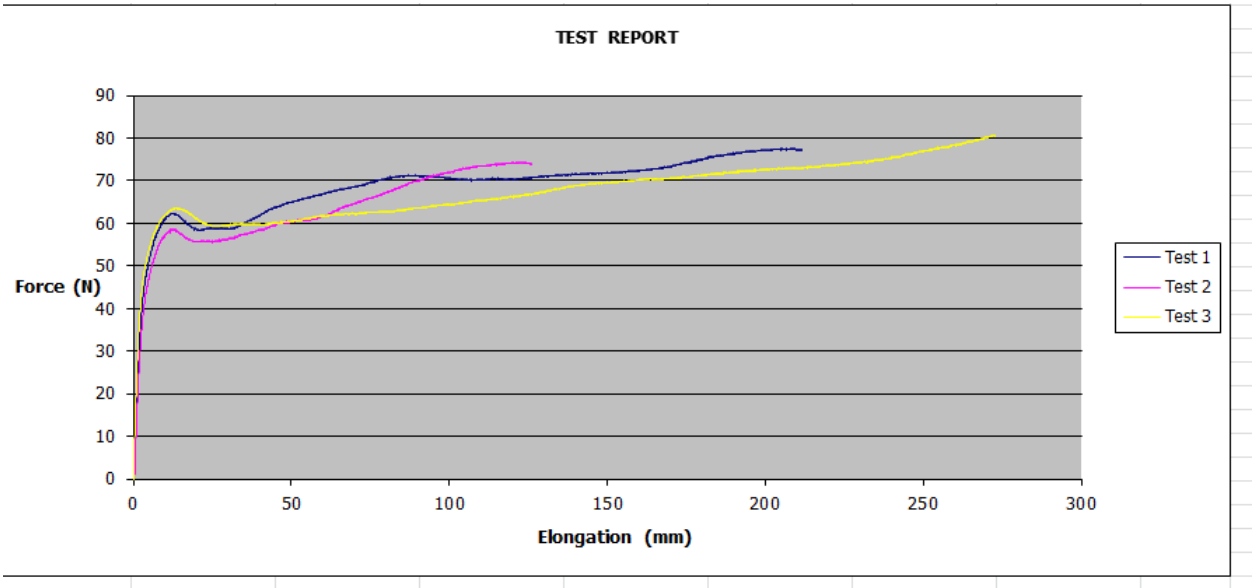

Appendix -7: Mechanical property Test for Neat PLAwith annealing

TEST REPORT
PE BAG

SAMPL TYPE : Bioplastic
LDS : 14248040
CUSTOMER :
ANALIST : ZEMENE/yezihalem
STANDARD : ES ISO 1184:2000

Test Name : BIOPLASTIC TEI
Test Type : Tensile
Test Date : 19/05/2022 11:
Test Speed : 50.000 mm/mi
Pretension : Off
Width : 13.000 mm
Thickness : 0.243 mm
Sample Length : 100.000 mr

Comments :

Test No	Force @ Break (N)	Elong. @ Break (mm)	Youngs Modulus (N/mm²)	Stress @ Break (N/mm²)
1	210.73	3.939	3494.919	66.708
2	246.39	3.053	2237.152	77.996
3	188.19	1.927	3912.487	59.573
4	200.77	2.82	3670.711	63.555
Mean	211.52	2.935	3328.817	66.958
S.D.	25.009	0.827	747.637	7.917
C. of V.	11.824	28.176	22.46	11.824
L.C.L.	171.725	1.619	2139.176	54.361
U.C.L.	251.315	4.25	4518.458	79.555
Mean - SD	186.511	2.108	2581.18	59.041
Mean + SD	236.529	3.762	4076.455	74.875
Mean - 1.96 SD	162.502	1.314	1863.448	51.441

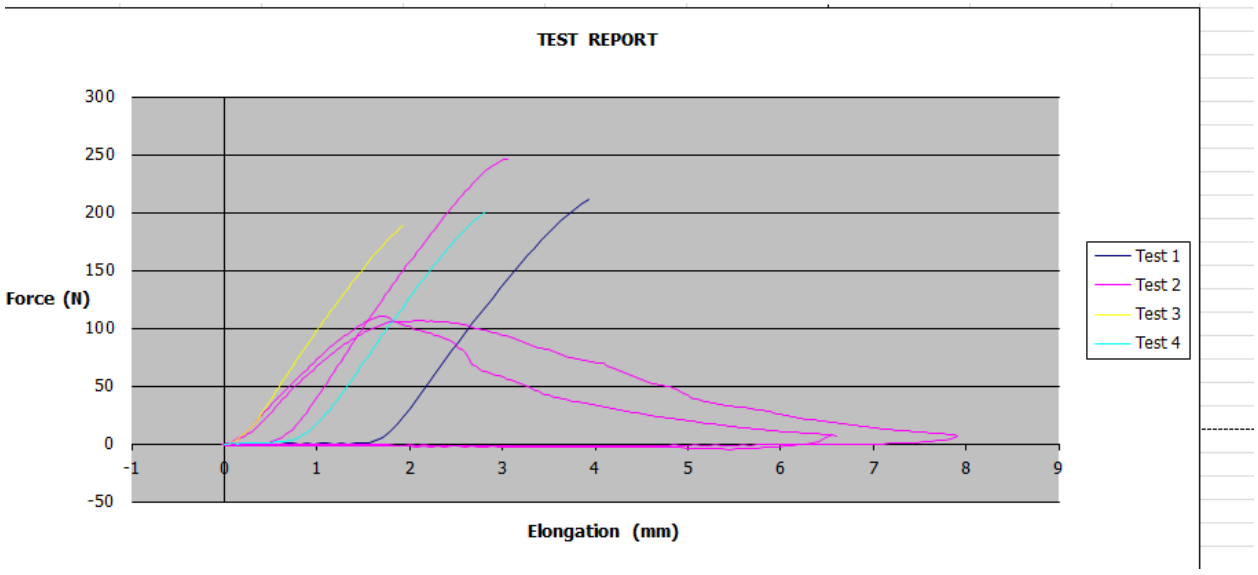

Appendix -8: Mechanical property Test for PLA/ELL-COLL-10% with annealing

TEST REPORT
PE BAG

SAMPL TYPE : Bioplastic
LDS : 14248041
CUSTOMER :
ANALIST : ZEMENE/yezihalem
STANDARD : ES ISO 1184:2000

Test Name : BIOPLASTIC TEI
Test Type : Tensile
Test Date : 19/05/2022 12:(
Test Speed : 50.000 mm/mi
Pretension : Off
Width : 13.000 mm
Thickness : 0.250 mm
Sample Length : 100.000 mr

Comments :

Test No	Force @ Break (N)	Elong. @ Break (mm)	Youngs Modulus (N/mm²)	Stress @ Break (N/mm²)
1	198.5	4.397	3827.028	61.077
2	189.33	4.286	3562.981	58.255
3	193.35	3.948	3563.651	59.492
4	201.45	3.426	3623.872	61.985
Mean	195.658	4.014	3644.383	60.202
S.D.	5.385	0.436	125.065	1.657
C. of V.	2.752	10.866	3.432	2.752
L.C.L.	187.089	3.32	3445.379	57.566
U.C.L.	204.226	4.708	3843.386	62.839
Mean - SD	190.273	3.578	3519.318	58.545
Mean + SD	201.042	4.45	3769.448	61.859
Mean - 1.96 SD	185.103	3.159	3399.255	56.955

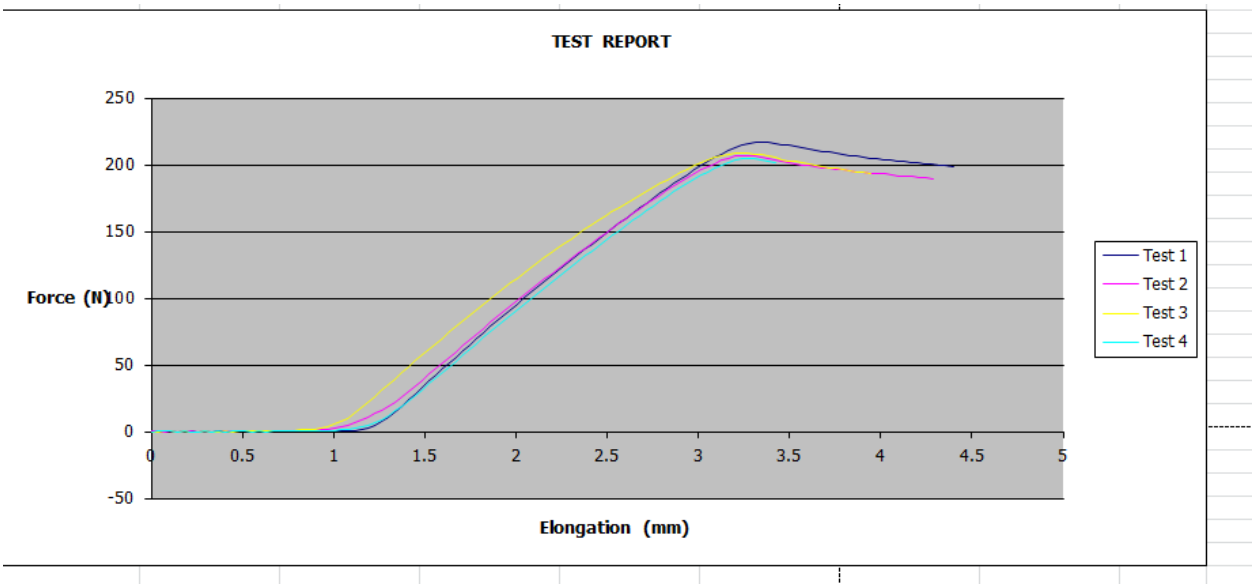

Appendix -9: Mechanical property Test for PLA/ELL-COLL-20% withannealing

TEST REPORT
PE BAG

SAMPL TYPE : Bioplastic
LDS : 14248042
CUSTOMER :
ANALIST : ZEMENE/yezihalem
STANDARD : ES ISO 1184:2000

Test Name : BIOPLASTIC TEI
Test Type : Tensile
Test Date : 19/05/2022 12:1
Test Speed : 50.000 mm/mi
Pretension : Off
Width : 13.000 mm
Thickness : 0.327 mm
Sample Length : 100.000 mr

Comments :

Test No	Force @ Break (N)	Elong. @ Break (mm)	Youngs Modulus (N/mm²)	Stress @ Break (N/mm²)
1	144.48	5.059	2409.728	33.987
2	152.78	5.89	2539.099	35.94
3	145.04	6.998	2457.046	34.119
4	143.86	6.223	2591.947	33.841
Mean	146.54	6.043	2499.455	34.472
S.D.	4.188	0.803	81.6	0.985
C. of V.	2.858	13.295	3.265	2.858
L.C.L.	139.876	4.764	2369.613	32.904
U.C.L.	153.204	7.321	2629.297	36.039
Mean - SD	142.352	5.239	2417.855	33.487
Mean + SD	150.728	6.846	2581.055	35.457
Mean - 1.96 SD	138.332	4.468	2339.518	32.541

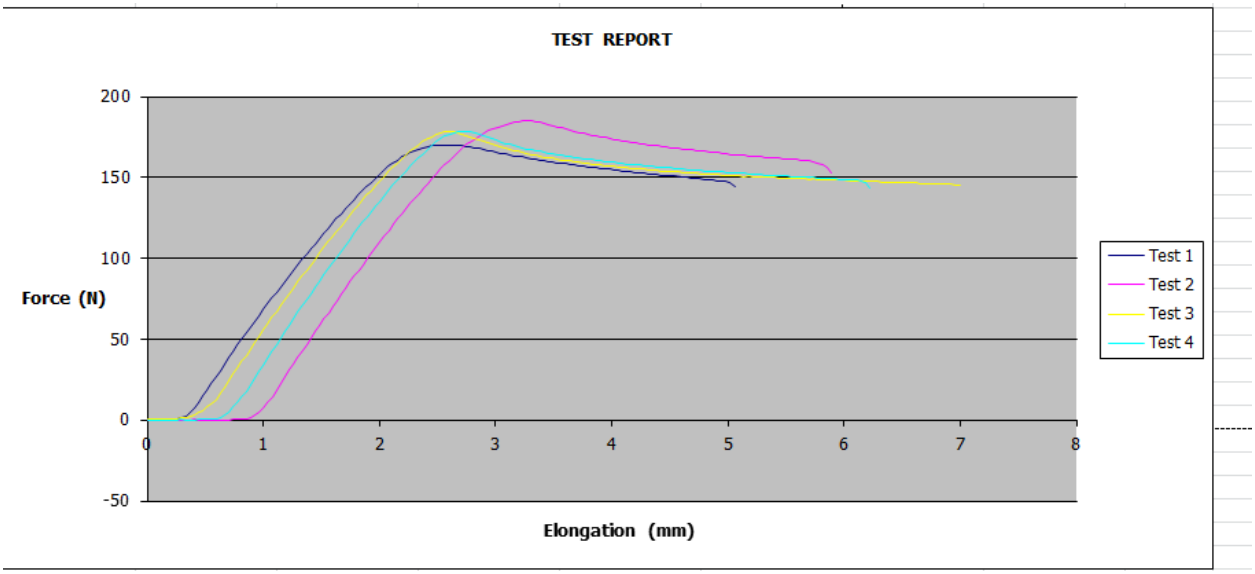

Appendix -10: Mechanical property Test for PLA/ELL-COLL-30% witht annealing

TEST REPORT
PE BAG

SAMPL TYPE : Bioplastic
LDS : 14248043
CUSTOMER :
ANALIST : ZEMENE/yezihalem
STANDARD : ES ISO 1184:2000

Test Name : BIOPLASTIC TEI
Test Type : Tensile
Test Date : 19/05/2022 13:3
Test Speed : 50.000 mm/mi
Pretension : Off
Width : 13.000 mm
Thickness : 0.316 mm
Sample Length : 100.000 mr

Comments :

Test No	Force @ Break (N)	Elong. @ Break (mm)	Youngs Modulus (N/mm²)	Stress @ Break (N/mm²)
1	124.19	5.845	2556.646	30.231
2	124.12	11.149	2221.842	30.214
3	152.72	4.245	2593.928	37.176
4	128.93	7.002	2474.001	31.385
Mean	132.49	7.06	2461.604	32.252
S.D.	13.673	2.951	167.513	3.328
C. of V.	10.32	41.796	6.805	10.32
L.C.L.	110.733	2.365	2195.057	26.955
U.C.L.	154.247	11.756	2728.151	37.548
Mean - SD	118.817	4.109	2294.091	28.923
Mean + SD	146.163	10.011	2629.118	35.58
Mean - 1.96 SD	105.69	1.276	2133.279	25.728

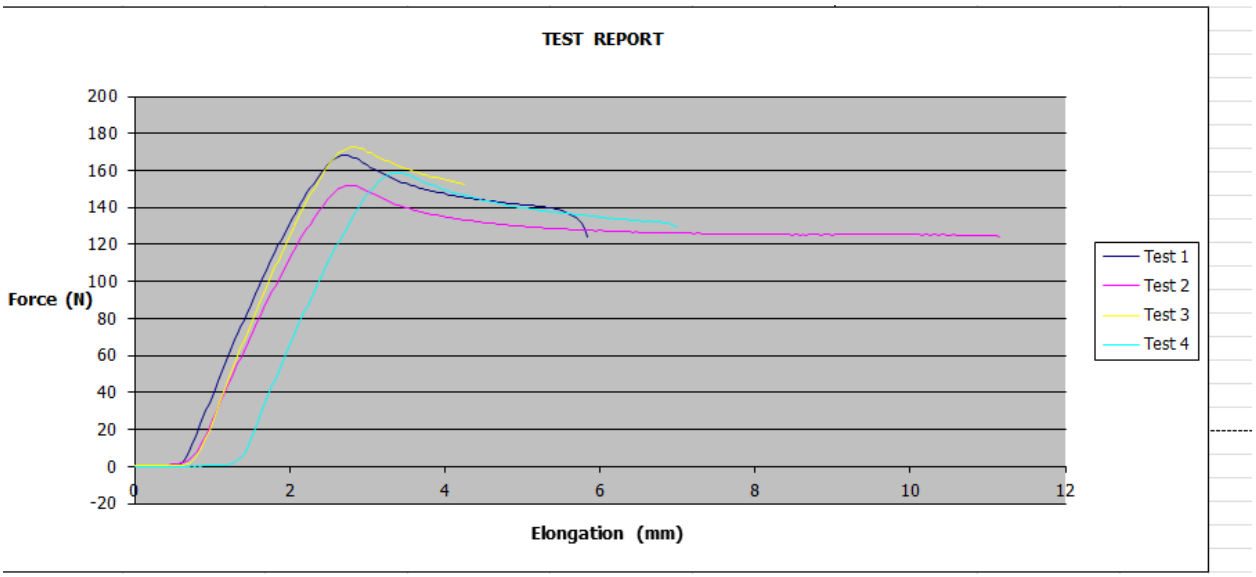

Appendix -11: Mechanical property Test for PLA/ELL-COLL-40% with annealing

TEST REPORT
PE BAG

SAMPL TYPE : Bioplastic
LDS : 14248044
CUSTOMER :
ANALIST : ZEMENE/yezihalem
STANDARD : ES ISO 1184:2000

Test Name : BIOPLASTIC TEI
Test Type : Tensile
Test Date : 19/05/2022 13:!
Test Speed : 50.000 mm/mi
Pretension : Off
Width : 13.000 mm
Thickness : 0.316 mm
Sample Length : 100.000 mr

Comments :

Test No	Force @ Break (N)	Elong. @ Break (mm)	Youngs Modulus (N/mm²)	Stress @ Break (N/mm²)
1	119.92	6.351	2375.632	29.192
2	132.92	9.038	2339.793	32.356
3	141.16	5.768	2452.696	34.362
4	160.7	7.384	2658.258	39.119
Mean	138.675	7.135	2456.595	33.757
S.D.	17.089	1.434	142.456	4.16
C. of V.	12.323	20.094	5.799	12.323
L.C.L.	111.482	4.854	2229.92	27.138
U.C.L.	165.868	9.417	2683.27	40.377
Mean - SD	121.586	5.702	2314.139	29.597
Mean + SD	155.764	8.569	2599.05	37.917
Mean - 1.96 SD	105.18	4.325	2177.382	25.604

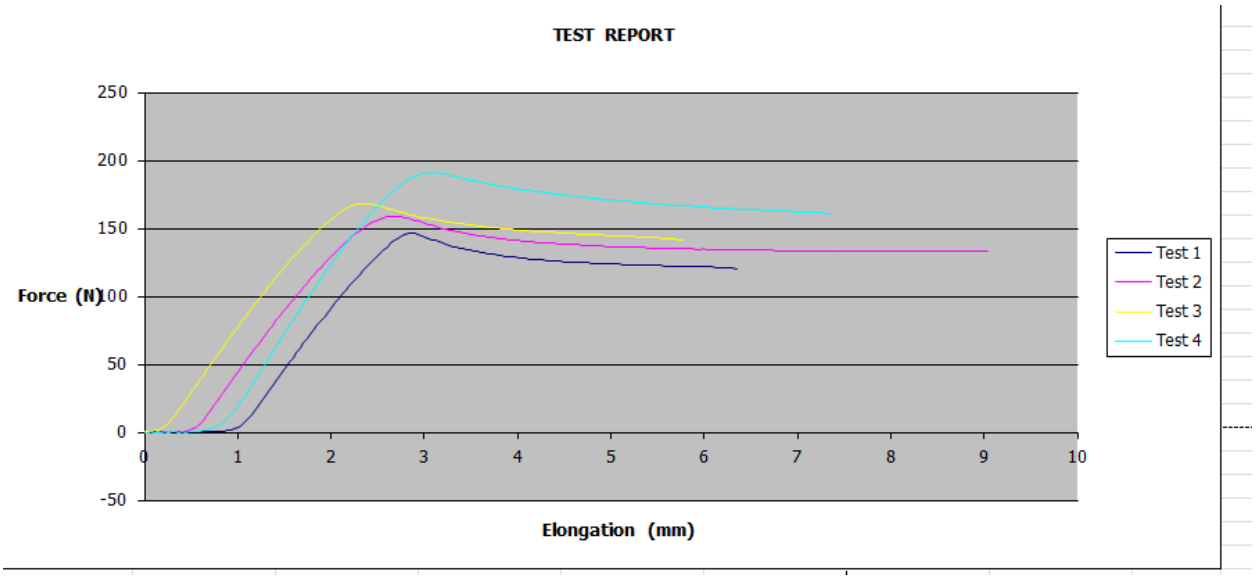

Appendix -12: Thermal conductivity of nanocomposite films

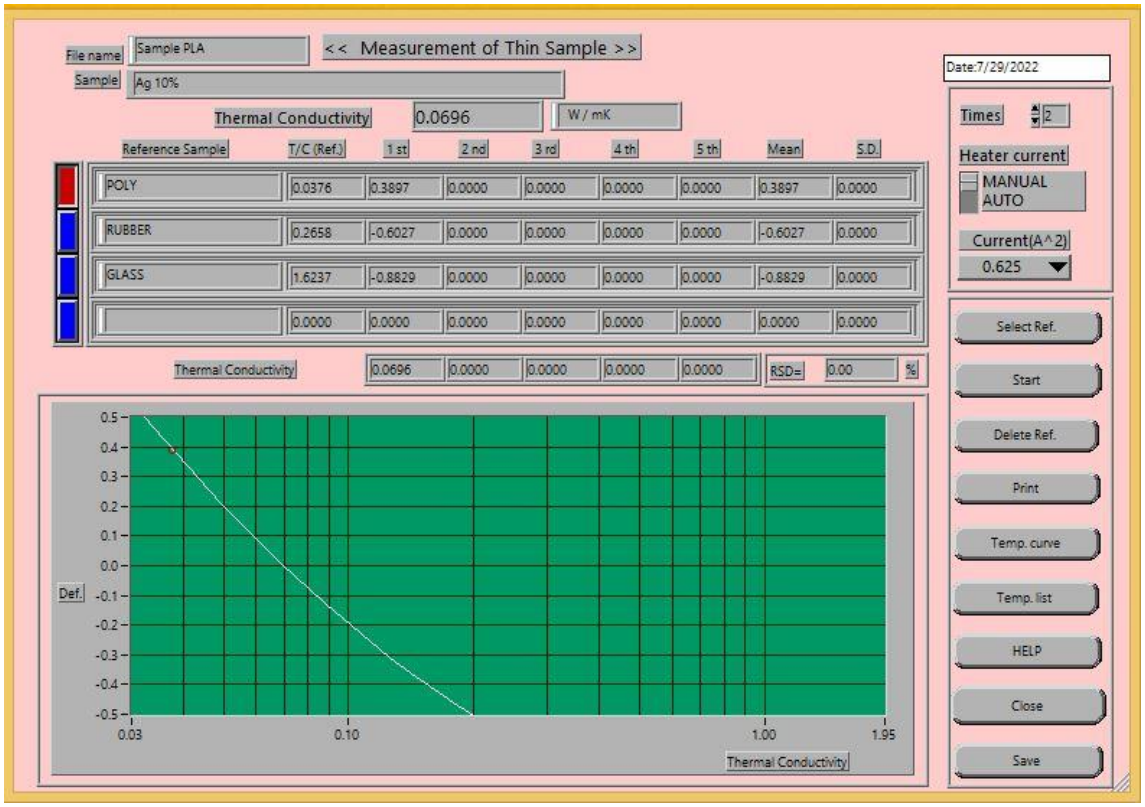

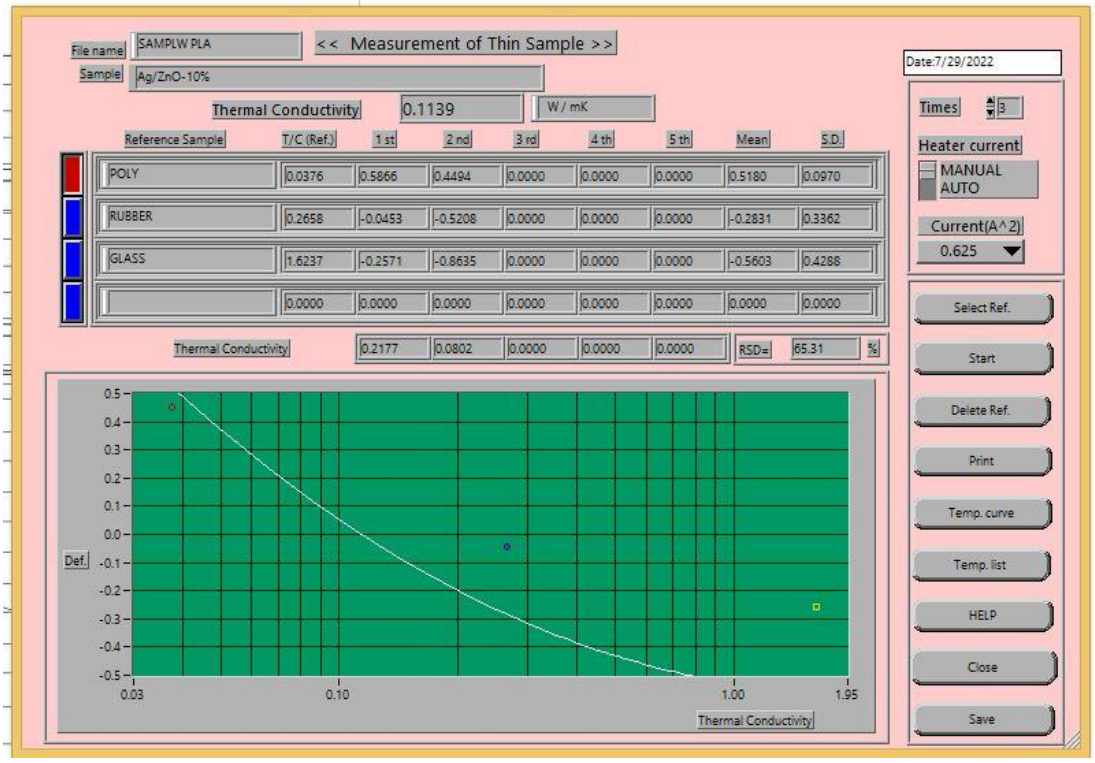
File name
SAMPLW PLA
<< Measurement of Thin Sample >>
Sample
Ag/ZnO-10%
Thermal Conductivity
0.1139
W / mK
Date:7/29/2022
Times
3
Heater current
MANUAL
AUTO
Current(A^2)
0.625
Reference Sample
T/C (Ref.)
1 st
2 nd
3 rd
4 th
5 th
Mean
S.D.
POLY
0.0376
0.5866
0.4494
0.0000
0.0000
0.0000
0.5180
0.0970
RUBBER
0.2658
-0.0453
-0.5208
0.0000
0.0000
0.0000
-0.2831
0.3362
GLASS
1.6237
-0.2571
-0.8635
0.0000
0.0000
0.0000
-0.5603
0.4288
0.0000
0.0000
0.0000
0.0000
0.0000
0.0000
0.0000
0.0000
Thermal Conductivity
0.2177
0.0802
0.0000
0.0000
0.0000
RSD=
65.31
%
Def.
0.5
0.4
0.3
0.2
0.1
0.0
-0.1
-0.2
-0.3
-0.4
-0.5
0.03
0.10
1.00
1.95
Thermal Conductivity
Select Ref.
Start
Delete Ref.
Print
Temp. curve
Temp. list
HELP
Close
Save

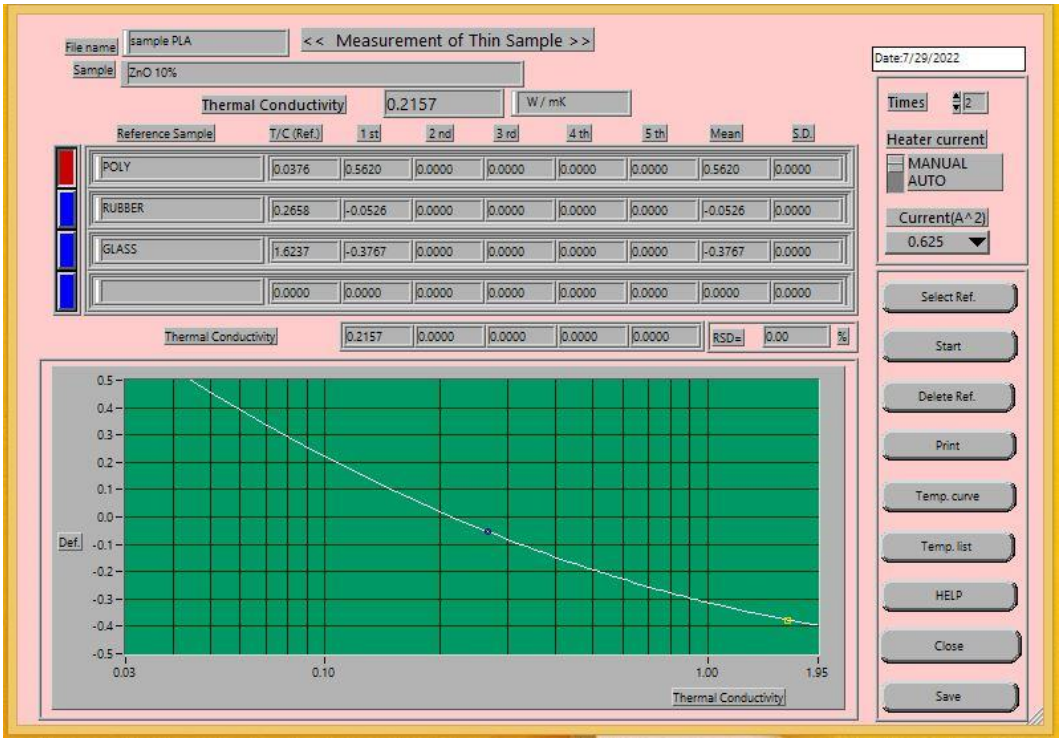
File name
sample PLA
<< Measurement of Thin Sample >>
Sample
ZnO 10%
Thermal Conductivity
0.2157
W / mK
Date:7/29/2022
Times
2
Heater current
MANUAL
AUTO
Current(A^2)
0.625
Reference Sample
T/C (Ref.)
1 st
2 nd
3 rd
4 th
5 th
Mean
S.D.
POLY
0.0376
0.5620
0.0000
0.0000
0.0000
0.0000
0.5620
0.0000
RUBBER
0.2658
-0.0526
0.0000
0.0000
0.0000
0.0000
-0.0526
0.0000
GLASS
1.6237
-0.3767
0.0000
0.0000
0.0000
0.0000
-0.3767
0.0000
0.0000
0.0000
0.0000
0.0000
0.0000
0.0000
0.0000
0.0000
Thermal Conductivity
0.2157
0.0000
0.0000
0.0000
0.0000
RSD=
0.00
%
Def.
0.5
0.4
0.3
0.2
0.1
0.0
-0.1
-0.2
-0.3
-0.4
-0.5
0.03
0.10
1.00
1.95
Thermal Conductivity
Select Ref.
Start
Delete Ref.
Print
Temp. curve
Temp. list
HELP
Close
Save

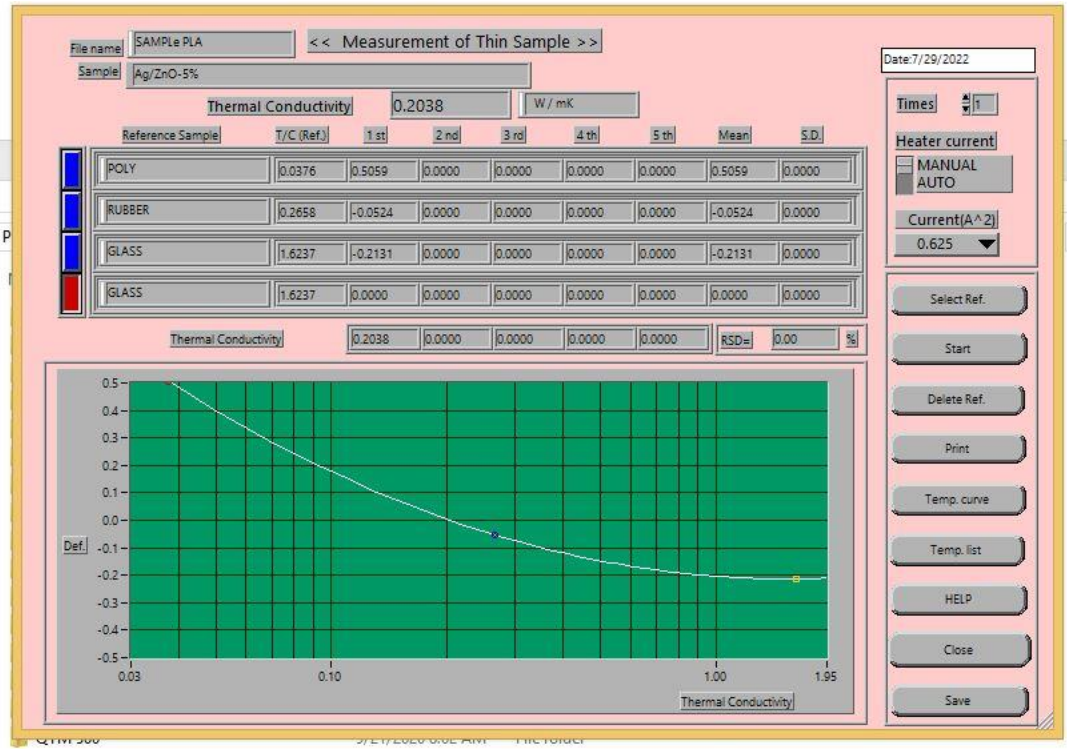
File name
SAMPLe PLA
<< Measurement of Thin Sample >>
Sample
Ag/ZnO-5%
Thermal Conductivity
0.2038
W / mK
Date:7/29/2022
Times
1
Heater current
MANUAL
AUTO
Current(A^2)
0.625
Reference Sample
T/C (Ref.)
1 st
2 nd
3 rd
4 th
5 th
Mean
S.D.
POLY
0.0376
0.5059
0.0000
0.0000
0.0000
0.0000
0.5059
0.0000
RUBBER
0.2658
-0.0524
0.0000
0.0000
0.0000
0.0000
-0.0524
0.0000
GLASS
1.6237
-0.2131
0.0000
0.0000
0.0000
0.0000
-0.2131
0.0000
GLASS
1.6237
0.0000
0.0000
0.0000
0.0000
0.0000
0.0000
0.0000
Thermal Conductivity
0.2038
0.0000
0.0000
0.0000
0.0000
RSD=
0.00
%
Def.
0.5
0.4
0.3
0.2
0.1
0.0
-0.1
-0.2
-0.3
-0.4
-0.5
0.03
0.10
1.00
1.95
Thermal Conductivity
Select Ref.
Start
Delete Ref.
Print
Temp. curve
Temp. list
HELP
Close
Save